Review Article

Pablo Cuartas-Restrepo*

Planetary Magnetic Fields and Habitability in Super Earths

https://doi.org/10.1515/astro-2018-0026
Received Oct 16, 2017; accepted May 22, 2018

Abstract: This work seeks to summarize some special aspects of a type of exoplanets known as super-Earths (SE), and the direct influence of these aspects in their habitability. Physical processes like the internal thermal evolution and the generation of a protective Planetary Magnetic Field (PMF) are directly related with habitability. Other aspects such as rotation and the formation of a solid core are fundamental when analyzing the possibilities that a SE would have to be habitable. This work analyzes the fundamental theoretical aspects on which the models of thermal evolution and the scaling laws of the planetary dynamos are based. These theoretical aspects allow to develop models of the magnetic evolution of the planets and the role played by the PMF in the protection of the atmosphere and the habitability of the planet.

Keywords: Planets and satellites: magnetic fields, physical evolution, terrestrial planets. Planet–star interactions. Methods: numerical

1 Earth-like planets and super Earths

The discovery of planets orbiting other stars in our galaxy has revealed a great diversity of possible worlds. These include giant gas planets like Jupiter orbiting so closly to their star that their atmospheres are eroded, icy Neptune-like planets, and most interesting kind of planets for us, terrestrial and oceanic Earth-like planets. These planets are good candidates for habitability.

Since 1995 more than 3800 exoplanets[1] have been discovered by different teams using different observational methods, and more than 4700 are waiting to be confirmed[2]. In 2005 a team led by Eugenio Rivera found the first SE (Rivera et al. 2005). The planet designated as Gl 876 b has 7.5 $M_\oplus$, and was the first Earth-like planet found around a main sequence star. Since then a few hundred exoplanets in the range of masses from 1-10 $M_\oplus$ have been discovered. One of the most exciting discovery was that the Earth-mass planet orbiting the stars in our closest neighbor stellar system: Alpha Centauri B (Dumusque et al. 2012; Anglada-Escudé et al. 2016).

Traditionally we refer to planets composed basically of rocks, iron, and water (ice) as terrestrial or Earth-like planets. In our Solar System, Mercury, Venus, and Mars have been considered Earth-like planets. The discovery of hundreds of planets with similar masses or superior to that of the Earth, but less massive than Neptune, brought with it the need to classify them within a new type of small planets. The term super-Earth (SE) refers to planets with masses in the range between 1 $M_\oplus$ to around 10 $M_\oplus$. This definition and the first description of these new types of planets were originally presented in the works of Valencia et al. (2006) and Fortney et al. (2007).

The work of Valencia et al. (2006) presents a first assessment of the interior structure of this type of terrestrial planet, assuming that they have a composition similar to that of Earth. This initial work scales the properties of the interior of planets up to 10 $M_\oplus$, including the profiles of density and the temperature inside the planet. On the other hand, Fortney's models of planets include a wider range of planetary masses, from terrestrial planets to gas giants, in addition to a range of compositions that includes planets made of iron, rock, and water (Earth-like), passing through planets covered by gigantic oceans that cover half of its mass (Ocean planets or water worlds), to planets dominated by huge layers of hydrogen and helium (Jovian giants) (Fortney et al. 2007).

Corresponding Author: Pablo Cuartas-Restrepo: FACom-SEAP-Instituto de Física-FCEN, Universidad de Antioquia, Calle 70 No. 52-21, Medellín, Colombia; Email: pablo.cuartas@udea.edu.co

1 http://exoplanet.eu

2 https://www.nasa.gov/mission_pages/kepler

Since those first studies, other works have described characteristics of the SEs, such as their interiors (Valencia et al. 2007b,c; Sasselov et al. 2008), their atmospheres, their tectonic activity (Valencia et al. 2007a) and their rotational and orbital evolution (Cuartas-Restrepo et al. 2016).

These are special properties of SEs that make them a particular class of extrasolar planets. Their sizes and masses suggest that they may have dynamic interiors and be able to develop and maintain atmospheres and Planetary Magnetic Field (PMF), both necessary conditions for habitability (Haghighipour 2011). On the other hand, their close-in orbits and their composition represent a challenge to planetary formation theories.

The better-known model of planetary formation is based on the minimum-mass solar nebula (the protoplanetary disk that forms the solar system). According to this model, there was enough solid material in the original protoplanetary disk to form planets larger than the Earth. The upper mass reached by a planet in the inner side of a protoplanetary disk depends on the available amount of solid material (Ida and Lin 2004).

If a planet grows above the mass of the Earth, it begins to accrete gas from the disk. This gas accumulation process culminates in a runaway accretion that will form a gas giant. The value of the critical mass, for which such runaway growth could occur, would thus determine whether SEs are likely to exist at all. Some models predict that planets above 10 $M_\oplus$ grows so rapidly that can reach more than 100 $M_\oplus$ in a few million years (Ida and Lin 2004). The models predict a large number of SEs formed in the inner parts of the disk too. From current planetary formation models, it is possible to infer the existence of a lot number of planets with masses in the range 1 - 10 $M_\oplus$. The diversity of known planetary systems containing SEs suggest two different ways of formation: core accretion and planetary migration. The first is a process of in-place formation, the second is a formation process while the orbital dynamics of the disk were evolving, impliying that SEs were formed at large distances and were then scattered to their close-in locations by migration processes (Haghighipour 2011). Models combining core accretion and type-I migration produce objects in the range 3-4 $M_\oplus$ in close-in orbits (McNeil and Nelson 2010).

The formation of planets around low mass stars (M-dwarfs), where the solid material available is less than a solar-type nebula, implies that is no easy to achieve the formation of giants. The most probable formation is instead of low mass planets ranging from Earth-like to Neptune-like masses. The dynamic of the formation around M-dwarfs is a slow process compared with more massive protoplanetary disks. Another factor involved is the rapid dispersal of the gas in the disk, which is another disadvantage for the giant's formation. According to this, the planets formed around M-dwarfs must be mainly low mass planets, SEs or smaller (Haghighipour 2011). Nevertheless, several giant planets have been discovered around M-dwarfs, so there remains an interesting open problem with current models.

1.1 The Mass-radius relationship

Different types of planets are defined by their internal composition. With measured masses and radii, and models for the interior of the planet, the composition could be inferred. But naturally, there are many possible solutions, the only things that might be inferred are bounds on the bulk composition of the planet (Valencia 2011). From radial velocity and transit observations, astronomers can infer the mass and the radius of the planet. Using these values, the average density can be computed, and the result shows indirectly which kind of planet are you observing. High density planets like Earth or Mercury push us to classify them as rocky, but only deeper analyses on the likelihood of other materials present in their compositions can give us the certain about the terrestrial nature of these planets. The true challenge for numerical modeling of the planetary interiors is to differentiate the Earth-like planets, made mainly by iron, rock, and ice, from planets with huge volatile envelopes, as is believed to be the case for GJ 1214 b (Charbonneau et al. 2009).

The giant gaseous planets are structured by a very small core enveloped with a huge H/He layer that represents the main composition. Super-Earths and Neptune-like planets are composed mainly by rocky and icy materials and have thin atmospheres that play a negligible role in their bulk composition. The internal structure models must account for the different rock and ice properties. Combining internal structure models, H/He and H_2O envelopes it is possible to infer the main composition of SEs (Valencia et al. 2006; Seager et al. 2007; Fortney et al. 2007; Adams et al. 2008; Valencia 2011). The models of the internal components for SEs are based on the hypothesis they are made primarily of iron, silicates, and water, and to a lesser extent, some other carbon compounds (Seager et al. 2007). The possibilities include planets made of pure ice and ice/rock mixtures, which could be described as "water worlds" or "Ocean planets" (Fortney et al. 2007), they calculate radii and masses for different types of planets, from gas giants to hydrogen-rich and water-rich planets using the Equation of State (EOS) for different compositions, and thus find a mass-radio relationship. Other detailed models

of the mass-radius relation for solid planets can be found in Seager et al. (2007). Normally the models of solid planets seek comparisons with well-known planets as Venus or the Earth. These comparisons require that models of the composition give the radio and the masses of the planets.

The iron component of a planet corresponds to the *Core-Iron Mass Fraction* (CMF). In the same way, the rock-silicate component corresponds to the *Mantle-Rock Mass Fraction* (MMF) and the water-ice component corresponds to the *Ice Mass Fraction* (IMF) (Fortney et al. 2007). The differences in compositions of rocky planets depend mainly on the amount of iron located mostly in the core, with some in the mantle. The extremes for rocky planet compositions go from a pure iron planet to a planet with any iron (Moon-like planet (Valencia 2011)). Earth-like planets have CMF ~32% of iron while Mercury-like planets are iron-rich with more than CMF ~80% of their mass represented by its core.

To facilitate comparisons between small solid planets and the Earth, Zeng et al. (2016) developed a model of planets based on the *Preliminary Reference Earth Model* (PREM), developed by Dziewonski and Anderson (1981). Zeng et al. (2016) have proposed that terrestrial-type planets are composed in two layers and found an expression to calculate the mass-radius relation of these planets, depending on their CMF. This proposal is adjusted to the Earth's radius within 2%, and is valid for a mass range $1 - 8\ M_\oplus$ and CMF up to 0.4:

$$\left(\frac{R}{R_\oplus}\right) = (1.07 - 0.21 * CMF)\left(\frac{M}{M_\oplus}\right)^{1/3.7}. \qquad (1)$$

This semi-empirical mass–radius formula is in agreement with the mass–radius relation of SEs presented in Valencia et al. (2006), which is a scaling law of $R \propto M^{0.267-0.272}$.

To find this relationship, Zeng et al. (2016) extrapolated the EOS of the core and mantle of the Earth to more massive planets and then they adjusted the mass-radius ratio in such a way that the relationships lie within 0.01 for radius and 0.02 for CMF. Assuming that in general, solid exoplanets comply with a distribution of the CMF, the CMF of a planet can be expressed as:

$$CMF = \frac{1}{0.21}\left[1.07 - \frac{(R/R_\oplus)}{(M/M_\oplus)^{0.73}}\right]. \qquad (2)$$

There are many uncertainties in the result of the CMF distribution for rocky exoplanets, mainly due to errors in the measure of both the radius and the mass of the planets. Nevertheless, by applying a least squares adjustment, it is possible to infer the core and mantle fractions of extrasolar planets with different compositions to a good approximation (see tables 1 and 2 in Zeng et al. (2016)).

Figure 1 shows the mass-radius relationship for rocky planets. The figure was built using equation 1 and the results for radios and masses for ice-iron-rocky planets, showed in table 1 in Fortney et al. (2007). This figure shows the curves for different types of composition and different CMF, from planets composed entirely of iron, through planets like Earth, to planets composed entirely of water. By way of comparison, the figure also shows the observational data of radii and masses published for planets below 10 $M_\oplus$, published in the exoplanet catalog (http://exoplanet.eu/catalog/). Each black dot corresponds to one SE in the catalog. As can be seen from the dispersion of points, there is a diversity of possible compositions among the SEs. The figure includes some of the SEs considered with the greatest potential to be habitable, according to the consensus of the planetary scientists and astrobiologists, identified with their names in vertical position.

1.2 Habitability

The traditional concept of habitability was proposed by Huang (1960). Our modern concept of habitability is based mostly on the possibility of a planet to sustain liquid water on its surface (Kasting et al. 1993). This condition depends on the balance between the energy received, the energy released and any greenhouse effect of the atmosphere, which together determine the temperature on the surface of the planet.

There are other factors involved in the question of planetary habitability. The modern notion of habitability implies many other geophysical, geochemical, astrophysical and biotic criteria that must be met before a planet can support life. Some of these criteria are related to the internal structure and dynamics of the planet that determines properties like the recycling of volatile from the atmosphere, the tectonic activity and the formation and maintenance of a protective PMF.

The mass, possible composition, and structure of SEs imply that they could have the capability of developing and retaining atmospheres and to have a dynamic interior that can produce a PMF. The PMF acts as a shield that protects the atmosphere from the erosive effects of the stellar wind and cosmic rays (CR).

Stellar parameters, such as mass, luminosity and magnetic activity, and orbital dynamic properties such as the location of the Habitable Zone (HZ) determine a lot of properties shared between the star and planet. Structures such as the magnetosphere are created by the interaction between the stellar wind and the PMF. The sustaining of an atmosphere depends on the radiation and particle flux evolution of the star, and the presence of an active PMF that conforms a protective magnetosphere (Lammer et al.

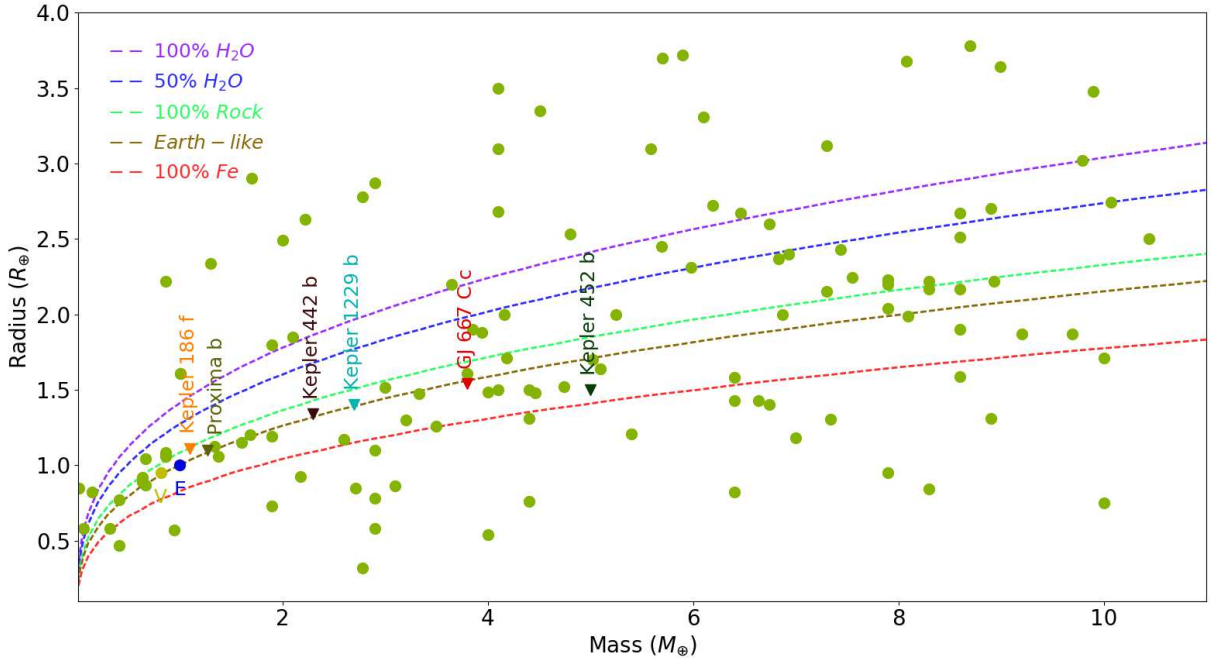

Figure 1. Mass-radius relationship. Earth-like planets have ~68% silicate mantle and ~32% iron core. The percentage of iron in the density profiles corresponds to the CMF. The percentage of water corresponds to the IMF. Extrasolar planets with known mass and radius and within the mass range of SEs are shown (green dots). There are also shown some of the most promising SEs in terms of posibilities of habitability currently

2010). All these conditions are related to the thermal evolution of the planet.

The flux of X-rays, Ultraviolet radiation (XUV) and stellar winds have a strong impact in the environments of close-orbit exoplanets, including terrestrial-type exoplanets in the HZ of low mass stars (Khodachenko et al. 2009). Normally, close planets are tidally locked, and their PMFs are weak to protect fully against winds and coronal mass ejections, in such a way that when they collide with the planetary magnetosphere, they compress it to heights where ionization and erosion can reduce the atmosphere.

1.3 Dynamics of the orbit and spin

Planets close to their host stars are subject to a strong tidal interaction. This leads to a gravitational locking on short timescales. The tidal forces change the orbits, limiting the time for the emergence and evolution of life on a planet. Based on the only example we know, the Earth, we can suppose that the time necessary for the chemistry of life to be able to experiment and reach complex organic molecules that lead to an evolutionary process is hundreds of millions of years. The time of evolution of the period of rotation of planets subjected to the tides of its star before they reach a low resonance or complete locking, is in almost all cases much smaller than hundreds of millions of years (Heller et al. 2011b; Correia et al. 2012; Rodríguez et al. 2012; Cuartas-Restrepo et al. 2016).

Planets inside the HZ of M-dwarfs are probably tidally locked. The planetary climate is dramatically affected, with a day-side hemisphere heated, where the surface material could reach the melt temperature forming a liquid rocky ocean, and a frozen night side hemisphere where the atmosphere could be condensed and/or collapsed.

Many numerical models of the evolution of the orbit of planets close to the host star has been developed. These models indicate that, regardless of the rotation of the planet, normally the tidal torque causes the planet to end in an orbital resonance (Makarov and Efroimsky 2012; Cuartas-Restrepo et al. 2016), not necessarily pseudo synchronic (Rodríguez et al. 2012).

A planet must remain habitable long enough for life to develop, in the case of the Earth this takes around 700 Myr. A planet in the HZ must also have a low orbital eccentricity, so that tidal interactions do not make it inhospitable. Planets with eccentricities larger than 0.5 suffer tides that reduce habitable lifetimes (Barnes et al. 2008), due to the changes in the semimajor axis and the eccentricity of the orbit. Planets with great eccentricities within the HZ will also suffer periods of very high radiation. The planet may not even stay within the HZ during its entire orbital period.

The majority of terrestrial planets inside the HZ of low-mass stars will be on nearly circular orbits (Barnes et al. 2008), and must be tidally locked in less than 1 Gyr. Nevertheless, recent works show that the 1:1 resonance for a planetary orbit is not so common (Makarov and Efroimsky 2012; Makarov et al. 2012; Cuartas-Restrepo et al. 2016), and is more probable to achieve 2:1 resonances. Depending on the eccentricity and the rheological properties of the planet, which includes the response of the mantle to tidal forces, the spin of the planet evolves to a low resonance but it is not necessarily locked. The spin of the planet is causally related to the appearance and maintenance of a PMF. The work of Zuluaga and Cuartas (2012) (hereinafter ZU12) shows how rotation determines the regime of the PMF and the structure of the magnetosphere.

Additionally, gravitational tides change the obliquity of the planet rotation axis. This process of tilt erosion, and likely occurs before life emerges in a planet. Tilt erosion can occur in just thousands to millions of years for planets orbiting in the HZ of low mass stars (Heller et al. 2011a). Obliquity determines atmospheric conditions, the amount of tidal heating and the rotation period, all these properties related directly with the habitability.

1.4 Planetary atmospheres

Terrestrial planets can obtain their atmospheres from three different processes: 1) the capture of gas from the original nebula, 2) the emission of gases from inside the planet during the process of accretion and 3) emission of gases by tectonic processes. These processes can produce massive atmospheres rich in hydrogen, and carbon compounds. This process can produce planets that contain up to 20% of their total mass in the form of water (Elkins-Tanton and Seager 2008).

Planetary atmospheres contain the main volatile material needed to develop and sustain life in a planet, especially H_2O. The atmosphere cycles are governed by the interaction between the interior and the surface of the planet. The content of greenhouse gases in the atmosphere controls the surface temperature and can determine the presence of liquid water on it. Any clouds in the atmosphere influence the equilibrium temperature of the planet, by the variation of the average albedo of the atmosphere. For example CO_2 clouds absorb infrared (IR) radiation warming the planet surface, on the other hand, low H_2O clouds like cumulus and stratus reflect visible light waves cooling the planet surface, and high H_2O clouds absorb IR coming out from the planet and warm up the surface. The presence of an atmosphere and its composition determine the physical limits for the habitability of a planet (Selsis et al. 2007). The atmosphere controls the flux of heat out of the planet, making the planet habitable or not.

The magnetosphere of terrestrial planets inside the HZ of low-mass stars might be compressed during epochs of increased stellar magnetic activity. In such cases, the interaction with the stellar wind can lead to heating of the upper atmospheres. This results in large atmospheric and water loss rates so that planetary habitability can be strongly affected (Khodachenko et al. 2007; Lammer et al. 2007).

The atmospheres of Earth-like planets are affected by thermal and nonthermal escape processes. The atmospheres can be eroded by the intense radiation, the stellar wind, and coronal mass ejections. Around M-dwarfs, this process is expected to be stronger, making planets around them less capable to sustain an atmosphere and to be habitable (Segura et al. 2010; Zendejas et al. 2010; Tian 2015; Luger and Barnes 2015; Owen and Mohanty 2016; Kopparapu et al. 2017). The thermal process by which the planetary atmosphere is lost happens when the planet temperature increases, then the atmosphere expands and its high layers are directly exposed to the erosive action of the stellar wind. In high layers, the UV photodissociates molecules of H_2O, and the hydrogen is lost into space. Planets like Venus and Mars lost their water through processes like these (Kulikov et al. 2006; Krasnopolsky 2015).

Some of the main atmospheric loss processes are (Lammer et al. 2010):

- **Exposure to X-ray and EUV radiation**: Terrestrial planets that form rich in water, placed within the HZ could be capable of evolving life as on Earth, as long as its water survives early bombardment events and the strong irradiation of X-ray and EUV from its young stars. The ionization of the outer atmosphere is mainly due to radiation at wavelengths ≤ 1000 Å. In these cases, the loss of atmospheric gases can be treated as a hydrodynamic problem. When the EUV radiation reaches the upper regions of the atmosphere, atoms like O and N are heated by radiation, and then they can reach escape velocities and expand into space (Tian et al. 2008). It has been shown that stellar winds can remove the N reserves in terrestrial planets when their outer atmospheric layers are exposed to intense X-ray and EUV radiation (Lammer et al. 2009).
- **Ion pickup**: Atoms and neutral molecules above the ionosphere can be ionized either by the exchange of charges with the stellar wind or by EUV radiation. The ions generated from this exchange are acceler-

ated by the interplanetary electric field and are finally dragged by the stellar wind around the magnetosphere. A fraction of the ions produced, come back through the lines of the PMF and collide with other particles, which allows them to reach escape velocity.

– **Atmospheric sputtering**: When charged particles with very high energy interacting with the atmosphere, they can produce the direct ejection of material. This process has been identified, for example, as one of the sources of loss of atmosphere on Mars, especially in the early stages of evolution of the planet, justly after the Martian magnetic field collapsed about 3.7 Gyr ago. This process of direct erosion is more effective on planets smaller than Earth. On planets more massive, particles accelerated by sputtering can reach heights where the ionization and pickup processes take place, and in this way, they are also eroded from the atmosphere.

2 The interior of massive terrestrial planets

Many models of the internal structure of SEs have been developed over the last ten years (Valencia et al. 2006, 2007b,c; Fortney et al. 2007; Seager et al. 2007; Selsis et al. 2007; Sotin et al. 2007; Adams et al. 2008; Baraffe et al. 2008; Grasset et al. 2009). These models are giving us an understanding of global properties such as the mass-radius relationship and its dependence on composition, as well as different geophysical phenomena such as mantle convection and plate tectonics (Olson 2007; Papuc and Davies 2008; Valencia et al. 2007a; Valencia and O'Connell 2009; Korenaga 2010). Models used to infer the internal structure of SEs suppose that the composition of these are the same as the Earth and their interior properties like density, temperature, gravity and pressure scale with the planetary mass (Valencia et al. 2006; Sotin et al. 2007; Fortney et al. 2007; Sasselov et al. 2008; Fortney et al. 2009).

Three primary characteristics of the planetary interior are related to habitability: composition, tectonic activity and PMF. The knowledge about the interior of planets is limited to Earth and Moon, where direct measurements have been done by seismographs. We do not have such direct access to the interior of other planets of the solar system and of course, exoplanets. There are data available for the gravitational field of planets such as Mars, Mercury, and Venus, but these are not enough to know their internal structure. It requires numerical models and assumptions about the composition in accordance with the measurements made by space probes.

For terrestrial planets the internal composition is not uniform, the pressure and temperature inside the planet change the state of materials, turning the structure of the planet into a collection of different layers with different composition and physical properties (Valencia et al. 2006; Sotin et al. 2007; Fortney et al. 2007; Sasselov et al. 2008; Fortney et al. 2009). For the Earth, the materials of the mantle and core are quite well determined. The mantle is mainly formed by two types of silicates: olivine at the upper mantle and perovskite in the lower mantle. The core is formed mainly by iron plus some light elements like sulfur, oxygen, and hydrogen. The main bulk composition of SEs can be reasonably assumed to be the combination of three ingredients: iron, silicates and water (Valencia et al. 2007b). This mix of materials implies different average densities and a maximum planetary radius for a given planetary mass. The water-rich planets must have larger radii than the water-poor ones. The minimum radius of a SE is a function of its mass. The mass and radius knowledge is not enough to determine the actual composition of a SE. The combination of components may result in the same mass and radius (Haghighipour 2011).

Assuming that these planets are made like the Earth, the internal structure could be inferred by scaling the structure and internal properties of the Earth itself and depending on the planetary mass. These models assumes a spherically symmetric planet that is chemically and mineralogically homogeneous. The equations describing density ρ, gravity g, mass m, and pressure P inside the planet are (Valencia et al. 2006):

$$\begin{aligned} \frac{d\rho}{dr} &= -\frac{\rho(r)g(r)}{\phi(r)} \\ \frac{dg}{dr} &= 4\pi G\rho(r) - \frac{2Gm(r)}{r^3} \\ \frac{dm}{dr} &= 4\pi r^2\rho(r) \\ \frac{dP}{dr} &= -\rho(r)g(r), \end{aligned} \tag{3}$$

where $\phi(r) = K_s(r)/\rho(r)$ is the seismic parameter that can be calculated from the equation of state, K_s is the adiabatic bulk modulus, G is the gravitational constant and r is the distance measured from the center of the planet.

It is necessary to solve an equation of state (EOS) for each material in the interior of the planet. Some authors chose a third-order EOS, the *Birch-Murnaghan* equation (Valencia et al. 2006), others authors chose a different EOS like the *Vinet* equation. The model that fit the interior of the Earth is the PREM, and in the Earth-like planets case, it is valid for comparison purposes, that is, for a 1.0 $M_\oplus$

planet, the interior model must reproduce the PREM to be acceptable.

Scaling the Earth's properties to larger planets gives an insight into the possible internal structure of a SE. These planets, due to their large compressional effects and high internal temperatures exhibit a mass to radius relationship that deviates from the cubic power relationship for constant density scaling (see section 1.1). Table 1 shows how some of the main properties could be calculated for SEs using a general form that scales the same property for the Earth:

$$P_{rop} = P_{rop\oplus}\left(\frac{M_p}{M_\oplus}\right)^{\beta_p}, \tag{4}$$

where $P_{rop\oplus}$ is the property measured for the Earth, M_p is the mass of the planet in Earth masses and β_p is the exponent which scale the property.

Table 1. Scaled properties exponent for massive terrestrial planets and its values for the Earth

Property	β_p	$P_{rop\oplus}$
Planetary Radius (R_p)	0.270	6.37×10^6 m
Mean Density ($\bar{\rho}$)	0.192	5500 kg m^{-3}
Core Radius (R_c)	0.244	3.48×10^6 m

2.1 Tectonic Activity

Planets are formed hot. After the accretion process the surface and interior of the planet are melted, and a slow cooling starts forming a solid surface first and removing heat from the interior. Other internal heat sources like radioactive decay, the slow gravitational contraction, and rotational friction must evolve in such a way that the planet interior is dynamic. The cooling of the interior is governed by convection. The mantle convection controls the cooling of the core and produces convection currents that travel from the core's upper limit to the solid crust. The convection operates in two different ways: moving the plates, this is called it the *mobile-lid* regime, as in the Earth's tectonism, or forming a rigid layer at the surface known as the *stagnant-lid* regime, as in Mars or Venus.

The tectonic activity of a planet determines thermal state at the surface, which is fundamental to habitability (Valencia et al. 2007a; Valencia and O'Connell 2009; Korenaga 2010; Foley et al. 2012; Tikoo and Elkins-Tanton 2017). It has been argued that habitable planet needs plate tectonics to remain active over billions of years. The cycling of volatile material from the atmosphere to the mantle is governed by plate tectonics, regulating the composition of the atmosphere, including greenhouse gases, CO_2 and H_2O, and hence, helps to control the surface temperature and planetary habitability (Kasting et al. 1993; Franck et al. 2000). Plate tectonics creates land surfaces that favor the appearance of life, and enhancing biodiversity through evolution on isolated continents (Lammer et al. 2010). A planet needs enough mass to drive mantle convection, and have a damp mantle to lubricate the plates' motion. Water affects the dynamics of the mantle and the planetary tectonic power. It makes the lithosphere deformable for subduction to occur and facilitates volcanic activity (Valencia and O'Connell 2009).

Plate tectonics evolves with the planet's thermal evolution (see section 4). A planet with tectonism must have enough heat flux to drive vigorous convection needed for active plates movement. The total heat flux varies with time as the interior of the planet undergoes in a long-term cooling. When the flux of heat from the interior falls below a threshold, plate tectonics will cease to operate on a planet. Planets close to their stars suffer tidal heating that could sustain the tectonism during more time. The tectonism in SEs still being an open problem and remains under debate.

Essentially all interior models for terrestrial planets start from the knowledge that we have of the planets of the solar system, so that in principle are biased. Normally, models of the interior present solutions to three canonical equations for solid planets: 1) mass conservation, 2) hydrostatic equilibrium and 3) the equation of state (Fortney et al. 2007; Seager et al. 2007; Sotin et al. 2007; Valencia et al. 2007b,c; Rogers and Seager 2010). Models assume, for example, spherical symmetry, and concentric layers. Most models assume that heavier materials will be located in the central core, and that the layers that surround the core are free of metallic materials (Fortney et al. 2007), or they possess the solar metallicity (Guillot et al. 2006). These simplifications are based on the fact that no matter where the heaviest materials are located, this does not affect, in general, the evolution of the planet (Baraffe et al. 2008).

The EOS is often assumed to be independent of temperature, when the latter is relatively low (Seager et al. 2007; Fortney et al. 2007). This assumption does not lead to great errors for Earth-like planets but is not correct when considering more massive planets (Baraffe et al. 2008). In many cases, the thermal evolution and the process of core cooling were ignored.

Baraffe et al. (2008) examines these assumptions. Their results suggest that models should improve the implementations of the EOS for material at very high pres-

sures and temperatures, including heat transport processes. Observational constraints on gravitational characteristics, like oblateness estimates using transit data, could shed light on periods of rotation, and could help to restrict models of internal structure.

Although most models adopt terrestrial composition, that is, iron, silicates and water (Valencia et al. 2007b; Seager et al. 2007; Fortney et al. 2007; Zeng et al. 2016), some models venture to propose planets rich in other materials such as carbon (Madhusudhan et al. 2012; Wagner et al. 2012), or with large differences in their water proportions, planets that have been called waterworlds (Marcus et al. 2010; Benneke and Seager 2013; Zeng and Sasselov 2013; Levi et al. 2014). In these cases, the limitations in the models have to do with two main processes: 1) the heat conduction from inside the planet, especially in planets with internal layers composed of materials at high pressures such as post-perovskite. Usually the actual thermal conductivity capacity of the materials in the SEs are greater than the models assume (Wagner et al. 2012). 2) There is doubt with respect to composition, given that observationally is possible to see a different type of planet having the same mass or the same radius. Sometimes what looks like a SE turns out to be a gaseous dwarf called mini-Neptune (Benneke and Seager 2013).

Most of the assumptions that refer to the thermal evolution, to heat conduction processes and to EOS have been improved in more recent models, such as those of Gaidos et al. (2010) (hereinafter GA10), Tachinami et al. (2011) (hereinafter TA11) and Zuluaga et al. (2013) (hereinafter ZU13), which are described with greater depth in section 4.

3 Planetary magnetic fields

In our solar system, magnetic fields have been measured from the Sun, through the planets and even in some of the moons. Interestingly these fields are different in all cases, even between similar objects in form or composition, such as the planets. Our understanding how a PMF emerges and evolves in SEs comes from the Earth's thermal evolution models (TEM) (Stevenson 2003; Labrosse 2003, 2007a,b; Nimmo 2009; Aubert et al. 2009; Breuer et al. 2010) and scaling laws for dynamos driven by convection and rotation, which are based upon numerical simulations (Christensen and Aubert 2006; Olson and Christensen 2006; Aubert et al. 2009; Christensen et al. 2009; Christensen 2010). The intensity of the PMF directly influences the evolution and the maintenance of planetary atmospheres and determines the conditions for the possible evolution of life (von Bloh et al. 2007; Grießmeier et al. 2005, 2009, 2010; van Thienen et al. 2007; Lammer et al. 2010). The PMF protects planets against the particles of the stellar wind and CR. Having a weak or no PMF, has serious implications for planetary habitability.

The PMF is generated in the interior of the planet through a dynamo (Stevenson 1983, 2003, 2010). This is precisely the case of the geomagnetic field. The properties of the PMF depend on the structure, composition and thermal history of the planet. These dynamos are sustained by thermal and compositional convection within an electrically conductive fluid (Olson and Christensen 2006). The sources of energy that maintain the PMF may vary, and the thermal history is directly related to the power available to keep the PMF alive.

The terrestrial planets are made mainly of iron and silicates that have condensed at very high temperatures. These materials remain liquid for a long period of the planet's history while it cools down. The conductive liquid required to generate the PMF is the molten iron in the core. The heat flow from inside the core produces the convection, which coupled with rotation, sustains the dynamo. The SEs can develop and sustain a dynamo, but the question is whether the dynamo can produce a strong PMF and if it is maintained during enough time to protect the planet until life appears and evolves.

3.1 PMF generation

The PMF requires an electrically conductive fluid in motion. On Earth-like planets, the conductive fluid is the layer of liquid iron within the core. The cooling process on low-mass planets produces the solidification of the innermost layers of the core and the growth of this provides a huge source of energy from the release of latent heat, in addition to the release of light elements that help convection. This energy turns on and maintains the dynamo. The buoyancy of light elements is derived of a difference in composition between the solid core and the liquid core. Elements such as sulfur and oxygen tend to be expelled from the solidified nucleus towards the liquid nucleus (Breuer et al. 2010).

Planetary dynamos operate in an environment of high electrical conductivity (Busse and Simitev 2009). The flow inside the core is turbulent and on a small scale, the PMF is chaotic. The large-scale structure can be regular as in the case of the Earth, but other dynamos like the one of the Sun presents activity and quiet periods. Dynamos convert mechanical energy into magnetic one, a process based on electromagnetic induction: the creation of electromag-

netic forces associated with currents and finally a magnetic field (Stevenson 2010). Mathematically this process is expressed by combining the laws of induction of Ohm, Ampere, and Faraday:

$$\frac{\partial \mathbf{B}}{\partial t} = \lambda \nabla^2 \mathbf{B} + \nabla \times (\mathbf{v} \times \mathbf{B}), \tag{5}$$

where $\mathbf{B}$ is the magnetic field, $\mathbf{v}$ represents the fluid motion relative to the rotating frame, and λ is the magnetic diffusivity. A good approximated solution of this equation is developed by Roberts and Glatzmaier (2000) in section 3 of their work.

If the conducting fluid does not move, then the field decays in a time scale $\tau \sim L^2/\pi^2\lambda$, where L is a length scale of the field that is related to the width of the layer that forms the liquid core (Stevenson 2010). Usually, the time of decay of the dynamo is of the order of thousands of years, this implies that the PMF must be generated continuously. A successful dynamo is one that remains active against ohmic dissipation, and requiring sources of energy to maintain fluid motion (Roberts and Glatzmaier 2000).

Two types of fluid dynamos could be modeled: *kynematic* and *magnetohydrodynamic* (MHD) (Roberts and Glatzmaier 2000). In the kinematic case, given the motion of the fluid $\mathbf{v}$, you must find $\mathbf{B}$. On the other hand, in the MHD case you try to find both $\mathbf{v}$ and $\mathbf{B}$ from a known power source. Analytically and numerically, the solutions suggest that the dynamo will only exist under certain conditions in the movement of the fluid. A fundamental characteristic is that the magnetic Reynolds number $Rm = vL/\lambda$ has a critical value between 10 - 100 (Stevenson 2010), but this is a vague criterion, since it depends on the velocity field and how it is determined. The problem of determining the parameters on real planets is even greater, we do not know their critical values. Assuming a spherical geometry of the liquid layer and if Coriolis forces and convection are taken into account, the critical value is of the order of $Rm_{crit} \simeq 50$ (Christensen and Aubert 2006).

The movement of the fluid produces a magnetic field which arises as a result of the Coriolis force and its effect on the flow (Stevenson 2010). The amount that relates the motion and the force of Coriolis is the *Rossby number*:

$$R_o = \frac{\mathbf{v}}{2\Omega L}, \tag{6}$$

where Ω is the frequency of rotation of the planet. A small value of the Rossby number implies a system which is strongly affected by Coriolis forces. On the other hand, a large value of the Rossby number corresponds to a system where the inertial and centrifugal forces are dominant.

3.2 The Geodynamo

The first suggestion about that a dynamo produces the Earth's PMF was made by Joseph Larmour in 1919. In his model the solid electrically-conducting disk that rotates on the axis of a device is replaced by the rotational movement of a electrically-conductive fluid. This idea was strengthened as other explanations for the origin of the field were discarded. One of the arguments in favor of a dynamo as the origin of the PMF of the Earth is the fact that there are no differences between the normal and reversal of field polarity states of the Earth's field. This behavior is especially hard to explain with models for the terrestrial magnetism, other than a self-excited dynamo (Roberts 2009).

Dynamo theory describes how a system in a rotation, with a conductive fluid and that has convection, can maintain a PMF during astronomical timescales. The paleomagnetic registers indicate that the Earth's PMF has been active at least for the last three and a half billion years (Tarduno et al. 2010), in contrast with a decay time of only a few tens of thousands of years. On the other hand, the polarity of the Earth's field has changed many times with periods of a few hundred thousands of years. There must be an internal mechanism to ensure permanent re-generation of the field within the planet.

The behavior of the Earth's magnetic field is directly related to the core's energy sources (see section 3.3). While the information about the terrestrial dynamo is limited, it is known that it behaves mainly like a dipole and that it presents reversals. We also know that the amplitudes of the field do not seem to have changed much through time. Surface measurements of the field are not a good source of information about what is happening in the core of the planet. The surface magnetic field is usually dominated by magnetic anomalies produced by the crustal minerals. In addition, the toroidal structure of the field at the core cannot be observed in the surface. As a result, the field we measure on the surface differs in frequency and amplitude of the field in the core. Particularly, the ohmic dissipation, dominated by very low amplitude fields, is not observable on the surface (Nimmo 2009).

On the surface of the Earth the magnetic field $\mathbf{B}$ is mainly dipolar, mathematically this is expressed as:

$$\mathbf{B} = -\nabla V, \tag{7}$$

$$\nabla \cdot \mathbf{B} = 0, \tag{8}$$

where V is the magnetic potential of the field:

$$V \sim \mathfrak{M} \cdot \nabla r^{-1}, \; r \to \infty. \tag{9}$$

where the intensity of the Earth's dipole is a function of time, $\mathcal{M}(t)$ and nowadays have a value of $|\mathcal{M}| = 7.835 \times 10^{22}\ A\ m^2$.

Currently, the magnetic axis is inclined 169°, if we consider that the positive magnetic pole points towards the geographic south pole of the Earth. The fact that the Earth's PMF decreases with distance supports the original idea by William Gilbert that the origin lies inside the planet.

The dipolar component of the field is just the first term of the expansion of the magnetic potential $V(r, \theta, \phi, t)$, that includes quadrupoles, octupoles, and orders each time smaller successively. The potential is usually expressed as an expansion in spherical harmonics that includes the functions of Legendre $P_l^m(\theta)$, with θ representing the colatitude coordinate ($\theta = 0$ corresponds to the North pole and $\theta = \pi$ to the South pole), and ϕ the longitude coordinate:

$$V = R_\oplus \sum_{l=1}^{\infty} \sum_{m=0}^{l} \left(\frac{R_\oplus}{r}\right)^{l+1} P_l^m(\theta)[g_l^m(t)\cos m\phi + h_l^m(t)\sin m\phi]. \quad (10)$$

Here $g_l^m(t)$ and $h_l^m(t)$ are known as Gauss coefficients and they define the field configuration. The term $(\frac{R_\oplus}{r})^{l+1}$ represents the proportionality of the internal harmonics of the field. Gauss demonstrated that the external harmonics of the field are so weak that they can be neglected. The term for $l = 1$ correspond to the dipolar component of the field, $l = 2$ to the quadrupole, $l = 3$ to the octupole etc. The terms decrease with distance as r^{-l}, so those of a higher order are more important near the surface of the planet.

These equations represent a PMF produced by currents of conductive material within the planet. Actually, the PMF deviates a bit from this ideal configuration. For example, currents in, and near the magnetosphere, induce other currents and electric fields that distort the lines of the PMF and modify its geometry, especially as it moves away from the planet.

On the other hand, inside the planet, the convection in the liquid core is due to temperature and buoyancy of light elements. As the Earth cools, the iron solidifies in the inner core releasing latent heat and lighter elements such as sulfur and oxygen. The combined action of convection and the rotation of the planet causes the fluid to move in a spiral path parallel to the axis of rotation. This continuous movement shakes the PMF, constantly writhes and replaces field against dissipation.

Why does the Earth's PMF have the intensity and structure that it shows us? Why is the magnetic dipole relatively aligned with the axis of rotation? Why does the dipole occasionally changes its polarity? Many authors have addressed the problem of modeling the geodynamo.

In a pioneerign work, Glatzmaier and Roberts (1995) developed numerical models that simulate the convection and the generation of the PMF, as well as reversals of polarity. The simulated PMF has an intensity and a dipole structure that is very similar to the real field. The numerical solution shows how planetary rotation plays a fundamental role in convection processes and is responsible for the structure and evolution of the PMF. Other models of geodynamo have been developed during the last years, all of them point more or less to the same conclusions.

Jones (2000) presented 3D simulations. In his model, the convection is, again, the main energy source for the PMF, both, thermal and compositional. The model reproduces the morphology and the intensity of the field in the core (CMB) reasonably, as well as the periods of the field reversals, that have been detected in the paleomagnetic observations. The model found problems with the values of the diffusivities, and the dynamic regime of the field still could not know. The model had to assume the nature of the flow near boundaries, which had serious implications for the dynamics of the PMF. Likewise, large-scale convection was not well understood, so the predictions of the model were deemed unreliable.

Later models such as Driscoll and Olson (2009) simulate the secular evolution of the core of the Earth trying to understand the behavior at large time scales of the geodynamo, but also including the frequency in the processes of polarity reversals. This work analyzes fundamental parameters such as convection, rotation and the growth rate of the inner core, in order to determine the dipole intensity and its duration over time for different regimes of convection and rotation. Their simulations find that the rate of the growth of the inner core determines, in many occasions, the frequency of the reversals and the intensity of the dipole.

The work of Christensen et al. (2010) establishes some conditions in the values of fundamental parameters such as the Ekman number, related to viscosity, and the magnetic number of Reynolds, in order to make the models closest to the observations. The main challenge to models is that the parameters values such as the Ekman number in the simulations are far from the real values for the Earth. Christensen et al. (2010) sets quantitative criteria based on the morphology of the magnetic field in the core.

An excellent review of the scope of geodynamo models is that of Christensen (2011a). By that time the models had already reached a state of sophistication such that they are considered by some as a fundamental tool to understand the morphology and the evolution of the terres-

trial PMF. Even through, many of the values of the parameters in the models are far from the real values for the Earth. However, some scaling laws suggest that the results of the models are not very far from the real behavior of the geodynamo, especially in the CMB. The results support the idea of columns of convection that concentrate the main magnetic flux, more or less parallel to the rotation axis. The values of the intensity of the field that result from the models are also, within the values measured for the geodynamo. Suprisingly, models reproduce the reversals of polarity, given that the origin of said reversals remains unknown.

3.3 Dynamo energy sources

By identifying the internal energy sources of a planetary dynamo we can to address two fundamental aspects of the problem of PMF: 1) How a planetary dynamo is viable and, 2) how a dynamo can survive for periods of time of Gyr. The fact that a PMF can sustain itself during billions of years, restricts the parameters of thermal evolution and the energy sources of the core of the planet (Nimmo 2009). The core contains a reserve of thermal energy that must be transported through the mantle of the planet, which in turn controls the transfer rate of the heat. This means that the thermal evolution of the mantle directly affects the core heat reserves (Nimmo 2009).

In the case of the Earth, the structure of the core has been inferred from seismic information. In general, density and core temperature are functions of depth, increasing along with the pressure. The density profile shows a discontinuity, which has allowed defining a boundary between an internal solid core and an external liquid layer. The discontinuity of density is due to the fact that, obviously, solid iron is denser, and the liquid layer also has a large number of light elements. This difference in composition constitutes one of the main factors affecting convection of the core.

The temperature in the core has an adiabatic profile (Nimmo 2009). Right on the boundary between the liquid and the solid cores (Inner Core Boundary - ICB), the temperature reaches the solidification point at that pressure, from there it must establish an adiabatic profile for the liquid layer. The solidification temperature of the iron at that pressures is difficult to establish experimentally. Models developed by Vočadlo et al. (2003) yield $T_{ICB} \approx 5650 \pm 600$ K for pressures ~330 GPa.

The heat fluxes from the interior of the Earth can be measured superficially, but the heat sources can only be inferred by using numerical models. A good description of the fluxes, energies, and entropies of the core of the Earth can be found in volume 8 of the *Treatise on Geophysics* especially in the chapter by F. Nimmo, *Energetics of the Core* (see table 1 in the chapter) (Nimmo 2009). According to Nimmo (2009), there are six sources of thermal energy in the solid and liquid cores, to each one of those corresponds to a source of entropy. The heats sources can be defined as:

- **Secular cooling heat,** Q_S: It is simply the heat released as the planet's core cools, which includes the effect of the core contraction. This source of heat depending on the cooling rate of the core:

$$Q_S = -\int \rho c_p \frac{dT_c}{dt} dV. \tag{11}$$

- **Latent heat,** Q_L: It is the heat released as the iron in the core changes state and solidifies, forming the internal solid core. The energy released depends on the solidification rate of the iron that depends on the latent heat L_H. The rate at which the inner core grows depends on the change in the temperature and the difference between the adiabatic temperature profile and the temperature of melting T_m:

$$Q_L = -\frac{4\pi R_{ic}^2 L_H T_{ic}}{\left(\frac{dT_m}{dP} - \frac{dT}{dP}\right) g} \frac{1}{T_c} \frac{dT_c}{dt}. \tag{12}$$

- **Radioactive decay,** Q_R: The decay of radioactive elements, as well as the gravitational tidal dissipation in the CMB, are processes that also release heat. It is assumed that the vigorous convection of liquid core homogenizes the distribution of elements throughout the entire volume of the liquid layer. h is the volumetric heating rate:

$$Q_R = \int \rho h dV. \tag{13}$$

- **The heat of reaction,** Q_H: This source of energy represents the change in the internal energy of the system due to chemical reactions. This energy depends on entropy and the concentration of light elements in the core. The energy released in chemical reactions between iron and light elements is also included in this heat source. R_H is the heat of reaction and D_c/D_t is the parameterized rate of expulsion of the light elements:

$$Q_H = \int \rho R_H \frac{D_c}{D_t} dV. \tag{14}$$

- **Compositional heat,** Q_g: This term refers to the release of light elements from the solid inner core. This release of elements change the density and hence

the gravitational potential ψ, of the core. The contribution of this heat source is proportional to the rate of expulsion of light elements D_c/D_t and the compositional expansion coefficient α_c:

$$Q_g = \int \rho\psi\alpha_c \frac{D_c}{D_t} dV. \tag{15}$$

– **Pressure heating,** Q_P: If the pressure in the core increases, then the melting temperature of the iron increases too, and the solid internal core growth, which produces an extra latent heat release that can be of the order of 10% - 20% (Gubbins et al. 2003).

$$Q_P = \int \alpha T P_T \frac{dT_c}{dt} dV. \tag{16}$$

In this way, the total inventory of heat released by the core, which is transported through the CMB, can be expressed as:

$$Q_{CMB} = Q_S + Q_L + Q_R + Q_H + Q_g + Q_P = \oint \mathbf{q} \cdot d\mathbf{S} \tag{17}$$

The heat produced by the ohmic dissipation is not included in this balance of energies. However, dissipation is an irreversible process, so it is a source of entropy. For each heat source, there is a corresponding entropy sink. The inventory of entropies in the core establishes criteria for the operation or the decay of the dynamo. In particular, sources of entropy can be identified due to diffusion E_k, by ohmic dissipation E_Φ, and by molecular conduction E_α.

In general, what can be calculated is the production rate of entropy, large heat fluxes mean large production rates of entropy. Each entropy sink could be expressed as:

$$E_S = -\int \rho c_p \left(\frac{1}{T_c} - \frac{1}{T}\right) \frac{dT_c}{dt} dV, \tag{18}$$

$$E_L = -\frac{4\pi R_{ic}^2 L_H (T_{ic} - T_c)}{\left(\frac{dT_m}{dP} - \frac{dT}{dP}\right) T_c g} - \frac{1}{T_c}\frac{dT_c}{dt}, \tag{19}$$

$$E_R = \int \rho h \left(\frac{1}{T_c} - \frac{1}{T}\right) dV, \tag{20}$$

$$E_H = -\int \rho \frac{R_H}{T} \frac{D_c}{D_t} dV, \tag{21}$$

$$E_g = \frac{Q_g}{T_c}, \tag{22}$$

$$E_P = \frac{Q_P}{T_c} - \int \alpha P_T \frac{dT_c}{dt} dV. \tag{23}$$

In this way, the sum of sinks of entropy must be equal to the production of entropy associated with each heat source

$$E_S + E_R + E_H + E_g + E_P = E_k + E_\Phi + E_\alpha \tag{24}$$

In this expression, the entropy associated with the latent heat has been added to the secular cooling.

In the case of the Earth, it is evident that the balance of entropies in the core is enough to hold the dynamo. The cooling process of the planetary core raises the question about the ratio between energy sources and entropy sinks. The equation (24) shows us the total entropy available to keep the dynamo in action. In general, the terms related to molecular conduction E_α and to the pressure E_P, are very small, so they need not be considered. Then, the available entropy production rate can be expressed as (Gubbins et al. 2003; Nimmo 2009):

$$\begin{aligned} \Delta E &= E_S + E_R + E_L + E_H + E_g - E_k \\ &= E_R + \tilde{E}_T \frac{dT_c}{dt} - E_k. \end{aligned} \tag{25}$$

Entropies E_S, E_L, E_H, E_g, depend on the cooling rate of the core dT_c/dt. E_R depends on the presence of radioactive elements in the core and E_k depends on the adiabatic profile just at the CMB. $\tilde{E}_T$ groups together all the terms that depend on the core cooling rate. A high cooling rate or a high radioactive decay increases the entropy available for the dynamo, but a high adiabatic contribution reduces the available entropy.

Now, given that the heats of pressure Q_P and reaction Q_H are very small compared with other heat sources, these can be ignored, and the equation for the energy balance can be written again as:

$$Q_{CMB} = Q_S + Q_L + Q_R + Q_g = Q_R + \tilde{Q}_T \frac{dT_c}{dt}. \tag{26}$$

Again $\tilde{Q}_T$ groups together terms dependent on the cooling rate. By combining the equations (25) and (26), we can find an expression that shows us the flux of heat through the CMB that is required to maintain a dynamo with an entropy production rate E_Φ:

$$Q_{CMB} = Q_R \left(1 - \frac{\tilde{Q}_T}{\tilde{E}_T}\frac{1}{T_R}\right) + \frac{\tilde{Q}_T}{\tilde{E}_T}(E_\Phi + E_k), \tag{27}$$

where $T_R = Q_R/E_R$. This is the equation of energy for a planetary dynamo. In section 4 we will see how the different models of thermal evolution make use of this equation.

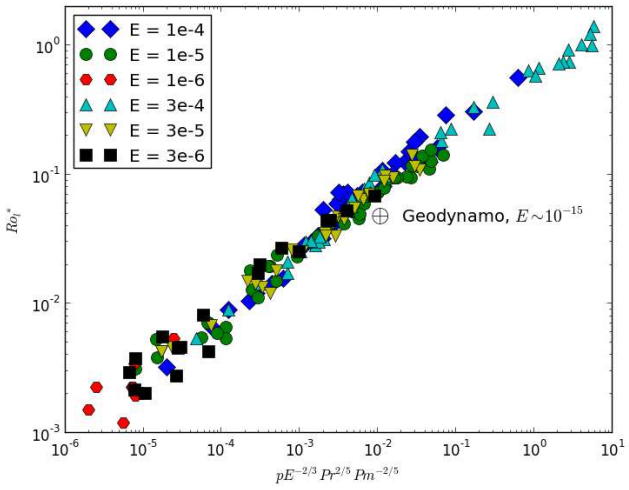

Figure 2. Modified local Rossby number Rol^* as a function of the combination $pE^{-2/3}Pr^{2/5}Pm^{-2/5}$ (implicitly χ). This figure reproduce the results showed in figure 8 in Aubert et al. (2009), but here including numerical dynamos results from (Christensen 2011b)

3.4 Magnetic scaling laws

Properties such as dipole moment, surface intensity and the intensity of the dipole component of the PMF of SEs, can be scaled from the properties of the geodynamo.

Magnetic scaling laws explain the PMF in terms of properties of the planet such as the core radius, conductivity and density of the core, rotation and convective energy flow (Christensen 2010). Scaled dynamos should be similar and differ only in some specific parameters. This means that the structure and evolution of Earth-like planets must be similar. The models of the thermal evolution of SEs suppose this input. Scaling laws based on our knowledge of the geodynamo provide a useful tool to estimate the PMF of extrasolar Earth-like planets.

Numerical experiments suggest that the main properties of convective dynamos can be expressed in terms of a power law of a modified Rayleigh number (Christensen and Aubert 2006; Olson and Christensen 2006; Aubert et al. 2009; Christensen et al. 2009). The properties that are scaled include the convective heat Q_{conv}, the radius of the core R_c, the thickness of the liquid core $D = R_c - R_{ic}$ and the rotational frequency Ω. Scaling laws are expressed using the formulation of Aubert et al. (2009), where the properties of the dynamo are scaled in terms of the dimensionless convective power density p,

$$p = \frac{Q_{conv}}{\Omega^3 D^2 \overline{\rho}_c V}. \tag{28}$$

Here, $\overline{\rho}_c$ is the mean density and V the total volume of the convection region. Two dimensionless parameters are have used to characterize the properties of the dynamo (Christensen and Aubert 2006; Christensen 2010): the Lorentz number Lo and the local Rossby number Ro_l. The Lorentz number is defined as (Aubert et al. 2009):

$$Lo = \frac{B_{rms}}{\sqrt{\overline{\rho}_c \mu_o} \Omega D}. \tag{29}$$

$B_{rms} = (1/V) \int B^2 dV$, is the rms amplitude of the field inside the convective layer with volume V and μ_o is the magnetic permeability.

Because the inertia implies a scale length, while the Coriolis force does not, Christensen and Aubert (2006) have defined a modified Rossby number, the *local Rosby number* Ro_l, that depends on the length scale of the flow rather than the thickness of the fluid shell and that is potentially a better measure for the balance between inertia and Coriolis force,

$$Ro_l = \frac{U_{rms}}{\Omega L}. \tag{30}$$

U_{rms} represents the velocity of the convection and $L \sim D/\bar{l}$ is the length scale. Assuming that the radial and horizontal scales are more or less similar, Christensen and Aubert (2006) estimate a characteristic value of the spectra of the kinetic energy in function of the spherical harmonic degree. The mean value of this harmonic, $\bar{l}$, it is obtained from the time-average kinetic energy spectrum. By definition, Ro_l will be large when the convection is intense, the length scale is small or the dynamo has a slow rotation. On the other hand, when the dynamo has a fast rotation, a large scale length or low convection, then Ro_l will have small values.

The scale relationships for Lo and Ro_l have been found from numerical experiments, covering a wide range of physical properties and boundary conditions (Christensen and Aubert 2006; Christensen et al. 2009; Aubert et al. 2009):

$$Lo = c_{Lo} f_{ohm}^{1/2} p^{1/3}, \tag{31}$$

$$Ro_l^\star \equiv \frac{Ro_l}{(1+\chi)} = c_{Rol}\, p^{1/2} E^{-1/3} (Pr/Pm)^{1/5}. \tag{32}$$

f_{ohm} is the fraction of convective energy that is lost by cause of the ohmic dissipation, $\chi = R_{ic}/R_c$ is the ratio between the radius of the inner core and the outer core, $E = \nu/(\Omega D^2)$ is the Ekman number that describes the ratio of viscosity to Coriolis forces, ν is the viscous diffusivity and $Pr/Pm = \lambda/\kappa$ is the ratio between the numbers of Prandlt, which describes the ratio between thermal (λ) and magnetic (κ) diffusivities. $Ro_l^\star$ is a modified Rossby number (Christensen and Aubert 2006), which depends on the size of the liquid layer. The relationship between $Ro_l^\star$ and

the convective energy p is shown in figure 2. The values of constants c_{Lo} and c_{Rol} are obtained by adjusting the results of numerical experiments for different boundary conditions (Christensen 2010). Usually, the value of c_{Lo} for the multipolar dynamos is smaller than for the dipole case.

The scaling law for Lo provides a simple way to scale the B_{rms} field with p, no matter what regime the field is in. Using equations (29) and (31) we find an expression for the magnetic field strength (Aubert et al. 2009):

$$B_{rms} = c_B f_{ohm}^{1/2} (\overline{\rho}_c \mu_o)^{1/2} \Omega D p^{1/3}. \tag{33}$$

The exact value of the exponent of p is close to $1/3$. Although in general, the intensity of the field does not depend on the rotation, the dipole component depends on it by means of Rol^* for all regimes: dipolar, reversing and multipolar.

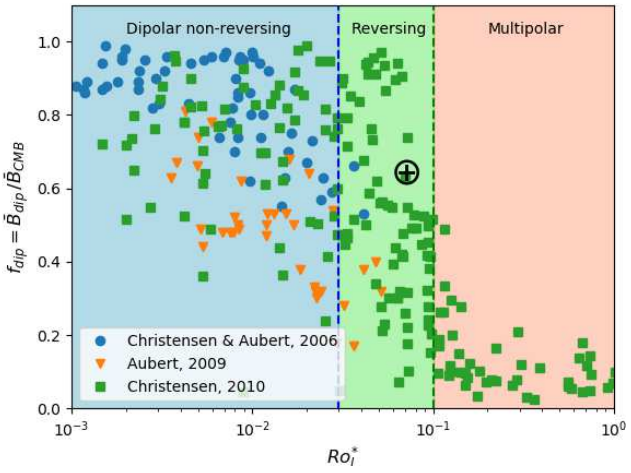

Figure 3. Values of f_{dip} for numerical dynamos. Data are from Christensen and Aubert (2006); Aubert et al. (2009), and Christensen (2011b) repectively. Colored regions corresponds to the different dynamo regimes. The value for the Earth is shown as $\oplus$ symbol

3.5 Dynamo Regimes

According to the energy spectrum of the field just in the *Core-Mantle Boundary* (CMB), dynamos can be classified into two groups: 1) Dipolar dynamos, in which the dipole component is larger than the others and 2) Multipolar dynamos that possess a flat multipolar spectrum or a weak dipole component. The dipolarity of the field f_{dip}, is measured by calculating the ratio of the intensity of the dipole in the CMB $\overline{B}_{dip}$, and the rms field strength $\overline{B}_{CMB}$, up to harmonic twelve,

$$f_{dip} = \frac{\overline{B}_{dip}}{\overline{B}_{CMB}}. \tag{34}$$

Dipolar dynamos have a dipole fraction $f_{dip} > 0.35$ (Aubert et al. 2009; Christensen 2010). If $f_{dip} \lesssim 0.35$, then the dynamo is classified as multipolar. Another quantity that can give us a measure of the dipolarity of the field is the ratio b_{dip} between the rms field strength B_{rms} inside the volume of the liquid layer, and the value of the dipole component just in the CMB,

$$b_{dip} = \frac{B_{rms}}{\overline{B}_{dip}}. \tag{35}$$

High values of b_{dip} usually involve multipolar fields, although in the numerical experiments have been found dipolar fields with high values of b_{dip}. On the contrary, small values of b_{dip} are only found in purely dipolar fields.

In the case of the Earth $f_{dip\oplus} \simeq 0.63$, $B_{dip\oplus} = 0.263$ mT and $B_{CMB\oplus} = 0.42$ mT (Olson 2007), which places our dynamo among the dipolar ones. The value of b_{dip} for the Earth is not known, but the value of B_{rms} can be estimated using, again, scaling laws. With the number of Elsasser, which relates the Lorentz forces with the Coriolis forces, a value of $B_{rms\oplus} \sim 4$ mT can be obtained (Roberts and Glatzmaier 2000; Olson 2007). From there $b_{dip\oplus} \sim 15$. Other models estimations made by Aubert et al. (2009) and Christensen (2010) have found $B_{rms} \sim 1.5$ mT and $b_{dip\oplus} \sim 5.0$.

Magnetic fields can be either, stable over time or, as in case of Earth, have reversals of polarity (Amit et al. 2010). In many cases the dipolar fields never present reversals and in other times fields that have reversals are multipolar. Sometimes the regimes overlap, showing fields that are dipole-reversible (Kutzner and Christensen 2002; Olson 2007).

Dipolarity and reversions define the field regime. Christensen and Aubert (2006) have discovered that the local Rossby number is a good indicator of the field regime (see figure 3). This has been checked by later works (Olson and Christensen 2006; Aubert et al. 2009; Driscoll and Olson 2009). Again, in the case of the Earth $\chi_\oplus \sim 0.35$ and $Ro^*_{l\oplus} \sim 0.07$. This places our geodynamo near the boundary between the dipole-reversible fields and multipolar.

The regimes are separated by borders that overlap and are limited by approximate values of Ro_l^*. Dipolar fields without reversals have $Ro_l^* < 0.04$. The transition between dipolar and multipolar fields is in the range $0.04 < Ro_l^* < 0.1$ and depends on convective processes. In this region, you can find all kinds of dynamos. Finally, the fields with $Ro_l^* > 0.1$ are clearly multipolar (see figure 3).

4 The thermal evolution

TEM for Earth-like planets have been developed for decades (Nimmo 2009). Specific TEM for SEs began to develop with the works by Papuc and Davies (2008); Gaidos et al. (2010); Tachinami et al. (2011); Driscoll and Olson (2011), and Stamenković et al. (2011). These TEMs predict that SEs can develop long-term PMF.

The thermal history of a planet determines the flux of heat from the interior, which provides the energy needed to generate and sustain the PMF. A large heat flux produces vigorous convection and a protective PMF. The intensity of the field is directly related to the heat that leaves the core and is transported through the mantle. For planets in which a solid inner core is formed, the growth of core and the cooling rate determine the heat flux. At the same time, the heat flux from the core depends on the capacity of the mantle to transport it out through conduction and convection processes (Breuer et al. 2010). The sources and amount of energy available to generate the field change with time as the planet cools. The intensity of the field depends essentially on the available convective energy Q_{conv} (Olson and Christensen 2006). The size of the convection region plays a key role in this.

Other TEMs for Earth and terrestrial planets, and for SEs, have been developed by Stevenson (2003); Labrosse (2003, 2007a); Papuc and Davies (2008); Nimmo (2009) and Breuer et al. (2010).

4.1 Core Thermal Evolution - CTE

GA10 used a TEM that we have called *Core Thermal Evolution* (CTE). In this TEM, a planet is composed by a homogeneous, fully convecting Mg/Fe–silicate mantle that surrounds a liquid/solid Fe core. They solved a third-order Birch–Murnagham EOS for each component:

$$P = \frac{3}{2}K_0(x^7 - x^5)\left[1 + \frac{3}{4}(4 - K_0')(1 - x^2)\right], \quad (36)$$

where, $x = (\rho/\rho_0)^{1/3}$, ρ_0 is density, K_0 is the bulk modulus and K_0' is its pressure-derivative at $P = 1$ bar respectively. The adiabatic temperature profile in the CTE is:

$$T(r) \approx T_c e^{[(R_c^2 - r^2)/d^2]}, \quad (37)$$

where d is a thermal length scale evaluated at the center of the planet:

$$d = \sqrt{\frac{3c_p}{2\pi\alpha_0\rho_0 G}}. \quad (38)$$

c_p and α_0 are the heat capacity and thermal expansivity of Fe in the surface, respectively. In CTE the density profile in the core is given by:

$$\rho(r) \approx \rho_c e^{[(R_c^2 - r^2)/L^2]}, \quad (39)$$

where L is a density scale length:

$$L = \sqrt{\frac{9K_0}{2\pi G\rho_0\rho_{cen}}\left(ln\frac{\rho_{cen}}{\rho_0} + 1\right)}. \quad (40)$$

The values for the Earth of these two scales are $d \sim 6400$ km and $L \sim 7400$ km respectively. These scales are weakly dependent on planet size, so the values are the same for SEs. On the other hand, if a inner core is growing, the temperature at the inner core boundary is the intercept between the adiabat and the iron melting point τ, then, the solidus profile is:

$$\tau(r) = \tau_0 e^{[-2(1-1/3y)(r/D)^2]}. \quad (41)$$

Here $y = L^2/d^2$ is the Grüneisen parameter.

Their dynamo predictions are sensitive to the properties of the core more than those of the mantle. In their model the Q_{conv} is obtained by solving the thermal equilibrium equations for both, the core and the mantle, and then the ohmic dissipation of the field is calculated from the balance between the sources of entropy (radioactive decay, secular cooling, sensible heat, latent heat and other sources of buoyancy), and the heat sinks (heat conduction, ohmic dissipation and other sources of dissipation) (Lister 2003; Labrosse 2003, 2007a; Nimmo 2009; Gaidos et al. 2010).

GA10 solves the equilibrium equations for entropy within the core. In CTE the condition for the maintenance of convective motions in the liquid core, needed for the dynamo activity and sustenance, can be expressed as a balance between sources and sinks of entropy in the core (see equation (25) for comparison):

$$\Phi + E_k = E_R + E_S + E_g + E_L. \quad (42)$$

Since the amount of radioactive elements in the core barely reaches a few tens of parts per million, GA10 disregards the radioactive source of entropy, and the final entropy balance is:

$$\Phi = E_S + E_g + E_L - E_k. \quad (43)$$

They calculate Φ, and dividing by the core mass M_c, they obtain $\phi = \Phi/M_c$, that is the entropy available per unit mass and time. From magnetic scaling laws, PMF intensity at the CMB is calculated in terms of the mean density of the core $\overline{\rho}$, the outer R_c and inner R_{ic} boundaries of the convecting zone (liquid core), and $p = \phi\overline{T}/[\Omega^3(R_c - R_{ic})^2]$ (see equation (28)), $\phi\overline{T}$ is the available convective

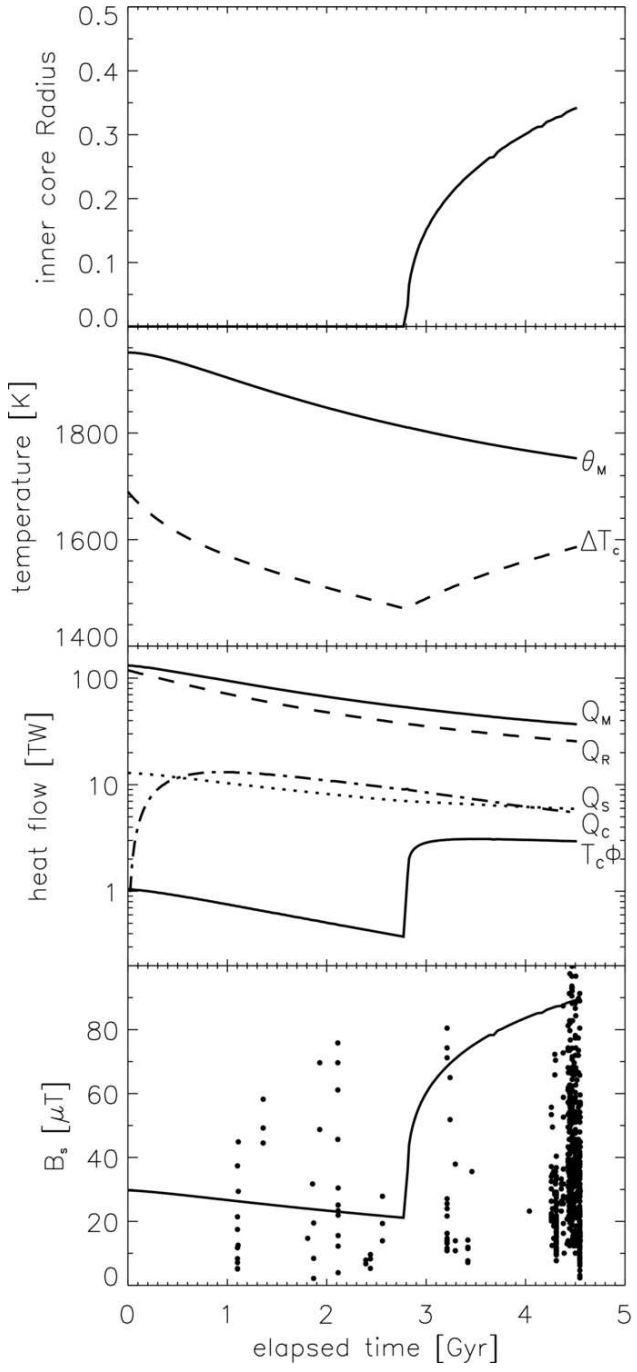

Figure 4. Evolution of the Geodynamo. Top to bottom: 1) Inner core to outer core ratio. 2) Mantle potential temperature θ_M (solid) and temperature contrast across the CMB Δ_{CMB} (dashed). 3) Total surface heat fluxes: Q_M (solid), Q_R (dashed), Q_S (dot-dashed), Q_{CMB} (dotted) and ΦT_c is the convective power Q_{conv}, available for the dynamo action (dash-triple-dotted). 4) Average surface magnetic field, the black dots are 606 measurements taken from the IAGA paleointensity database (Biggin et al. 2009) and three recent measurements in 3.45 Ga rocks form Herrero-Bervera and Valet (2009); Tarduno et al. (2010). (Figure from GA10, with permission of the author).

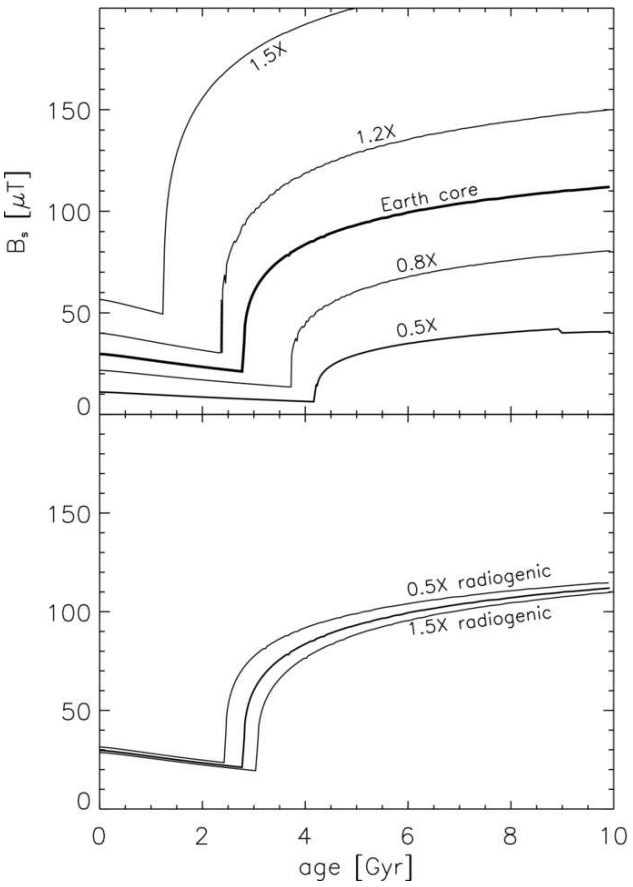

Figure 5. Evolution of the average surface PMF of Earth-like planets with plate tectonics and $T_s = 288$ K. Dynamos are assumed dipolar. Top: planets with core masses between 0.5 and 1.5 that of Earth. Bottom: planets with an Earth-size core but initial radiogenic element abundances that are 0.5 or 1.5 the terrestrial case (heavy solid line). (Figure from GA10, with permission of the author)

power per unit of mass and $\overline{T}$ is an effective dissipation temperature:

$$B_c = a_1\sqrt{\mu_0\overline{\rho}}\Omega(R_c - R_{ic})p^{b_1}. \quad (44)$$

a_1 and b_1 are dimensionless parameters. (Aubert et al. 2009) find that $a_1 \approx 1.65$ and $b_1 = 1/3$. This eliminates the dependence of the PMF on the rotation rate Ω:

$$B_c \approx a_1\sqrt{\mu_0\overline{\rho}}[\Omega^3(R_c - R_{ic})^2]. \quad (45)$$

On the other hand, the balance of heat sources in GA10, that corresponds to the heat that flows through the CMB, is expressed as:

$$Q_{CMB} = Q_S + Q_L + Q_g. \quad (46)$$

Recall that the terms of the right depend on the core cooling rate dT_c/dt. All this heat must be transported

through the mantle to the surface of the planet. Basically, this transport is given by conduction, although we know that there is convection in the subsolid material, which implies that the convection also helps to the extraction of heat.

CTE describes the thermal evolution of planets with masses between 1 and 4.8 $M_\oplus$, and assumes that the planets are rapid rotators. On the other hand, the model predicts the evolution of the PMF intensity based on the scaling laws (Christensen and Aubert 2006; Aubert et al. 2009; Christensen 2010). CTE combines the thermal properties of the core, the formation and the growth of a solid inner core, the properties of the mantle, the possible presence of tectonic plates and the temperature on the planet surface, to determine the emergence and sustaining a PMF.

An important result found by CTE is that only the planets with masses $\lesssim 2.0\, M_\oplus$ develop a protective PMF. Planets with larger masses were not cooled enough to form a solid inner core, that is fundamental for the support of the convective energy and therefore the PMF. SEs with masses $M \gtrsim 2.0 M_\oplus$ develop magnetic fields that decay and turn off.

4.2 Mantle Thermal Evolution - MTE

The TEM of TA11 aims to calculate the lifetime of the PMF in SEs. We have called this model the *Mantle Thermal Evolution* (MTE). The authors emphasize the fact that there are no observational data of internal thermal structures for SEs. Their model finds that the lifetime of the PMF depends on the planet mass and on the initial conditions and rheological properties. These conditions greatly affect the thermal evolution of the planet.

In order to reduce the uncertainties in the parameters, TA11 consider planets with a surface temperature T_s = 300 K and a mass ratio between the mantle and the core of 7/3, just like Earth. They consider also planets within the HZ in circular orbits, which prevents drastic changes in the T_s. Other rheological parameters are calibrated using known values for Earth.

For heat transport through the mantle, they use the *Mixing Length Theory* (MLT) modified for solid planets. This theory was developed by Ludwig Prandtl at the beginning of the twentieth century. This theory is adapted to the conditions of the convection in the mantle including the rheological properties. TA11 found that the PMF lifetime is shorter for SEs than for low mass planets. The mechanism that suppresses the dynamo in SEs is independent of that in GA10, suggesting that SEs may be magnetically inactive.

For the thermal evolution of the core, TA11 assume that each point inside the inner core maintains the temperature of solidification due to the low conductivity inside. The liquid core possesses, just like in GA10, an adiabatic profile of temperature, and a vigorous convection. The growth of the inner core and the temperature in the CMB depends on the energy sources within the solid and liquid cores. These sources of energy are given as functions of the flux of heat through the CMB.

According to their model, the initial distribution of temperature directly affects the lifetime of the PMF. For this reason, they calculate the profiles of temperature, both, for core and mantle. MTE calculates the hydrostatic stratification using equations (3) (see section 2) for pressure and mass of the planet, and a Vinet EOS dependent on pressure and independent of the evolution of temperature:

$$P = 3K_0 \frac{1-y}{y^2} e^{[\phi(1-y)]}, \tag{47}$$

where $\phi = 3/2(K_0' - 1)$ and $y = \rho_0/\rho$. The adiabatic temperature gradient in the outer core is given by:

$$\frac{\partial T}{\partial r} = \frac{\rho g y}{K_s} T, \tag{48}$$

where K_s is the bulk modulus of the liquid core. With the temperature profile, it is possible to calculate the radius of the inner core of the planet, according to the temperature of melting that depends on pressure and composition. Given a value for R_{ic}, MTE calculate the total energy budget of the core as the sum of gravitational, latent and thermal heats, all of them depending on r:

$$Q_g = -\int_0^{R_{ic}} 4\pi r^3 \rho_{ic}(r) g_{ic}(r) dr - \int_{R_{ic}}^{R_c} 4\pi r^3 \rho_c(r) g_c(r) dr, \tag{49}$$

$$Q_L = \mathcal{L} M_{ic}, \tag{50}$$

$$Q_{th} = \int_0^{R_c} 4\pi r^2 \rho(r) c_p(r) T(r) dr, \tag{51}$$

where $\mathcal{L}$ is the latent heat per unit of mass of the iron, $\mathcal{L} = 1.2 \times 10^6$ J kg^{-1}. It is clear that the model of heat flux in MTE is a simple one-dimensional flux in r.

TA11 put special attention on the role that the mantle plays in the process of core heat extraction. We have already said that MTE uses a MLT modified for solid planets, in order to calculate the energy transported by convection through the mantle and the energy in the CMB. The heat is transported through the mantle according to the transport equation:

$$\rho c_p \frac{\partial T}{\partial t} = \frac{1}{r^2} \frac{\partial}{\partial r} \left\{ r^2 k_c \left(\frac{\partial T}{\partial r} \right) \right. \tag{52}$$

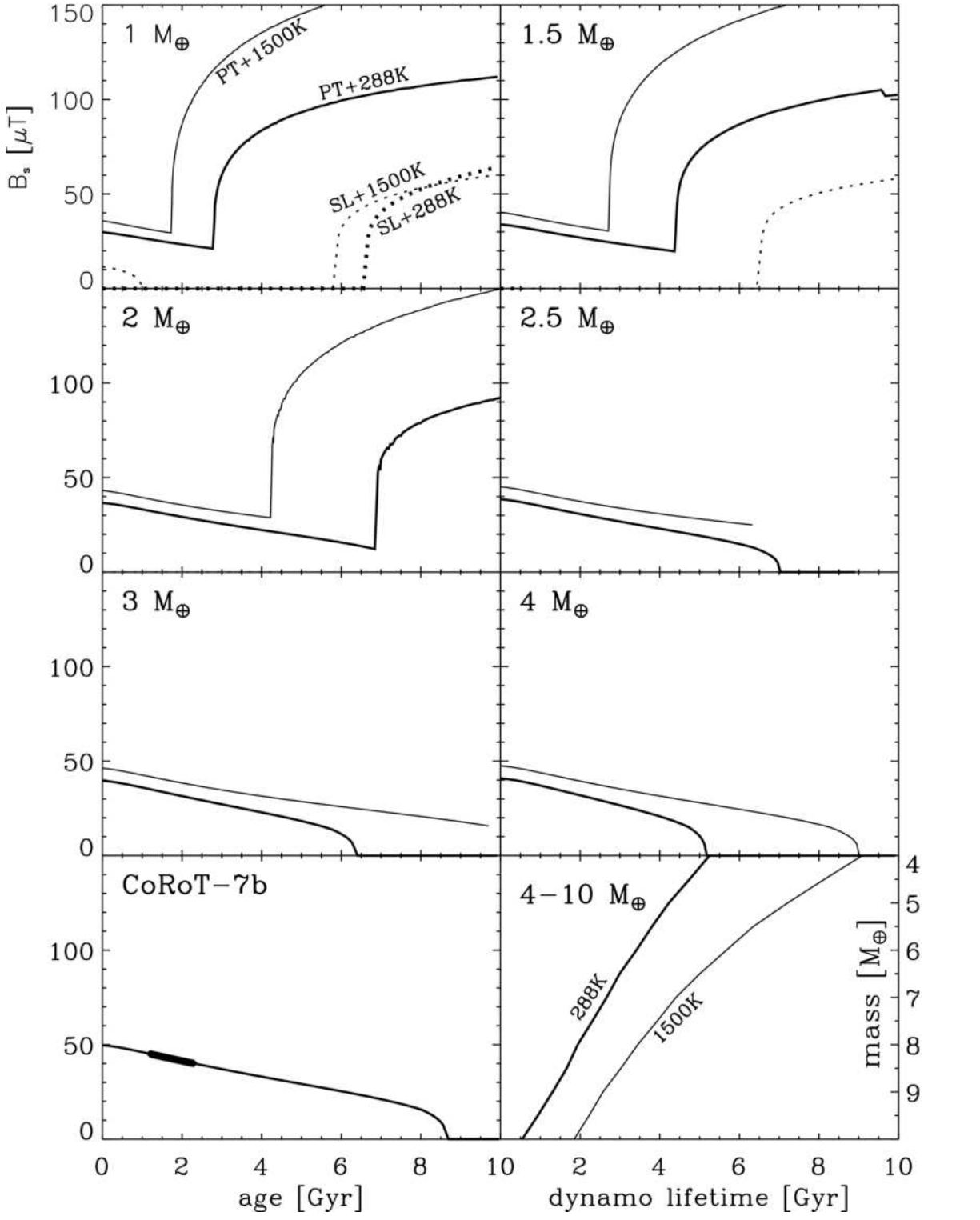

Figure 6. Evolution of the surface PMF of planets with masses of 1–10 $M_\oplus$ and the $\sim$ 4.8 $M_\oplus$ planet CoRoT-7b. Absence of a line indicates that the dynamo is inoperative. Dynamos are assumed dipolar. Heavy solid lines: Earth-like planets with plate tectonics and T_s = 288 K. Light solid lines: a hot Earth with plate tectonics and T_s = 1500 K. Light dashed lines: Venus-like planets with stagnant lid, 10 times the Earth's mantle viscosity, and T_s = 1500 K. Heavy dashed lines: a balmy Venus with T_s = 288 K. For the case of CoRoT-7b, T_s $\approx$ 1810 K, assuming efficient redistribution of heat (Léger et al. 2009). The thick part of the CoRoT-7 curve spans the range of the system's estimated age (1.1 to 2.3 Gyr). The bottom right-hand panel is the evolution of dynamos as a function of mass > 4 $M_\oplus$ and the two values of the surface temperature.(Figure from GA10, with permission of the author)

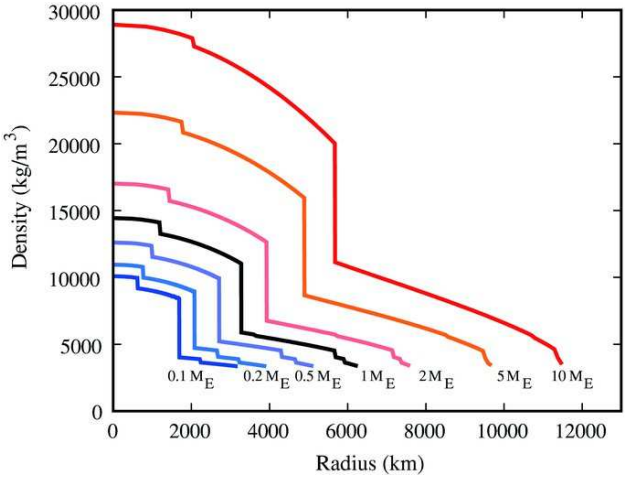

Figure 7. Radial density profiles for 0.1, 0.2, 0.5, 1, 2, 5, and 10 $M_\oplus$ planets (inner core is 6% mass of the complete core). Profiles obtained with MTE in the nominal case.(Figure from TA11, with permission of the author)

$$+ r^2 k_v \left[\left(\frac{\partial T}{\partial r} \right) - \left(\frac{\partial T}{\partial r} \right)_s \right] \Big\} + \rho Q_R .$$

k_c and k_v are thermal diffusion coefficients, for conductivity and convection respectively, $(\partial T/\partial r)_s$ is the adiabatic temperature gradient, and the terms inside the brackets are conductive and convective fluxes respectively. Likewise, the model takes into account the production of heat in the mantle by means of the radioactive decay of elements like K, Th, and U, and assume that the SEs have an abundance equal to the Earth's.

An important aspect of the MTE is the mantle's viscosity since it determines the efficiency in the heat transport through the mantle. This is one of the least known parameters of the rheological properties of the planetary interior. TA11 adopt an Arrhenius-type formulation in which the viscosity depends on pressure and temperature:

$$\eta(P, T) = \frac{1}{2} \left[\frac{1}{B^{1/n}} exp \left(\frac{E^* + PV^*}{nRT} \right) \right] \dot{\epsilon}^{(1-n)/n}, \qquad (53)$$

where R, $\dot{\epsilon}$, n, B, and E^* are the universal gas constant, the strain rate, the creep index, the Barger coefficient and the activation energy respectively. One of the main parameters in MTE is the activation volume of the mantle V^*, that determines the dependence of the viscosity on pressure. In the mantle, this can be increased by orders of magnitude as the planetary mass increases. The gravitational heat is released by thermal contraction. MTE assumed this as an increase in the specific heat of the core. A temperature contrast between the CMB and the first convective layer of the mantle is chosen $\Delta T_{CMB} = 1000$ K. This reproduces the Earth's present condition.

Finally, MTE define the lifetime of the PMF as a parameter that depends on a critical heat flux necessary for the dynamo action:

$$Q_{crit} = k_c \left(\frac{\partial T_{CMB}}{\partial r} \right)_s = k_c \frac{\rho g y G}{K_s} T_{CMB}. \qquad (54)$$

The lifetime of the PMF is the period during which the flux of heat from the core is higher than Q_{crit}. Q_{conv} is estimated by solving the transport equations for the core and the mantle. The difference between the total heat coming out through the CMB and the amount of energy transported by conduction is calculated. After solving the thermal transport equations, MTE calculates the heat flux through the CMB, Q_{CMB}, the heat conducted through the CMB adiabat, Q_{cond}, and the radius of the solid inner core R_{ic} as a function of time. In order to predict the intensity of the PMF and its duration, the convective heat is:

$$Q_{conv} = (Q_{CMB} - Q_{cond}) \times 4\pi R_c^2 \qquad (55)$$

The MTE is applied to planets with masses between 0.1 and 10 $M_\oplus$ which have a mass ratio between the core and the mantle similar to that of the Earth and are rapid rotators with dipolar PMF. There are a couple of important results from MTE:

1. The thermal evolution of the planet is strongly linked to the viscosity of the mantle, which in turn depends on pressure and temperature.
2. The intensity and duration of the PMF in this model depends on the initial temperature profile characterized by ΔT_{CMB}.

The temperature difference between the CMB and the lower mantle is determined from the beginning of the history of the planet by the processes of accretion and differentiation. If from the beginning there are very high values of ΔT_{CMB}, this will favor the emergence of an intense and long-lived PMF. For example, if ΔT_{CMB} varies from 1000 K to 2000 K, this difference increases the duration of the dynamo up to an order of magnitude for massive planets with $M > 2\ M_\oplus$.

Both models, CTE and MTE give us the first description of the PMF generated by a dynamo for Earth-like extrasolar planets. The results of CTE and MTE point more or less in the same direction: SEs with masses $\lesssim 2.0 M_\oplus$ seem to have the best possibilities of developing long-term and sustainable PMFs. This is one of the most important predictions arising from both models. MTE finds an important effect in the thermal evolution related to the dependence of the viscosity on the pressure as well as temperature, that limits the mantle's ability to extract the heat from the core. This is especially important for massive planets.

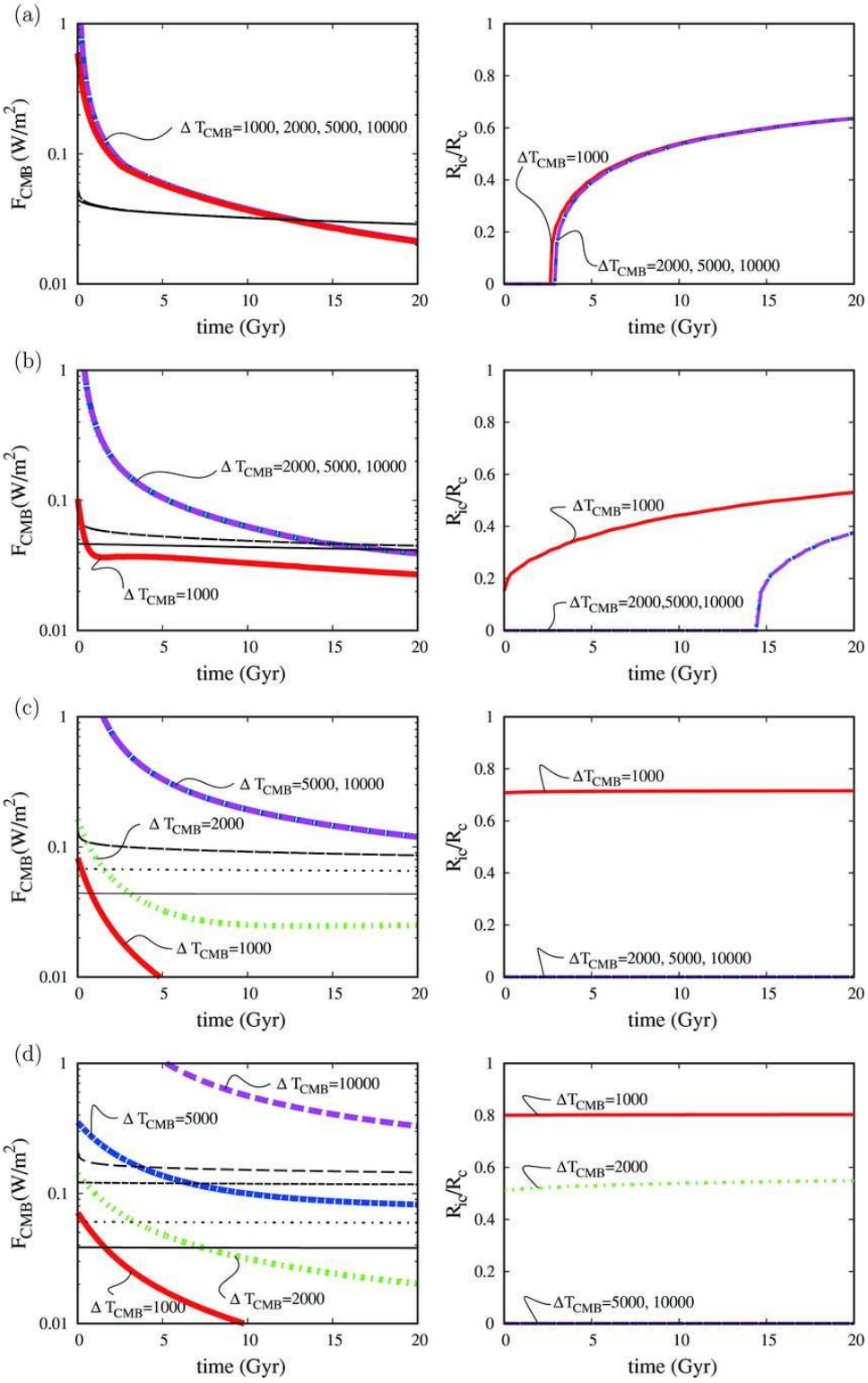

Figure 8. Evolution of the Q_{CMB} (left column) and R_{ic} (right column) for M = (a) 1, (b) 2, (c) 5, and (d) 10 $M_{\oplus}$ with different initial Δ_{CMB}. Left column: critical flux of heat for each Δ_{CMB} is expressed by a thinner line of the same type. Some lines with different initial Δ_{CMB} are overlapped by each other. For these parameters, the initial conditions do not affect the evolution because self-regulation of mantle heat transfer works due to temperature dependence of mantle viscosity. Inner cores never nucleate in the cases of Δ_{CMB} = 2000, 5000, and 10,000 K for M_p = 5 $M_{\oplus}$ and Δ_{CMB} = 5000 and 10,000 K for M_p = 10 $M_{\oplus}$. (Figure from TA11, with permission of the author)

Both models use planets with unspecified but low rotation periods, in the dipole regime. Both predict that the density of magnetic energy and therefore the intensity of the field do not depend heavily on rotation. We will see that the rotation of the planet can be important when it comes to determining the field regime (see section 5), especially in the case of SEs that may be tidally locked.

In table 2 can be seen different configurations for CTE and MTE. There, SEs within HZ were analyzed that have surface temperatures of 288 K in CTE and 300 K in MTE respectively, and that possess intense long-lived PMF. In the case of CTE, the possibility of having tectonic plates is included. The models must fit the values of the Earth for planets with masses of 1 $M_\oplus$ and must be consistent with terrestrial thermal evolution. The time of appearance of the Earth's inner core must be accurately calculated.

4.3 Reference Thermal Evolution - RTE

ZU13 developed the *Reference Thermal Evolution Model* (RTE), by combining the heat transport of the core and the mantle. In this way is possible to have a more complete idea of a planet's magnetic evolution. As commonly accepted, ZU13 assumes that the main source of the PMF is the action of a convective dynamo within the liquid core (Stevenson 1983, 2003).

RTE implements different characteristics compared with earlier works. The most important is a novel treatment of mantle rheology. In this model new parameters are used to describe viscosity. In addition, the density and temperature profiles in the mantle are treated as for the core, avoiding the isothermal approximation. RTE assigns initial values to the temperature of the lower mantle and core, which are among the most uncertain parameters in the TEM, but uses a unified method to assign initial temperatures to planets with different masses. Other models assigned these temperatures arbitrarily (Papuc and Davies 2008), or as free parameters [TA11].

An acceptable TEM must correctly predict six fundamental properties of the PMF: 1) The total convective energy Q_{conv}, 2) the convective heat flux $q_{conv} = Q_{conv}/4\pi R_c^2$, both, 1) and 2) are necessary for the operation and amplification of the PMF, 3) the radius of the solid inner core R_{ic}, 4) the thickness of the convective layer $D \approx R_c - R_{ic}$, 5) the time in which the inner core appears t_{ic}; and 6) the total lifetime of the dynamo t_{dyn}.

In order to know these quantities, RTE solve the energy and entropy balance equations that describe the heat flux in both, core and mantle. A detailed description of the physics on which the RTE is based can be found in the following works: Schubert et al. (1979); Stevenson (1983); Nimmo and Stevenson (2000); Labrosse et al. (2001); Labrosse (2003); Gubbins et al. (2003, 2004); Aubert et al. (2009); Gaidos et al. (2010), and Stamenković et al. (2011).

RTE assumes the internal structure of the planet proposed by Valencia et al. (2006), as composed of two well-differentiated layers, chemically and mineralogically homogeneous: A mantle of rock made mainly by olivine and perovskite and a core of Fe+Alloy. The mechanical conditions inside the planet, *i.e.* Pressure P, density ρ and gravitational field g, are calculated by solving Adams-Williamson's continuity equations, in addition to the equations of hydrostatic equilibrium (3).

RTE assumes boundary conditions for all masses: $\rho(r = R_p) = 4000$ kg m^{-3} and $P(r = R_p) = 0$ Pa. The model makes use of an integrator RK4 and calculates consistently both, the core radius R_c, and the radius of the planet R_p. RTE uses the Vinet equation of state since this predicts better the dependence of compressibility for the typical pressures of the interiors of the SEs, *i.e.* 100 – 1000 GPa for $M_p = 1 - 10 M_\oplus$ (Valencia et al. 2006; Tachinami et al. 2011). The model ignores thermal corrections for adiabatic compressibility *i.e.* $K_S(\rho, T) \approx K_S(\rho, 300\text{ K}) + \Delta K_s(T)$ (Valencia et al. 2006), as well as first-order temperature effects on the mechanical structure of the interior. However, it does take into account effects produced by the phase change within the core and mantle.

From the initial mantle temperature profile, RTE calculates where the transition from olivine to perovskite occurs using a linear function of pressure and temperature: $T = 400P - 4287$ (Valencia et al. 2007b). This border between layers is assumed constant throughout the entire evolution of the planet.

The thermal profile is used at each step of the integration to calculate the instantaneous radius of the solid core. In the phase transition, it is assumed that the density of iron changes as $\Delta\rho = (\rho_s - \rho_l)/\rho_l$, ρ_s (solid) and ρ_l (liquid), are computed using the Vinet equation. $\Delta\rho$ is assumed to be equal at all points within the solid core. Table 3 summarizes the values of the physical parameters used by RTE.

4.3.1 Core Thermal Evolution in RTE

In order to calculate the thermal evolution of the core, the energy and entropy balance equations must be solved (Labrosse et al. 2001; Nimmo 2009):

$$Q_{CMB} = Q_S + f_{ic}(Q_g + Q_L). \tag{56}$$

$$\Phi = E_S + f_{ic}(E_g + E_L) - E_k. \tag{57}$$

Table 2. Summary of results for the evolution of PMF for CTE (GA10) and MTE (TA11). For every mass and each pair of independent planetary properties (tectonics and surface temperature, T_s in CTE, activation volume, V^* and temperature contrast at CMB, ΔT_{CMB} in MTE), there is the value of three properties of the dynamo and the predicted PMF: t_{ic} (Gyr) is the time for the starting of the inner core nucleation, $B_s(t_o)$ (μT) are surface magnetic field at a reference time taken as the present age of the Earth, 4.54 Gyr and t_{dyn} (Gyr) is the lifetime of the dynamo. In the CTE stagnant lid (SL), as opposed to plate tectonics (PT) configurations, are not able to produce a dynamo for masses larger than 1.5 $M_\oplus$ and are not included in the Table

CTE model (t_{ic},B_s,t_{dyn})			
M ($M_\oplus$)	Tectonics	T_s	
		288K	1500K
$1M_\oplus$	PT	2.8, 90, >10	1.7,140,>10
	SL	6.5, 0, >10	5.9, 0, >10
$1.5M_\oplus$	PT	4.4, 20, >10	2.7, 130, >10
	SL	–	6.5, 0, >10
$2M_\oplus$	PT	6.8, 20, >10	4.2, 90, >10
$2.5M_\oplus$	PT	>10, 20, 7	>10, 30, 6.4
$3.0M_\oplus$	PT	>10, 20, 6.5	>10, 30, 10
$4.0M_\oplus$	PT	>10, 20, 5.2	>10, 30, 9

MTE model(t_{ic},B_s,t_{dyn})					
$M(M_\oplus)$	V^*	ΔT_{CMB}			
		1000K	2000K	5000K	10000K
$1.0M_\oplus$	3 m^3 mol^{-1}	4, 80, >20	6.5, 110, >20	7.5, 130, >20	7.5, 130, >20
	10 m^3 mol^{-1}	2.7, 80, 10	2.8, 80, 10	2.8, 80, 10	2.8, 80, 10
$2.0M_\oplus$	3 m^3 mol^{-1}	0, 90, >20	7, 120, >20	8, 140, >20	8, 140, >20
	10 m^3 mol^{-1}	0, 0, 0.5	14, 100, >20	14, 100, >20	14, 100, >20
$5.0M_\oplus$	3 m^3 mol^{-1}	0, 0, 1	7.5, 130, >20	11, 160, >20	11, 160, >20
	10 m^3 mol^{-1}	0, 0, >20	>20, 0, >20	>20, 150, >20	>20, 150, >20

In RTE the contributions due to radioactive decay and pressure are negligible inside the core (Nimmo 2009). The components of gravitational redistribution and latent heat only exist in the case of a solid core are formed. If this happens, RTE uses a factor $f_{ic} = 1$ that becomes effective whenever the core starts its process of solidification, other way $f_{ic} = 0$.

Energy and entropy balances are functions of the temperature profile: $\partial T(r,t)/\partial t$. The heat related to the release of light elements depends on the growth of the inner core (Gubbins et al. 2004). The radial and temporal dependence of temperature must be decoupled: $T(r,t) = f_c(r)T_c(t)$, where $T_c(t)$ is the time-dependent temperature at R_c. When these dependencies decouple, equation (56) becomes a first order differential equation:

$$Q_{CMB} = M_c[C_S + f_{ic}(C_g + C_L)]\frac{dT_c}{dt}. \tag{58}$$

M_c is the mass of the core, C_S, C_g and C_L are the *bulk heat capacities* expressed as volumetric integrals, which include the radial dependence of temperature $f_c(r)$:

$$C_S = -\frac{1}{M_c}\int \rho c_p dV \tag{59a}$$

$$C_g = \frac{1}{M_c}\int \rho\psi\alpha_c C_c C_R dV \tag{59b}$$

$$C_L = -\frac{C_c}{c}\frac{L_H}{(dT_m/dP - dT/dP)\rho g T_c}. \tag{59c}$$

Both, core and mantle have adiabatic profiles of the temperature (see equation (48)):

$$\frac{dT(r)}{dr} = \frac{\rho(r)g(r)T(r)}{K_s(r)}y(r), \tag{60}$$

If an exponential adjustment is used for the density of the core (Labrosse et al. 2001), then the adiabatic temperature profile is approximately:

$$T(r,t) = T_c(t)\exp\left(\frac{R_c^2 - r^2}{\mathcal{D}^2}\right), \tag{61}$$

where $\mathcal{D} = \sqrt{3c_p/2\pi\alpha\rho_{cen}G}$ is the adiabatic height, α is the thermal expansivity that is assumed constant, and ρ_{cen} is the density at the center of the planet. It can be seen that $T_c(t) = T(r = R_c, t)$.

If this parameterization is used, the secular bulk heat capacity $C_S \equiv Q_S/(M_c\ dT_c/dt)$ is:

$$C_S = -4\pi\int_0^{R_c}\rho(r)c_p\exp\left(\frac{R_c^2 - r^2}{\mathcal{D}^2}\right)r^2 dr. \tag{62}$$

Similar expressions can be found for C_g and C_L from heats Q_g and Q_L (Gubbins et al. 2004) and using the caloric capacities (59a...c).

Table 3. Interior structure and thermal evolution model parameters

Parameter	Definition	Value	Reference
		Bulk	
CMF	Core mass fraction	0.325	–
T_s	Surface temperature	290 K	–
P_s	Surface pressure	0 bar	–
		Inner core	
–	Material	Fe	(Valencia et al. 2006)
ρ_0, K_0, K_0', γ_0, q, θ_0	Equation of state parameters	8300 kg m^{-3}, 160.2 GPa, 5.82, 1.36, 0.91, 998 K	(Valencia et al. 2006)
k_c	Thermal conductivity	40 W m^{-1} K^{-1}	(Nimmo 2009)
ΔS	Entropy of fusion	118 j kg^{-1}K^{-1}	GA10
		Outer core	
–	Material	$Fe_{(0,8)}FeS_{(0,2)}$	(Valencia et al. 2006)
ρ_0, K_0, K_0', γ_0, q, θ_0	Equation of state parameters	7171 kg m^{-3}, 150.2 GPa, 5.675, 1.36, 0.91, 998 K	(Valencia et al. 2006)
α	Thermal expansivity	1.4 ×10^{-6} K^{-1}	TA11
c_p	Specific heat	850 j kg^{-1} K^{-1}	GA10
k_c	Thermal conductivity	40 W m^{-1} K^{-1}	(Nimmo 2009)
κ_c	Thermal diffusivity	6.5 × 10^{-6} m^2 s^{-1}	(Ricard 2009)
ΔS	Entropy of fusion	118 j kg^{-1} K^{-1}	GA10
ϵ_{ad}	Adiabatic factor for $T_c(t = 0)$	0.71	–
ξ_c	Weight of T_c in core viscosity	0.4	–
		Lower mantle	
–	Material	perovskita+fmw	(Valencia et al. 2006)
ρ_0, K_0, K_0', γ_0, q, θ_0	Equation of state parameters	4152 kg m^{-3}, 223.6 GPa, 4.274, 1.48, 1.4, 1070 K	(Valencia et al. 2006)
d, m, A, b, D_0, m_{mol}	Viscosity parameters	1×10^{-3} m, 2, 13.3, 12.33, 2.7×10^{-10} m^2 s^{-1}, 0.10039 kg mol^{-1}	(Stamenković et al. 2011)
α	Thermal expansivity	2.4 ×10^{-6}K^{-1}	TA11
c_p	Specific heat	1250 j kg^{-1} K^{-1}	GA10
k_m	Thermal conductivity	6 W m^{-1} K^{-1}	GA10
κ_m	Thermal diffusivity	7.5 × 10^{-7} m^{2}s^{-1}	(Ricard 2009)
ΔS	Entropy of fusion	130 j kg^{-1} K^{-1}	GA10
		Upper mantle	
–	Material	olivine	(Valencia et al. 2006)
ρ_0, K_0, K_0', γ_0, q, θ_0	Equation of state parameters	3347 kg m^{-3}, 126.8 GPa, 4.274, 0.99, 2.1, 809 K	(Valencia et al. 2006)
B, n, E^*, $\dot{\epsilon}$	Viscosity parameters	3.5 × 10^{-15} Pa^{-n}s^{-1}, 3, 430×10^3 j mol^{-1}, 1 × 10^{-15} s^{-1}	TA11
V^*	Activation volume	2.5 ×10^{-6} m^3 mol^{-1}	(Stamenković et al. 2011)
α	Thermal expansivity	3.6 ×10^{-6} K^{-1}	TA11
c_p	Specific heat	1250 j kg^{-1} K^{-1}	GA10
k_m	Thermal conductivity	6 W m^{-1} K^{-1}	GA10
κ_m	Thermal diffusivity	7.5 × 10^{-7} m^2 s^{-1}	(Ricard 2009)
θ	Potential temperature	1700 K	(Stamenković et al. 2011)
χ_R	Radiactive heat correction	1.253	–

Table 4. Symbols and quantities.

Symbol	Meaning	Notes
	Acronyms	
CMB	Core Mantle Boundary	
PMF	Planetary Magnetic Field	Surface magnetic field
$CoMF$	Core Magnetic Field	
CTE	Core Thermal Evolution Model	GA10
MTE	Mantle Thermal Evolution Model	TA11
RTE	Reference Thermal Evolution Model	ZU13
HZ	habitable zone	(Kasting et al. 1993)
	Planetary Properties	
R_p	Planetary radius, $R_p = 6371(M/M_\oplus)^{0.265}$	km, (Valencia et al. 2006)
R_c	Radius of the core, $R_c = 3480(M/M_\oplus)^{0.243}$	km, (Valencia et al. 2006)
$\overline{\rho}_c$	Average core density, $\overline{\rho}_c = 1.1 \times 10^4 (M/M_\oplus)^{0.271}$	kg m^{-3}, (Valencia et al. 2006)
Ω, T	Rotation rate, period of rotation, $T = 2\pi/\Omega$	rad s^{-1}, days
R_{ic}, χ	Radius of the solid inner core, $\chi = R_{ic}/R_c$	km
D	Vertical height of the liquid core, $D = R_c - R_{ic}$	km
V	Volume of the dynamo region, $V = 4/3\pi(R_c^3 - R_{ic}^3)$	km^3
	Dynamo Properties	
Q_{conv}	Total convective power	Ws^{-1}
p	Total convective power density	Adimensional
Lo	Lorentz number, $Lo \sim < E_{mag} >^{1/2}$	Adim., (Christensen and Aubert 2006)
Ro	Rossby number, $Ro \sim < E_{kin} >^{1/2}$	Adim., (Christensen and Aubert 2006)
Ro_l	Local Rossby number, $Ro_l \sim < l_u >< E_{kin} >^{1/2}$	Adim., (Christensen and Aubert 2006)
f_{ohm}	Fraction of ohmic dissipation	Adim., (Christensen and Aubert 2006)
	Magnetic Field Properties	
B_{rms}	rms amplitude of the magnetic field inside the convecting shell	μT
$\overline{B}_{dip}$	Dipolar component intensity of the core magnetic field	μT
$\overline{B}_{s,dip}$	Dipolar component of the PMF, $\overline{B}_{s,dip} = \overline{B}_{dip}(R_c/R_p)^3$	μT
f_{dip}	Dipolar fraction of the core magnetic field, $f_{dip} = \overline{B}_{dip}/\overline{B}_{CMB}$	Adim., (Christensen and Aubert 2006)
b_{dip}	Ratio between the rms strength of the field and the dipolar component at the CMB, $b_{dip} = B_{rms}/\overline{B}_{dip}$	Adim., (Christensen et al. 2009)
t_{ic}	Starting time for the inner core nucleation	Gyr
t_{dip}	Dipolar lifetime	Gyr
t_{sw}	Dipolarity switch time	Gyr
t_{dyn}	Dynamo lifetime	Gyr

The total heat released by the core that flux through the CMB is obtained using the boundary layer theory (Stevenson 1983). Q_{CMB} is given by (Ricard 2009):

$$Q_{CMB} = 4\pi R_c k_{lm} \Delta T_{CMB} Nu_c, \tag{63}$$

where k_{lm} is the thermal conductivity of the lower mantle, $\Delta T_{CMB} = T_c - T_{lm}$ is the temperature difference just in the CMB, T_{lm} is the temperature of the lower mantle and $\mathrm{Nu}_c \approx (\mathrm{Ra}_c/\mathrm{Ra}_\star)^{1/3}$ is the Nusselt number for the core (Schubert et al. 2001). RTE assumes a critical Rayleigh number $\mathrm{Ra}_\star \approx 1000$. The Rayleigh local number Ra_c in the CMB is calculated assuming that the heat comes from below (Ricard 2009),

$$\mathrm{Ra}_c = \frac{\rho\, g\, \alpha\, \Delta T_{CMB} (R_p - R_c)^3}{\kappa_c \eta_c}, \tag{64}$$

where g is the gravitational field, κ_c is the thermal diffusivity and η_c is the dynamic viscosity, all averaged within the liquid core.

In order to calculate the average viscosity in the liquid layer, RTE uses the pressure in the CMB and weighted average temperature (average value between the temperature of the core and the temperature of the lower mantle):

$$T_{\eta c} = \xi_c T_c + (1 - \xi_c) T_{lm}, \tag{65}$$

where $\xi_c \simeq 0.4$ is a parameter that reproduces the values for the Earth.

Now, for the formation and growth of the inner core, the temperature profile must be compared with the solidification temperature of the iron at each step. Lindemann's law is used to calculate the temperature of the solidus for Fe+Alloy (Labrosse et al. 2001):

$$\frac{\partial \log \tau}{\partial \log \rho} = 2[y - \delta(\rho)], \tag{66}$$

where $\delta(\rho) \approx 1/3$ and τ is the temperature of solidification. To integrate this equation, RTE used the density profile and take values of density, $\rho_0 = 8300 \text{kg/m}^3$ for pure iron, and temperature $\tau_0 = 1808$ K. Temperature at the center $T(r = 0, t)$, and the solidus $\tau(r = 0)$, are compared step by step. When $T(0, t_{ic}) \approx \tau(0)$, t_{ic}, solidification initiates, and the inner core appears. Then sources of latent heat and light elements release are turned on (see equations (56) and (57)) and the integration is continued.

The radius of the inner core at any time $t > t_{ic}$, is calculated by solving the following equation (Nimmo 2009; Gaidos et al. 2010),

$$\frac{dR_{ic}}{dt} = -\frac{\mathcal{D}^2}{2R_{ic}(\Delta - 1)} \frac{1}{T_c} \frac{dT_c}{dt}, \tag{67}$$

where Δ gives the relative slopes of the solidus and adiabat measured in R_{ic} (see equation (7) in Nimmo (2009)). When the material cools below a certain temperature, the outer layers of the core begin to stratify. This effect can be introduced in the calculation by correcting the radius and temperature of the core at each step. When stratification begins, the actual radius of the core is reduced and the temperature on its surface increases (GA10). Stratification of the core reduces the thickness of the convective layer and intensifies the PMF.

Recall that the calculation of the properties of the PMF requires to know the available convective heat Q_{conv},

$$Q_{conv} \approx \Phi T_c. \tag{68}$$

When Q_{conv} becomes negative, convection can not transport sufficient energy through the liquid core and the dynamo turns off. At this point, the integration is completed and we obtain the lifetime of the dynamo t_{dyn}.

4.3.2 Mantle Thermal Evolution in RTE

The balance of energy within the mantle can be expressed as:

$$Q_m = \chi_R Q_{Rm} + Q_{Sm} + Q_{CMB}. \tag{69}$$

Q_m is the total heat transferred through the mantle outside the planet, Q_{Rm} is the heat released by the radioactive decay inside the mantle and Q_{Sm} is the secular heat due to cooling of the interior layers in the mantle. The radioactive heat is calculated using the expressions and parameters proposed by (Kite et al. 2009). Due to the inhomogeneity of the distribution of radioactive elements in the mantle, RTE introduce a factor $\chi_R = 1.253$ that fits the values for the Earth and the same value is assumed for SEs.

Secular heat is calculated using equation (11). As in the case of the core, the radial $f_m(r)$ and temporal $T_m(t)$ dependence of the temperature are separated to facilitate the integration of the energy equation. It is assumed that the radial temperature profile does not change during the thermal evolution of the planet. Inside the mantle $T(r, t) = T_m(t) f_m(r)$. Here, $T_m(t) = T(r = R_p, t)$ is the temperature of the upper mantle, just below the surface of the planet (see figure 9). RTE assumes an adiabatic temperature gradient across the convective mantle and an exponential adjustment for density. The scale of height of mantle temperature D_m, related to the density height scale L_m as $D_m^2 = L_m^2/y$ (Labrosse 2003), is obtained by fitting the density profile:

$$f_m(r) = \exp\left(\frac{R_p^2 - r^2}{D_m^2}\right), \tag{70}$$

RTE takes values of the density at the borders of the mantle and estimates analytically the value of L_m and D_m. The energy balance is completed when you get Q_m on the surface of the planet as a function of T_m.

The presence or absence of tectonic plates can play an important role in the efficiency of heat flow through the mantle. For mobile plates, RTE assumes that the upper mantle layer is completely convective and uses the boundary layer theory to calculate Q_m for the case where Mobile Lids (ML) are present,

$$Q_m^{LM} = \frac{4\pi R_p^2 k_m \Delta T_m \text{Nu}_m}{R_p - R_c}, \tag{71}$$

here $\Delta T_m = T_m - T_s$ is the temperature difference across of the surface frontier of the planet (SB) and T_s is the surface temperature which is assumed to be $T_s = 290$ K.

Neither, the internal structure and the thermal evolution, are sensitive to the value of surface temperature, in fact, the properties are basically the same for a temperature range between 250-370 K.

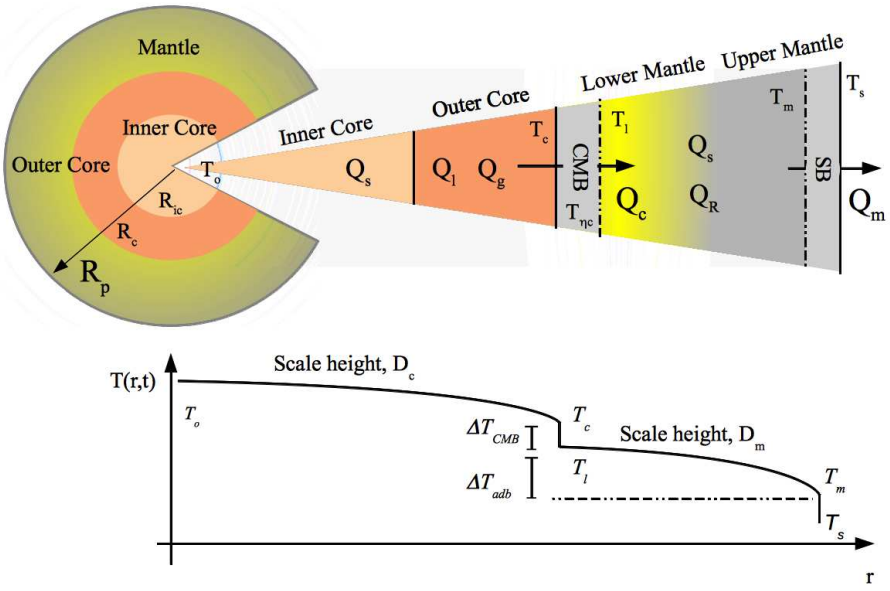

Figure 9. Schematic representation of the planetary interior. The temperature profile depicted below the slice does not use real data. Distances and sizes are not to scale. (Figure from ZU13, with permission of the editor)

In the case of mobile plates the Nusselt number for the mantle Nu_m, defined as the average heat flux at the top of the lid normalized to the conductive heat flux across the layer, is also related to the Rayleigh number. RTE calculates Rayleigh's local number assuming that the mantle material is heated from inside [GA10],

$$\mathrm{Ra}_m = \frac{\alpha g \rho^2 H (R_p - R_c)^5}{k_m \kappa_m \eta_m}, \tag{72}$$

where $H = (Q_R + Q_{CMB})/M_m$ is the heat density within the mantle, k_m is the thermal conductivity, κ_m is the diffusivity and η_m is the viscosity of the upper mantle. When no moving plates are present (Stagnant Lids, SL), the SB becomes a rigid boundary for heat flux (Nimmo and Stevenson 2000) and the heat can be approximated as:

$$Q_m^{SL} = 4\pi R_p^2 \frac{k_m}{2} \left(\frac{\rho g \alpha}{\kappa_m \eta_m} \right)^{1/3} \Gamma^{-4/3}, \tag{73}$$

$$\Gamma \equiv \frac{-d(ln\ \eta_m)}{dT_m}. \tag{74}$$

Since Q_m is estimated independently, the energy balance for the mantle can be described as an ordinary differential equation that depends on T_m,

$$Q_m = \chi_R Q_R + Q_{CMB} + C_m \frac{dT_m}{dt}, \tag{75}$$

where C_m is the heat capacity of the upper mantle, obtained from an expression equal to the equation (62).

4.3.3 Initial Conditions in RTE

By solving equations (58), (67) and (75), this implies defining some initial conditions. The temperature of the upper mantle, $T_m(t = 0)$ (Stamenković et al. 2011) is found by integrating the adiabatic equation up to an average pressure inside the mantle $\langle P_m \rangle$,

$$T_m(t = 0) = \theta \exp \left(\int_0^{\langle P_m \rangle} \frac{y_0}{K_s(P')} dP' \right). \tag{76}$$

$\theta = 1700$ K is the potential temperature, assumed equal for all planetary masses. The initial value of the core's temperature $T_c(t = 0)$, is one of the most uncertain parameters in TEM since it depends on the history of the formation of the planet. Some assume that the initial temperature is the same order of the melting temperature of silicates in the lower mantle. More complex models (Papuc and Davies 2008) suppose a dependence of mass for $T_c(t = 0)$.

The difference of temperature through the CMB can be assumed of the same order of the difference between lower and upper mantles, ΔT_{adb}, since the heat released by the core through a temperature gradient ΔT_{CMB} is then carried by the mantle with a gradient ΔT_{adb}. For the case of the Earth,

$$T_c(t = 0) = T_{lm} + \epsilon_{adb} \Delta T_{adb}, \tag{77}$$

where $\epsilon_{adb} = 0.7$ is a free parameter. In these conditions $T_c(t = 0)$ is close to the melting temperature of the perovskite at the pressure of the CMB.

4.3.4 Rheological Model

The greatest source of uncertainty in TEMs is the value of the rheological properties of silicates and iron at high pressures and temperatures (Stamenković et al. 2011; Tachinami et al. 2011). RTE uses two models to calculate viscosity over a wide range of pressures and temperatures. For the lower mantle, RTE used the model of Nabarro-Herring (Yamazaki and Karato 2001),

$$\eta_{NH}(P, T) = \frac{R_g d^m}{D_0 A m_{mol}} T\rho(P, T) \exp\left(\frac{b\ T_{melt}(P)}{T}\right). \quad (78)$$

Here $R_g = 8.31$ Jmol^{-1} K^{-1} is the gas constant, d is the size of the grains and m is the exponent of growth, A and b are free parameters, D_0 is a diffusion coefficient, m_{mol} is the molar density and $T_{melt}(P)$ is the melting temperature of the perovskite (Stamenković et al. 2011). The Nabarro-Herring expression allows to calculate $\eta_c = \eta_{NH}(T_{\eta c})$, where $T_{\eta c}$ is the temperature of the layer.

The upper mantle has a different mineralogy, and pressures and temperatures are smaller, so an Arrhenius-type model for non-Newtonian fluids is used to estimate the viscosity (Ranalli 2001; Tachinami et al. 2011):

$$\eta_A(P, T) = \frac{1}{2}\left[\frac{1}{B^{1/n}}\left(\frac{E^\star + PV^\star}{nR_g T}\right)\right]\dot{\epsilon}^{(1-n)/n}, \quad (79)$$

where $\dot{\epsilon}$ is the strain rate, n is the creep index, B is the Barger coefficient, $E^\star$ is the activation energy and $V^\star = 2.5 \times 10^{-6}$ m^3 mol^{-1} is the activation volume of the upper mantle [TA11]. From this, the viscosity of the upper mantle is $\eta_m = \eta_A(\langle P_m \rangle, T_{up})$.

Table 3 summarizes the parameters used by RTE that fit the properties of the Earth. The parameters used for the stagnant lid case are those suggested by GA10, which reproduce the properties of Venus. Figure 10 shows the RTE results applied to planets with masses $0.5 - 4.0\ M_\oplus$.

Normally the TEMs contain uncertainties in many critical parameters. ZU13 did a sensitivity analysis of the model, by changing the values of five of the most important parameters:

- **The core mass fraction, CMF**: This parameter is determined by the Fe/Si ratio of the planet that it is fixed at planetary formation. Its value could be altered by exogenous processes like planetary impacts, as the one that formed our moon. RTE uses the Earth's value CMF = 0.325 and assumes that SEs are dominated by a silicate-rich mantle. As a comparison, Mars has a CMF = 0.23 and the value for Mercury is CMF = 0.65, Mercury could have lost a significant fraction of its mantle probably by a large impact. The CMF determines the size of the core and the thermal properties of the convective shell where the PMF is generated. RTE take two extreme values: CMF = 0.23 (a Mars-like core) and CMF = 0.43 (an iron-rich core). Planets with larger cores have low-pressure olivine mantles and the rheological model becomes unreliable.
- **The initial temperature contrast at the CMB**: ΔT_{CMB} is one of the most uncertain properties in TEMs. The initial core temperatures would be determined by random processes during the assembly and differentiation of the planet. To fit the thermal history of the Earth, RTE set $\epsilon_{\rm adb} = 0.7$ and applied the same value to SEs. They varied this parameter between 0.6 and 0.8. Their analysis provides the magnitude and sign of the effect that this parameter has in the dynamo properties.
- **High-pressure viscosity rate coefficient,** b: Rheological properties of silicates inside the mantle are one of the most uncertain aspects of TEMs. They critically determine the amount of heat that could be transported out of the planet. RTE found that the viscosity of the lower mantle (perovskite) is the most important source of uncertainties in the TEM. Equation (79) strongly depends on temperature and pressure and the parameter controlling this dependence is the "rate coefficient" b. RTE used $b = 12.3301$ to reproduce the thermal properties of the Earth. To study the impact of b in TEM, RTE varied it in the interval 10 – 14.
- **Iron thermal conductivity,** k_c: This parameter controls the amount of heat coming out from the core. RTE used k_c=40 Wm^{-1}K^{-1} that fits the thermal evolution history and present magnetic field of the Earth. Although recent first-principles analysis suggest that values as large as 150-250 Wm^{-1}K^{-1} could be common at Earth's core conditions (Pozzo et al. 2012), RTE varied k_c between 35 and 70 Wm^{-1}K^{-1}.
- **Grüneisen parameter for iron,** y_{0c}: This is one of the most critical parameters of the EOS, especially under core conditions. It affects the mechanical structure, temperature profile and phase of iron in the metallic core. RTE used the reference value y_{0c}=1.36 that fits the values of the Earth. Grüneisen parameter values have been found in the range of 1.36-2.338. RTE value is at the lower end of this range, so RTE recalculated the model for a larger value of 2.06.

Other uncertain parameters such as the critical Rayleigh number, have also been studied (Gaidos, E. 2011). The TEM is insensitive to such uncertainties.

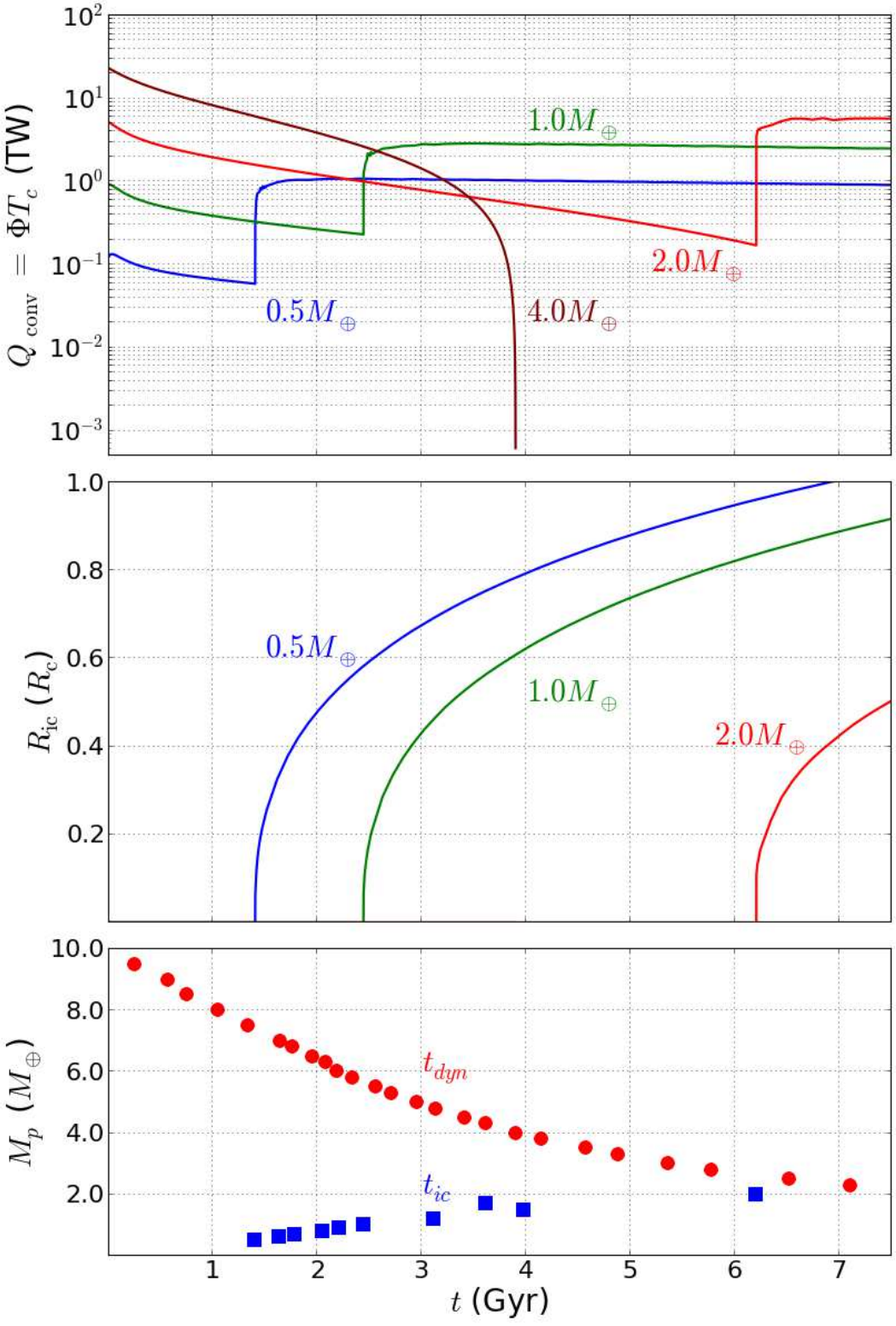

Figure 10. Thermal evolution for Earth-like composition ($CMF = 0.325$) using the RTE. Upper panel: convective power flux Q_{conv}. Middle panel: radius of the inner core R_{ic}. Lower panel: time of inner core formation (blue squares) and dynamo lifetime (red circles). In RTE the metallic core is liquid at $t = 0$ for all planetary masses. Planets with a mass $M_p < 2.0M_\oplus$ develop a solid inner core before the shut down of the dynamo. The core of more massive SEs remains liquid at least until the dynamo shut down. (Figure is taken from ZU13, with permission of the editor)

Planetary composition, CMF, and mantle viscosity are responsible for the largest uncertainties in the predicted magnetic properties of the planet. Planets with small metallic cores have on average low magnetic dipole moments. This is mainly due to a geometrical effect. The total heat produced by the core and hence the magnetic field strength at core surface is of the same order for Fe-poor and Fe-rich planets. However, a small core means also a lower magnetic dipole moment, *i.e.* $\mathcal{M} \sim R_c^3$. Planets with a lower content of iron also have small and hot cores and therefore the solid inner core formation and the shutting down of the dynamo are slightly delayed.

Viscosity dependence on pressure and temperature, as quantified by the parameter b, has the opposite effect on planetary magnetic properties than CMF, at least for SEs. A low viscosity lower mantle will favor the extraction of heat from the metallic core increasing the convective energy available for dynamo action. On the other hand a viscous lower mantle will delay the formation of a solid inner core and extend the lifetime of the dynamo.

The effect of the Grüneisen parameter under core conditions is negligible, at least on what respect to the PMF strength and lifetime. Only the time of inner-core formation is strongly affected by changes in this parameter. In planets smaller than Earth, inner-core solidification can be delayed up to three times. On the other hand, with a larger Grüneisen parameter, SEs could get a solid inner-core very early in their thermal histories.

A larger initial temperature contrast across the CMB implies a larger initial temperature at the core. Although a hotter core also produces a larger amount of available convective energy, the time required for iron to reach the solidification temperature is also larger. The dynamo of planets with $M_p < 2M_\oplus$ and hot cores (large ϵ_{adb}) is weaker than that of more massive planets during the critical first couple of gigayears. Planets with a colder core develop a solid inner core almost from the beginning and the release of latent and gravitational energy feeds a stronger dynamo. For more massive planets, $M_p > 2M_\oplus$, the condition for an inner core formation is never reached during the dynamo lifetime. In this case, planets with hot cores (large lower mantle viscosities or high-temperature contrasts along the CMB) produce large amounts of convective energy. A larger convective power will produce a larger value of the local Rossby number. Thus massive planets with hot cores also have multipolar dynamos and hence lower dipole magnetic moments and a reduced magnetic protection.

Thermal conductivities affects the results of the TEM less. Besides the case of massive planets where differences in the order of 10-30% in the magnetic properties are found when k_c varies, the magnetic properties calculated with RTE seem very robust against variations in these two properties. However, it should be mentioned that this result applies only when a standard value of k_c is assumed.

TEMs, scaling laws of dynamos, stellar winds and magnetospheric evolution are all necessary ingredients to analyze the magnetic protection of SEs. There are two quantities that characterize the global magnetic properties of SEs: 1) the average of the surface dipolar component of the PMF, B_{avg} and 2) the total time T_{dip} spent by the dynamo in the dipolar dominated regime. Intense PMFs with strong dipolar components (Stadelmann et al. 2010), are better to protect planets against stellar winds or CRs. Large values of B_{avg}, irrespective of the dynamo regime, are consistent with planetary habitability. The long-term preservation of water and other volatiles in SEs atmospheres and the development of life would require long-lived protective PMFs, *i.e.* large values of T_{dip}. Intense and protective PMF in the early phases of planetary and stellar evolution will be also suited for the preservation of an atmosphere.

The RTE model is based on three main hypothesis: 1) the thermal evolution models by GA10 and TA11 provide global robust features of the thermal evolution of SEs, 2) the scaling laws fitted with the numerical dynamo experiments can be extrapolated to real planetary dynamos, 3) the local Rossby Number could be used as a proxy for dynamo regime.

It is important to solve a complete model including a rigorous treatment of convection in the mantle, as was done in MTE, but also taking into account a detailed model of the structure and entropy balance in the core as done by CTE. The RTE model tries to look for this more complete model. There are two robust predictions from these models that may be confirmed by more complete models or even by observations: 1) there is a maximum planetary mass, $\sim 2\ M_\oplus$ beyond which conditions to develop strong and long-lived PMF decline; 2) the formation of a solid inner core is favored in the case of $\approx O(1)M_\oplus$ planets.

Hypothesis (2) is still studied in models of planetary dynamos (Christensen 2010). Although the application of numerical scaling laws to planetary dynamos have had some success (Olson and Christensen 2006), higher resolution in numerical experiments aimed at exploring a wider region of the parameter space is required to confirm or reject this hypothesis. Further advances in the understanding of how non-dipolar dynamos behave will also be required to support the procedure devised in RTE to estimate the PMF intensity.

Hypothesis (3) is based on numerical results (see figure 3). From numerical parametric studies (Sreenivasan and Jones 2006) it is known that dipolarity decreases with the increase of the ratio of inertial to Coriolis forces. Chris-

tensen and Aubert (2006) identified a critical value for $Ro_l^\star$ that has been confirmed by more studies performed by Aubert et al. (2009); Driscoll and Olson (2009) and Christensen (2010). Less clear are the properties of the dynamos between the dipolar and multipolar regimes, like the Earth's dynamo that lies in this regime. Driscoll and Olson (2009) discussed the relationship between the reversal history of the Earth's dynamo and the unknown properties of the transitional region between dipolar and multipolar regimes. An interesting question remains: why is the Earth's dynamo so close to this boundary? The scaling law for $Ro_l^\star$ could shed light into this. It is noted that the particular thermal history of our planet does not affect to a large extent the order of magnitude of $Ro_l^\star$. One or two orders of magnitude variation in p are not enough to change the order of magnitude of $Ro_l^\star$. This quantity is more sensitive to the rotation and the core radius of the planet. The rotation of the Earth has been of the same order since the formation of the planet (Denis et al. 2011). The core radius is mainly determined by the (Fe/SiO) ratio, a quantity that is not well known, even for the Earth.

RTE assumed that planetary properties very similar to Earth. GA10 studied the modifications to this model as the case of planets with a different relative core size. GA10 found that an increase in core size (a larger (Fe/SiO) ratio) essentially has two effects: 1) an earlier nucleation of the solid inner core and 2) an increase of the surface PMF intensity. The latter effect is mostly due to the smaller attenuation of core field and not to a noticeable modification of the convective power density. A different core size for RTE results in two important conclusions: 1) the predicted maximum dipolar component of the PMF is increased and 2) the dipolar field lifetime, especially in the case of slow rotators, is decreased. Assuming that a different core size does not affect the convective power p, the $Ro_l^\star$ will not change so much.

The RTE model predicts the thermal histories of planets with masses in the range of 0.5 to 6.0 $M_\oplus$. Then applying dynamo scaling laws, the model predicted the magnetic properties of SEs inside the HZ and its evolution depending on time, planetary mass, and rotation.

5 The role of rotation

Summarizing up to this point, it can be said that by using TEM and scaling laws, it is possible to restrict the properties of the PMFs of SEs. The works of GA10 and TA11 focussed on planets with low rotation periods and dipolar dynamos. The work of ZU13 also includes the effect of rotation in order to determine the regime of the PMF and its properties for planets which have both, dipolar and multipolar core magnetic fields (CoMF).

5.1 Rotation and the CoMF regime

To predict the evolution of the CoMF, and the intensity of the PMF, be required at least an expression for the local Rossby Number as a function of time, mass, and rotation. Replacing the available energy density p and using $E = \nu/(\Omega D^2)$, we found that:

$$Ro_l^\star = c_{Rol} \times \left[Q_{conv}^{1/2}\Omega^{-3/2}D^{-1}(\overline{\rho}_c V)^{-1/2}\right] \times \left[\nu^{-1/3}\Omega^{1/3}D^{2/3}\right] \times (\lambda/\kappa)^{1/5}. \quad (80)$$

Q_{conv} and $\chi = R_{ic}/R_c$ are obtained from TEM. With the value of χ, it is possible to calculate $D = R_c(1-\chi)$ and $V = (4\pi/3)R_c^3(1-\chi^3)$. The radius of the core and the average density for SEs are scaled as $R_c \propto M_p^{0.243}$ and $\overline{\rho}_c \propto M_p^{0.271}$ (Valencia et al. 2006). Rotation is expressed in terms of period $\Omega = 2\pi/P$. We have:

$$Ro_l^\star(t, M, P) = C\left[\overline{\rho}_c^{-1/6}R_c^{-11/6}\right] \times \left[Q_{conv}^{1/2}(1-\chi)^{-1/3}(1-\chi^3)^{-1/2}\right] \times P^{7/6}. \quad (81)$$

Here the quantities that depend directly on the mass (left bracket) are separated from those that depend directly on time and indirectly on the mass (right bracket). The dependence on rotation is included in the term $P^{7/6}$. C depends on the viscosity of the core. The thermal and magnetic diffusivities are considered constant and independent of the planetary mass. C takes a value such that a planet with 1 $M_\oplus$, at a time $t = 4.54\ Gyr$, with rotation $P = 1$ day, has a value of $Ro_l^\star(t = 4.54\ Gyr, M = 1\ M_\oplus, P = 1\ day) = 0.07$ [ZU12].

Planets with large periods (slow rotators) have large $Ro_l^\star$ values and their PMF tends to be multipolar. Dynamos created from a fully liquid core ($\chi = 0$), have low $Ro_l^\star$ and tend to be dominated by the dipole, even for different periods of rotation. In this case, the absence of compositional and latent heat make the convection, and thus the PMF, much weaker. For constant convective energy, the most massive planets will have smaller values of $Ro_l^\star$ and its PMF will tend to be dipolar.

5.2 Scaling the PMF intensity

To calculate the intensity of the CoMF, Q_{conv} and $D = R_c(1-\chi)$ are provided by TEM. Having b_{dip} and B_{rms}, the

intensity of the dipolar component at the CMB can be calculated as,

$$\begin{aligned}\overline{B}_{dip} &= \frac{1}{b_{dip}} c_B f_{ohm}^{1/2} \sqrt{\overline{\rho}_c \mu_o} \Omega D p^{1/3} \\ &= \frac{1}{b_{dip}} c_B \sqrt{f_{ohm} \mu_o} \times \left[\overline{\rho}_c^{1/6} R_c^{-2/3}\right] \\ &\times \left[Q_{conv}^{1/3} (1-\chi)^{1/3} (1-\chi^3)^{-1/3}\right].\end{aligned} \tag{82}$$

Here D and V were substituled by terms of R_c and χ. For rapid rotators $b_{dip} \sim 1$ and $\overline{B}_{dip} \sim B_{rms}$. This is the approximation used by GA10 and TA11 to calculate the PMF intensity. This approach is not always valid. The values of b_{dip} for numerical dynamos (Christensen and Aubert 2006; Aubert et al. 2009; Christensen 2010), vary over a wide range for both regimes [ZU12]. It is possible to determine a minimum value of b_{dip}^{min} as a function of the dipolar fraction of the field,

$$b_{dip}^{min} = c_{bdip} f_{dip}^{-\alpha}, \tag{83}$$

where $c_{bdip} \simeq 2.5$ and $\alpha \simeq 11/10$ are adjustment parameters. This restriction allows us to calculate a maximum value for the dipolar field in the CMB directly from the equation (82), by replacing b_{dip} as b_{dip}^{min},

$$\begin{aligned}\overline{B}_{dip} \lesssim \overline{B}_{dip}^{max} &= \frac{c_{Lo}}{c_{bdip}} f_{dip}^{11/10} \sqrt{f_{ohm} \mu_o} \\ &\times \left[\overline{\rho}_c^{1/6} R_c^{-2/3}\right] \times \left[Q_{conv}^{1/3} (1-\chi)^{1/3} (1-\chi^3)^{-1/3}\right]\end{aligned}$$

c_{Lo} is a constant coefficient related with the Lorentz number and has values that depends on the regime of the dynamo. In the multipolar case, $f_{dip} \lesssim 0.35$ and $c_{Lo} \simeq 1.0$, in the dipolar case, $f_{dip} > 0.35$ and $c_{Lo} \simeq 0.6$, c_{Lo} depends implicitly on f_{dip} and in the minimum value of b_{dip}^{min} [ZU12].

Here we see how f_{dip} and b_{dip} do not adopt unique values for a dynamo in a given regime. Moreover, their values are restricted above and below respectively. This allows us to restrict the value of the dipole component of the CoMF.

After estimating the value of $Ro_l^\star$ for a dynamo with a given period of rotation, it is possible to calculate the maximum value of f_{dip} that the dynamos could reach that value of $Ro_l^\star$ (see figure 3). With this value, it is possible to calculate the maximum value of the dipole component of the CoMF, at a certain time t, calculated as follows:

1. Using the thermal evolution model find $Q_{conv}(t)$ and $\chi(t)$.
2. Compute $Ro_l^\star$ using eq. (81).
3. Using $Ro_l^\star$ compute the maximum value of f_{dip} as given by an envelope to numerical dynamo results in the $f_{dip} - Ro_l^\star$ space (see dashed line in figure 3).
4. Using f_{dip}, compute the maximum dipolar component of the CoMF, $\overline{B}_{dip}^{max}$ using eq. (84). Values adopted for c_{Lo} are ≈ 1 for dipolar dynamos ($f_{dip} > 0.35$) and ≈ 0.6 for multipolar dynamos ($f_{dip} < 0.35$) (Aubert et al. 2009; Christensen 2010).

With the maximum intensity of the dipole component of the CoMF and assuming a non-conductive mantle, it is possible to estimate the value of the PMF at the surface of the planet. If the CoMF is dipolar, then the surface field scales as $(R_c/R_p)^3$. If, on the other hand, the CoMF is multipolar, the PMF properties on the surface can not be known so easily.

Suppose we have a dipole field in the CoMF, our interest is to analyze the properties of a protective PMF, which depends fundamentally on its dipole component (Stadelmann et al. 2010). Under this condition, the maximum dipole component of the PMF $\overline{B}_{s,dip}^{max}$ can be calculated as:

$$\overline{B}_{s,dip}^{max} = \overline{B}_{dip}^{max} \left(\frac{R_c}{R_p}\right)^3. \tag{84}$$

5.3 Evolution of the rotation period

The long-term evolution of the period of rotation of a planet depends on aspects such as the dynamic conditions, the impacts suffered during the formation process, the internal processes of the planet that redistribute the material and the gravitational interactions with its star and other planets in the system, in addition to the possible action of moons, if present (van Hoolts 2009).

To understand the long-term variations of the rotation period two scenarios must be taken into account: 1) The case in which the period is constant P_o, that would be the case of planets tidally locked or those that retain their prime periods; 2) A steady increase in the period of rotation, which would be the case of planets affected gravitationally by its star, a moon or other planets. RTE assumed a simple linear variation of the period [ZU12],

$$P(t) = P_o + \dot{P_o}(t - t_o). \tag{85}$$

P_o is the the rotation period at t_o and $\dot{P_o}$ its the rate of variation respectively. For an Earth-like planet it is assumed $t_o = 4.54$ Gyr, $P_o = 24$ h and $\dot{P}_o \approx 1.5$ h Gyr^{-1}. These values are compatible with a primordial rotation of $P(t = 0) = P_{ini} \approx 17$ h (Varga et al. 1998; Denis et al. 2011).

The $Ro_l^\star$ evolution is calculated using the equation (81), $Q_{conv}(t)$ and $\chi(t)$ are obtained from CTE and MTE (see table 2). Figure 12 shows the results for different planetary masses assuming $P_o = 1$ d, for both cases, constant and variable period, respectively. CTE and MTE obtain different results. This is mainly due to the value and evolution of p for both models (see figure 11).

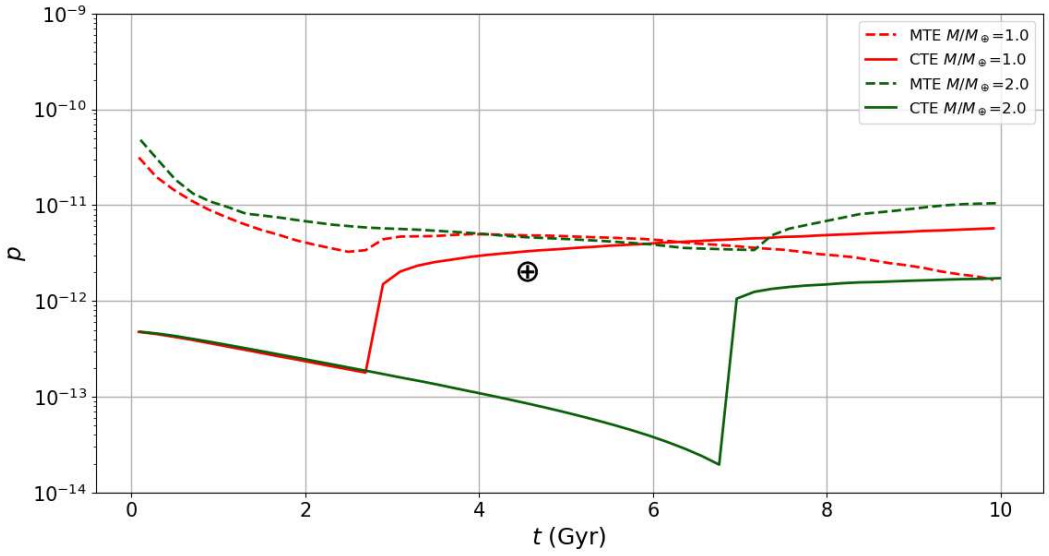

Figure 11. Evolution of the convective power density p in CTE (solid lines) and MTE (dashed lines) for two different planetary masses 1.0 and 2.0 $M_\oplus$. p is one order of magnitude larger in MTE and falls faster than in the CTE model due to differences in the estimations of the convective power

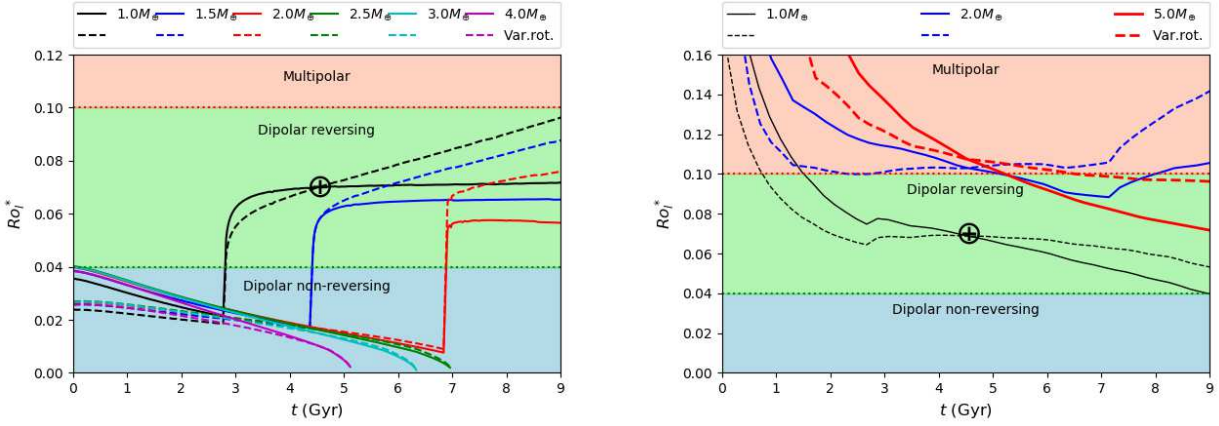

Figure 12. Evolution of the local Rossby number computed from selected results for CTE and MTE. Solid curves correspond to constant period of rotation, dashed lines correspond to a variable period. Earth-like values were assumed, *i.e.* P_o=1 d. For variable period of rotation (dashed lines) dP_o/dt = 1.5 h Gyr^{-1}. Shaded regions corresponds to dynamo regimes

For CTE, p comes directly from the dissipation of entropy within the core. In MTE p is limited by the amount of heat extracted from the core through the CMB. Because of this, p is one order of magnitude greater in MTE, and also grows more quickly with the planetary mass. The energy flux through the CMB decays more rapidly in MTE than the energy dissipated by entropy in the core for CTE. This effect produces a long-term reduction in p, especially for low mass SEs.

There is an evident change in the evolution of Ro_l^* that happens when p jumps abruptly just after the solidification of the inner core begins at t_{ic}. In CTE, p shows a big increase due to the renovated convection, resulting from the release of light elements and latent heat, in addition to the reduction of the thickness of the convective layer. In the case of MTE, the increase of p is mainly due to the reduction in the thickness of the convective layer. The heat flux through the CMB that determines Q_{conv}, is not as sensitive to the new sources of entropy.

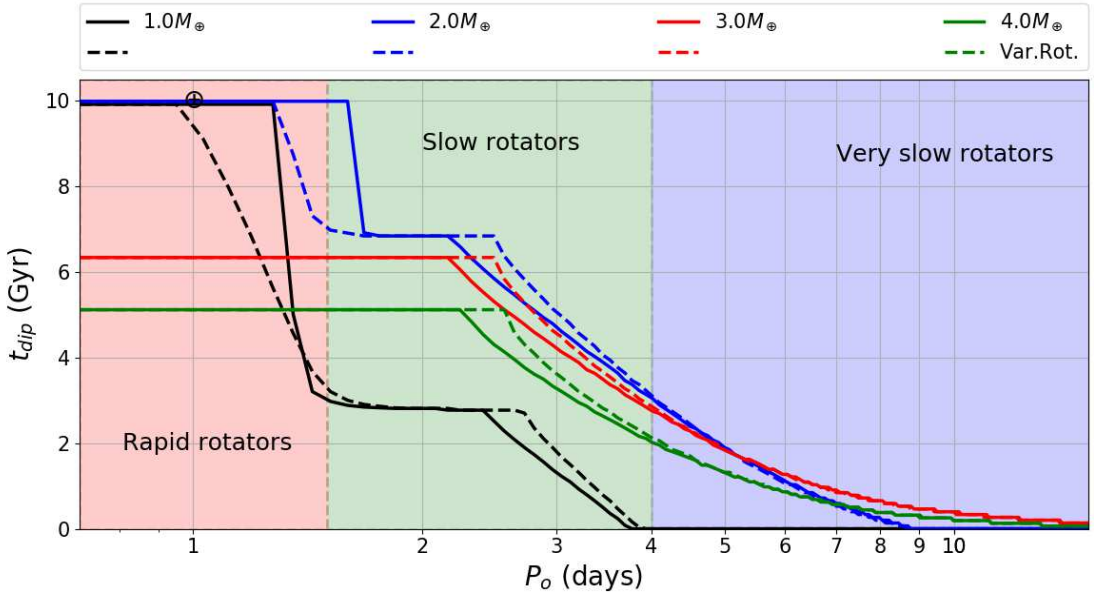

Figure 13. Lifetime of the dipolar dominated CoMF in CTE obtained from the analysis of the $Ro_l^\star$ evolution for planets with different masses. Constant (solid line) and variable (dashed lines) periods of rotation have been assumed. The gray regions are limited by the maximum rotation periods of low mass planets ($M < 2\ M_\oplus$) in three categories

5.3.1 Rotation in the CTE

Figure 12 shows how $Ro_l^\star$ varies over time, in a similar manner to p. With variable rotation periods, an interesting effect is shown, as p and D decreases, $Ro_l^\star$ increases rapidly. It can be seen that the minimum value of $Ro_l^\star$ corresponds at the moment when the nucleation begins in t_{ic}. On the other hand, the beginning of the formation of a solid core establishes the transition from the dipolar to the multipolar field regime.

For massive SEs, in which an internal core is not formed, $Ro_l^\star$ continues decreasing until the dynamo turns off. This makes the planet unable to establish a dipolar CoMF, especially if the period of rotation continues increasing.

Planets possessing a constant rotation period $P \lesssim P_{mul} = P_o(0.1/Ro^\star_{l,\min})^{6/7}$, could develop a dipolar CoMF at some epoch [ZU12]. There is a critical value for the rotation period P_{mul} from which the CoMF becomes multipolar. For planets with $M \lesssim 2.0\ M_\oplus$, the critical value of the rotation period is $P_{mul} \sim 4 - 9$ days. For SEs with $M \gtrsim 2\ M_\oplus$, the critical period is $P_{mul} \sim 30 - 50$ days. This result sets an upper limit on the period to be considered as a rapid rotator.

In the case of a planet with $1.0\ M_\oplus$, the CoMF is dipolar only during the first 2-3 Gyr, while the formation of the solid core has not begun and the convection is kept low, *i.e.* low $Ro_l^\star$. Just after the solidification of the core has begun, the intensification of convection does the CoMF becomes multipolar. The time while the dipolar component governs the CoMF is called the *dipolar lifetime*, t_{dip}.

Massive SEs with $M > 2\ M_\oplus$ behave differently. While its period of rotation is $P \lesssim P_{mul}$ the CoMF remains in the multipolar regime. After some time called dipolarity switch time, t_{sw}, the period $P > P_{mul}$ and the field becomes dipolar. For this case, the lifetime of the dipole, t_{dip}, will be the difference between the total duration of the dynamo and t_{sw}.

Figure 13 shows the value of t_{dip} for planets with different masses as functions of the initial rotation period. For rapid rotators ($P_o \simeq 1.0$ day), t_{dip} equals the total lifetime of the dynamo. The critical period of rotation for which this condition is met increases with the mass of the planet, especially on planets with $M \leq 2\ M_\oplus$, as a result of the appearance of the inner core (see figure 12). Planets with $M > 2\ M_\oplus$ have a critical period for dipolarity more or less equal for periods the order $P_c \simeq 2 - 2.5$ days, because for these planets $Ro_l^\star$ evolves approximately in the same way (see figure 12).

When rotation periods are variable, the critical period P_c decreases for small planets and increases on massive planets. Low mass SEs can maintain their CoMF within the dipole regime even above the P_c until the solidification of the core has not begun, *i.e.* $t < t_{ic}$. During this period, the

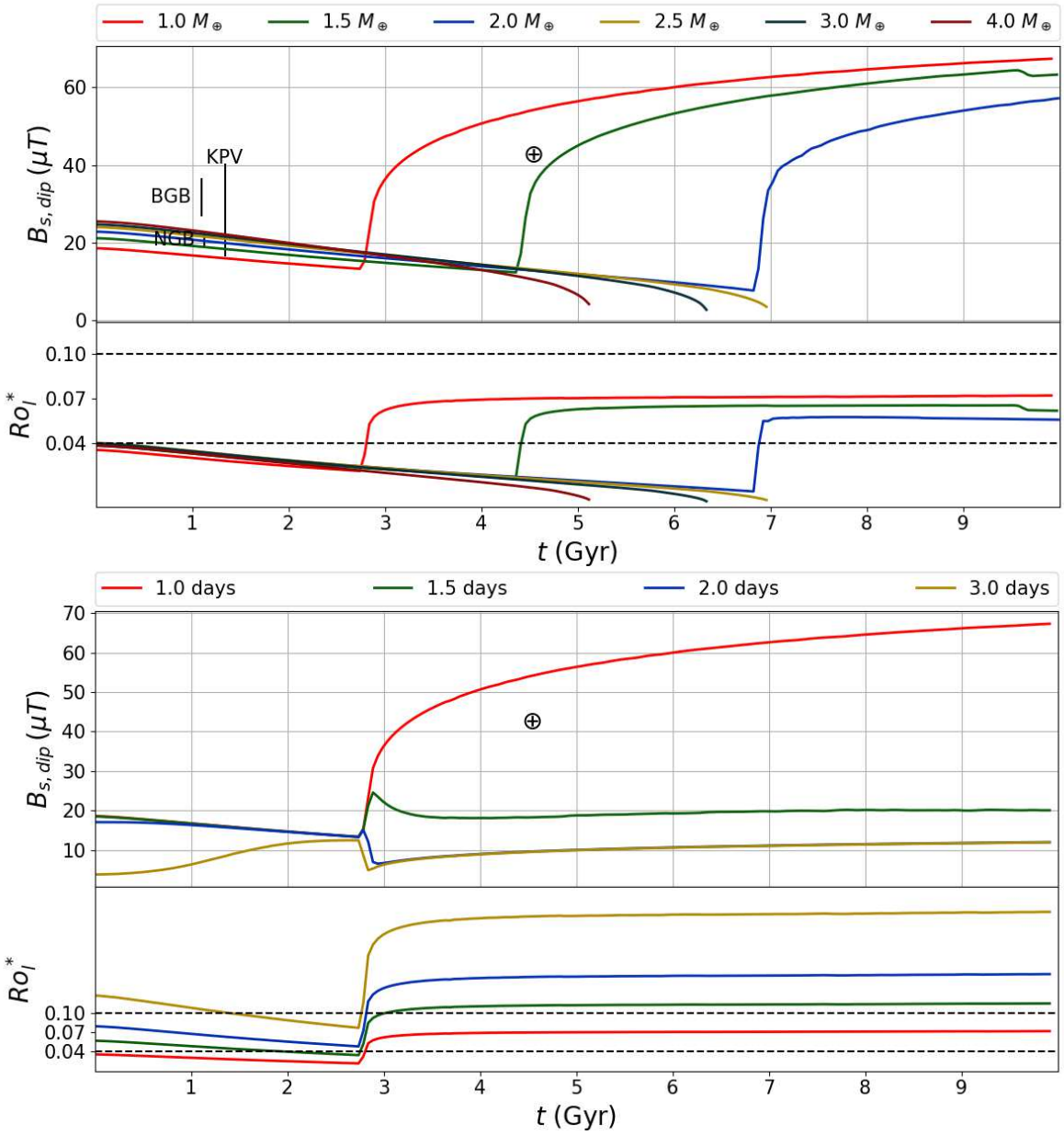

Figure 14. Maximum dipolar component of the PMF at the surface estimated using CTE. Upper panel: $B_{s,dip}$ for a constant rotation period=1.0 day and differet planetary masses. Lower panel: $B_{s,dip}$ for a constant planetary mass = 1.0 $M_\oplus$ and different rotation periods. The value of the Ro_l^* has also been plotted to illustrate the effect that a transition between dynamo regimes have in the evolution of the PMF. The black dashed lines in the lower Ro_l^* panels are the limits between the regimes (dipolar non reversing, dipolar reversing and multipolar). The value of $B_{s,dip}$ for the present Earth's and paleomagnetic measurements made at Kaap Valley (KPV), Barberton Greenstone Belt (BGB), and Nondweni Greenstone Belt (NGB), dacite localities has also been included (Tarduno et al. 2010).

dipolarity of the CoMF can be guaranteed for different periods of rotation. This effect explains why the time of the dipole is very close to the time of nucleation, $t_{dip} \simeq t_{ic}$. This result allows us to establish a limit to the periods of rotation required for a long live dipole, *i.e.* $t_{dip} \gtrsim 3$ Gyr. No matter the mass of the planet, SEs with $P \lesssim 2-3$ days comply with this condition.

The works of GA10 and TA11 chose low mass planets such as those with greater potential to develop intense and long life PMF. This is mainly due to to the early appearance of a solid core and to the rheological properties of the mantle, favorable for development of the PMF.

ZU12 find the same result, especially for planets with periods of rotation ≈ 1.5 days. However, when periods are greater the results are exchanged and massive planets de-

velop dipolar CoMFs of greater duration. This is due to the appearance of the solid core in small planets, which triggers p, which does not happen to the massive ones. The thermal evolution of massive planets, *i.e.* $M > 2\ M_\oplus$, does not present this increase in p, so that the rotation can be increased much more before the CoMF turns multipolar. From the evolution of $Ro_l^\star$ and knowing the CoMF regime, it is possible to calculate the intensity of the dipole component of the PMF, $\overline{B}_{s,dip}$.

Figure 14 shows how the dipole component of the PMF on the surface evolves for SEs of up to 4.0 $M_\oplus$, assuming a constant period of rotation $P = 1.0$ day in all cases. We see how the $Ro_l^\star$ value plays an important role in the intensity of the PMF at the surface. For all masses the surface dipole component behaves in the same way as $Ro_l^\star$. It is obvious how $\overline{B}_{s,dip}$ decreases during the first few Gyr. This decline ends for low-mass SEs at the time when solidification begins. Although the emergence of the inner core implies a change in the CoMF regime, for the surface PMF this means an increase in its dipole component, which is advantageous for the magnetic protection of the planet. Conversely, we see as in the SEs with masses $M > 2\ M_\oplus$, which do not develop a solid core, the surface dipole continues decaying until it goes out.

The bottom panel shows the results for an SE with $M = 1.0\ M_\oplus$ in which the period of rotation varies between 1-3 days. When the period is $P \gtrsim 1.5$ days, the dipole component reaches its maximum intensity, just a couple of hundred million years after the start of the solidification of the core. From this maximum value, the dipole decays as a consequence of the increase in the convection, that can not be balanced by the weak Coriolis forces, due to the low rotation. In 3 Gyr the CoMF is completely multipolar. This regime transition is relatively fast, when compared to the time scale of the thermal evolution.

If most of the habitable SEs are tidally locked, having large periods of rotation, future efforts must consider the direct and indirect effects that rotation has in their PMF properties. The assumption of rapidly rotating planets ($P \lesssim 2.0$ days), is invalid for tidally locked SEs inside the HZ of M-dwarfs. On the other hand assuming that tidally locked planets lack completely of an intense PMF is also an oversimplification. As has been shown, there is a range of periods of rotation where planets could sustain moderate PMFs.

Figure 14 includes the current value of the terrestrial dipole, as well as intensity values for 3.2 and 3.4 Gyr ago (Tarduno et al. 2010). It should be noted that the variation of $Ro_l^\star$ could not explain the polarity reversal frequency observed in the Earth's field.

5.3.2 Rotation in the MTE

The behavior of $Ro_l^\star$ for MTE is shown in figure 12. Unlike the CTE model, in MTE all the fields are multipolar from the outset. This is due to the large amount of heat which flows through the CMB, F_{CMB} while the planet is young. Recall that this heat is used to calculate the convective power of the core.

In MTE model, the dynamos change from multipolar regime to dipolar in a switch time t_{sw}. The increase of p caused by nucleation and the variation in rotation reduce the time during which the dynamo is dipolar. It is required that the CoMF be come dipolar as soon as possible, *i.e.* in a small t_{sw}, in order to provide a protective PMF. This protection is more important at the beginning of evolution of the planet, when the star is more active (Lichtenegger et al. 2010). It would be hoped that dipolarity would last for a long time, *i.e.* large t_{dip}.

However, in figure 12 can be seen how in the MTE model a low-mass planet, $M = 1.0\ M_\oplus$, takes more than 9 Gyr to reach the dipole regime and remains in the reversals regime during most of its evolution. More massive planets, *i.e.* $M > 2\ M_\oplus$, fail to achieve dipolarity throughout their lives.

In MTE the effects of having a variable period are more remarkable. The development of a dipolar field of long life is fulfilled in just few cases. In fact, only planets with periods $P \lesssim 1.0$ day develop an intense and durable dipolar CoMF.

5.4 Rotator classifications

Rotation can be classified in three different types of SE dynamos, according to their period of rotation (see figure 13):

- **Rapid rotators**
  These planets have magnetic fields dominated by dipole component that last billions of years. They have values of $Ro_l^\star$ bellow the critical value, and operate in the dipolar regime during the majority of the dynamo's lifetime. ZU12 propose a dypolar time for these planets $t_{dip} \gtrsim 0.5 t_{dyn}$. The Earth is in this group.
- **Slow rotators**
  There are SEs with dipole dynamos that do not last more than 50% of the dynamo's time, *i.e.* $t_{dip} < 0.5 t_{dyn}$. This type of dynamo spends the majority of their life time in the region of reversible fields, and can even spend some time above the critical value, which places them in the multipolar regime.

– **Very slow rotators**
This category corresponds to SEs that do not develop a predominantly dipolar field throughout its existence. These dynamos have big values of $Ro_l^\star$.

The periods of rotation that characterize these categories of rotators vary according to the mass of the planets and depend on TEM that is used to model the properties of the PMF.

In the case of CTE, fast rotators have periods $P \lesssim 1.5$ days, independently of the mass of the planet. Slow rotators with masses $M \lesssim 2\ M_\oplus$ are in a range of periods $4 \lesssim P \lesssim 10$ days. More massive SEs that are very slow rotators are in the range $10 \lesssim P \lesssim 20$ days. All planets with periods greater than $P \gtrsim 20$ days are considered also very slow rotators.

For the MTE model, the maximum rate of rotation in the category of rapid rotator is $\sim$ 1.0 day. The SEs with periods $P \gtrsim 1.0 - 1.5$ days already fall into the category of very slow rotators.

Many of the discovered SEs are very close to their stars, so that they may be tidally locked. This would allow, in principle, determination of its rotation periods. The SEs with masses $M < 2\ M_\oplus$ and periods of less than 50 days may be very common around low-mass stars (Howard et al. 2010). But for other SEs, rotation periods lie beyond current observational capabilities (Ford et al. 2001; Pallé et al. 2008).

Recently, synthetic spectra have been developed for tidally locked planets. Such spectral signatures be measured with future space telescopes like The Origins Space Telescope (OST). These models include the possibility of measuring the rotation of the planet (R.K. Kopparapu 2017).

The main limitation of such models is the assumption that the SEs have a composition similar to the terrestrial one, and that they have tectonic and a habitable temperature. These assumptions ignore the great variety of possible compositions.

Planets with different compositions such as GJ 1214 b, covered by huge atmospheres and deep oceans (Nettelmann et al. 2011), will develop PMFs through the extraction of heat, but under very different parameters. Even so, the CTE, MTE and RTE models show us that planetary rotation plays a fundamental role in the generation and maintenance of protective PMFs in diverse regimes.

SEs that are very close to their stars, as in the case of Corot 7 b, have such high surface temperatures that they do not allow the application of thes TEMs discussed. The high surface temperatures reduce the viscosity in the mantle, which favors the flux of heat from the core and increases the convection. GA10 has found that low mass SEs with higher temperatures at the surface could develop intense fields. In the case of massive SEs, a greater surface temperature produces fields of longer duration. In all cases, the value of $Ro_l^\star$ is also larger, lowering critical values of rotation to achieve the multipolar regimes. It seems that hot SEs would not be well protected. SEs could be rapid rotators ($P \lesssim 1.5 - 4$ days), slow rotators ($4 \lesssim P \lesssim 10 - 20$ days) and otherwise, very slow rotators. Planets in the HZ of low mass stars $M_\star < 0.6\ M_\odot$ could be tidally locked in less than 1 Gyr. These SEs will fall between slow and very slow rotator groups. In contrast, unlocked SEs could be any of the types according to their primordial period of rotation.

Physically speaking, the Rossby number represents the balance between rotational forces and the inertia of the fluid. It should be noted that the modified Rossby number depends on the characteristic length scale of the flow rather than on the shell thickness, and is potentially a better measure for the balance between inertia and Coriolis force (Christensen and Aubert 2006). The numerical models show that the dynamos are preferably dipolar when the effect of rotation is important. The dynamos dominated by inertial forces tend to be multipolar. These models can be applied to real planets, if it can be assumed that the scaling laws are still valid in reality. It has already been said that the numerical models of the geodynamo use values of the parameters that are far from the real ones, mainly because it is not possible to run simulations with the appropriate viscosity and thermal diffusivity values (Christensen and Aubert 2006). This problem is important if diffusive processes are important. Even so, when applying the scaling laws to true planets, like Jupiter or the Earth, the results are consistent with the measure PMF and values estimates of the intensity of the fields in the interior.

6 Magnetic protection of SE

The properties needed for a planet to be habitable have been discussed extensively over the last 25 years (Kasting et al. 1993; Lammer et al. 2009; Kasting 2010). Two basic conditions must be guaranteed: 1) the presence of liquid water on the surface and 2) the existence of an atmosphere (Kasting et al. 1993). Compliance with these two conditions depends on many factors such as the space environment and other physical conditions (Ward and Brownlee 2000; Lammer et al. 2010). One of the physical factors involved in habitability is the existence of a stable and durable PMF (Grießmeier et al. 2010). A strong PMF protects the atmo-

sphere, especially its content of volatile molecules such as water, against the erosive action of a stellar wind (Lammer et al. 2003, 2007; Khodachenko et al. 2007; Chaufray et al. 2007).

Most terrestrial planets in our galaxy orbit around low-mass stars, especially type M red dwarfs (Boss 2006; Mayor and Udry 2008; Scalo et al. 2007; Rauer et al. 2011; Bonfils et al. 2011). The planets located in the HZ of these stars ($M_\star \lesssim 0.6 M_\odot$), are likely to be tidally locked (Joshi et al. 1997; Heller et al. 2011a; Cuartas-Restrepo et al. 2016), a condition that is not very favorable for their potential habitability (Kite et al. 2011).

Previous work has extensively studied the protection that a PMF can provide to an exoplanet (Grießmeier et al. 2005; Khodachenko et al. 2007; Lammer et al. 2007; Grießmeier et al. 2009, 2010), including the influence of the thermal evolution on the properties and evolution of the PMF. Usually classic scaling laws are used to describe their magnetic fields (Christensen 2010; Zuluaga and Cuartas 2012). The work of ZU13 goes beyond previous works because it includes aspects such as the dependence of magnetic properties on the thermal evolution of the planet, as well as the planetary mass and composition, and includes the role of rotation in the determination of the intensity and the multipolar regime of the PMF [ZU12].

6.1 Star-Planet interaction

The interaction between the PMF and the stellar wind forms a complex magnetic system known as the magnetosphere. The properties of this system depend fundamentally on two physical variables (Siscoe and Christopher 1975): 1) The magnetic dipole moment of the field, $\mathcal{M}$, and 2) the dynamic pressure exerted by the stellar wind, P_{sw}.

The dipole moment is the first order term in the multipolar expansion of the magnetic field:

$$B_p^{dip}(r) = \frac{\sqrt{2}\mu_0 \mathcal{M}}{4\pi r^3}, \tag{86}$$

where $B_p^{dip}(r)$ is the dipolar component of the PMF at a distance r and $\mu_0 = 4\pi \times 10^{-7}\ H/m$ is the vacuum permeability.

The dynamical pressure of the stellar wind is given by:

$$P_{sw} = mnv_{eff}^2 + 2nk_B T, \tag{87}$$

where m is the mass of the proton and n its number density, $v_{eff} = (v_{sw}^2 + v_p^2)^{1/2}$ is the effective velocity of the stellar wind measured in the reference frame of the planet with orbital velocity v_p, T is the local temperature of the wind and $k_B = 1.38 \times 10^{-23}$ J/K is the Boltzmann constant.

Three properties are of particular interest: 1) The maximum magnetopause field intensity B_{mp}, which is a proxy of the flux of high energy particles entering into the magnetosphere, 2) The standoff distance, R_S, a measure of the size of the dayside magnetosphere and 3) The area of the polar cap A_{pc} that measures the total area of the planetary atmosphere exposed to open field lines through which atmosphere particles can escape. These quantities provides information about the level of exposure to the erosive effects of stellar wind and CR.

The maximum value of the magnetopause field intensity B_{mp} is estimated from the balance between the magnetic pressure $P_{mp} = B_{mp}^2/(2\mu_0)$ and the dynamical stellar wind pressure P_{sw},

$$B_{mp} = (2\mu_0)^{1/2} P_{sw}^{1/2}. \tag{88}$$

In simplified models B_{mp} is assumed proportional to the PMF intensity B_p^{dip} at $r = R_S$ (Mead 1964; Voigt 1995),

$$B_{mp} = 2 f_0 B_p(r = R_S) \approx \left(\frac{f_0 \mu_0}{2\pi}\right) \sqrt{2} \mathcal{M} R_S^{-3}, \tag{89}$$

f_0 is a form factor that depends on the shape and electrical currents flowing on the magnetopause (Voigt 1995). Grießmeier et al. (2010) used $f_0 = 1.16$. The dipolar component of the intrinsic field dominates at magnetopause distances even in a weakly dipolar PMF. From equations (88) and (89):

$$R_S = \left(\frac{\mu_0 f_0^2}{8\pi^2}\right)^{1/6} \mathcal{M}^{1/3} P_{sw}^{-1/6}. \tag{90}$$

R_S can also be expressed in terms of the dipole moment of the Earth $\mathcal{M}_\oplus = 7.768 \times 10^{22}$ A m^2 and the average dynamic pressure of the solar wind at 1.0 au $P_{sw\odot} = 2.24 \times 10^{-9}$ (Stacey 1992; Grießmeier et al. 2005):

$$\frac{R_S}{R_\oplus} = 9.75 \left(\frac{\mathcal{M}}{\mathcal{M}_\oplus}\right)^{1/3} \left(\frac{P_{sw}}{P_{sw\odot}}\right)^{-1/6}. \tag{91}$$

This estimate assumes a negligible value of the plasma pressure on and within the magentopause. This approximation is valid if: 1) PMF is very intense, 2) the dynamical pressure of the stellar wind is small, or 3) the planetary atmosphere is not expanded by the XUV radiation. This is an underestimation of the actual size of the magnetosphere.

The polar cap is the region in the magnetosphere where PMF lines can open into the space. (Siscoe and Chen 1975) have shown that the area of the polar cap A_{pc} scales with the dipole moment and dynamical pressure as:

$$\frac{A_{pc}}{4\pi R_p^2} = 4.63\% \left(\frac{\mathcal{M}}{\mathcal{M}_\oplus}\right)^{-1/3} \left(\frac{P_{sw}}{P_{sw\odot}}\right)^{1/6} \tag{92}$$

The polar cap area is given as a fraction of the total area of the atmosphere $4\pi R_p^2$. The atmosphere has a scale-height much smaller than planetary radius R_p.

Given $B_p^{dip}(R_p)$, we can obtain the dipole moment $\mathcal{M}$ and the density n, the velocity v_{eff} and temperature T of the stellar wind. All these quantities depend on time and also on different planetary and stellar properties.

6.2 Revisiting the scaling laws

Numerical experiments have defined scaling laws that can be used to determine properties of the PMF (Christensen 2010). For a large number of conditions, the properties of the PMF can be expressed in terms of the convective energy and the size of the convective layer. The volumetric average magnetic field strength B_{rms}, within the layer does not depend in general of the rotation (see equation (33)),

$$B_{rms} \approx C_{Brms}\, \mu_0^{1/2} \overline{\rho}_c{}^{1/6} (D/V)^{1/3} Q_{conv}^{1/3} \tag{93}$$

C_{Brms} is a fitting constant, in the case of dipolar dynamos $C_{Brms}^{dip} = 0.24$, and for multipolar dynamos $C_{Brms}^{mul} = 0.18$. $\overline{\rho}_c$, $D = R_\star - R_{ic}$ and $V = 4\pi(R_\star^3 - R_{ic}^3)/3$ are the average density, height and volume of the convective shell. The dipolar field intensity at the planetary surface, and hence the dipole moment of the PMF, can be estimated from the power spectrum of the CoMF. Although it is not possible to predict the relative contribution of each mode to the total CoMF strength, the local Rossby number $Ro_l^\star$ could be used to distinguish dipolar dominated from multipolar dynamos as we see in section 5.1:

$$Ro_l^\star = C_{Rol}\, \overline{\rho}_c{}^{-1/6} R_c^{-2/3} D^{-1/3} V^{-1/2} Q_{conv}^{1/2} P^{7/6}. \tag{94}$$

In this case $C_{Rol} = 0.67$ is another fitting constant and P is the period of rotation of the planet. Remember that dipolar fields arise systematically when dynamos have $Ro_l^\star < 0.1$. Multipolar fields arise in dynamos with $Ro_l^\star > 0.1$. From equation (94) we see that fast rotating planets have dipolar dominated CoMF while slow rotators produce multipolar fields and hence fields with a much lower dipole moment.

The independence of B_{rms} on rotation rate on the one hand, and the role that rotation has in the determination of the regime on the other, implies that even very slow rotators could have a comparable magnetic energy as rapid rotators with similar size and thermal histories. In this case the magnetic energy will be redistributed among other multipolar modes rendering the CoMF more complex.

With B_{rms} and $Ro_l^\star$ it is possible to calculate the *maximum dipolar component* of the CoMF by using the maximum dipolarity fraction f_{dip} (the ratio of the dipolar component to the total strength of the CoMF) that for dipolar dynamos is $f_{dip}^{max} \approx 1.0$ and for multipolar is $f_{dip}^{max} \approx 0.35$ [ZU12]. To connect this ratio to B_{rms}, is used the volumetric dipolarity fraction b_{dip}, from numerical experiments (see equation (35)):

$$b_{dip}^{min} = c_{bdip} f_{dip}^{max\,-11/10}, \tag{95}$$

$c_{bdip} \approx 2.5$ is a fitting constant. Combining equations (93) and (95) it is possible to find an upper bound to the dipolar component of the CoMF:

$$B_c^{dip} \lesssim \frac{1}{b_{dip}^{min}} B_{rms} = \frac{f_{dip}^{max\,11/10}}{c_{bdip}}\, B_{rms} \tag{96}$$

The surface dipolar field strength is estimated as,

$$B_p^{dip}(R_p) = B_c^{dip} \left(\frac{R_p}{R_c}\right)^3. \tag{97}$$

Finally, the total dipole moment is calculated using equation (86) at $r = R_p$. The surface PMF intensity determined using equation (97) overestimates the PMF dipolar component. The actual field could be much more complex and the dipolar component could actually be lower. As a consequence, this model can only predict the maximum level of protection that a planet could have from its PMF.

The results for planets in the range 0.5-4.0 $M_\oplus$ are summarized in figures 15 and 16. Figure 15 shows the local Rossby number, the maximum dipolar field intensity and the dipole moment as a function of time for planets with different mass and two different periods of rotation ($P = 1$ day and $P = 2$ days), and the effect that rotation has in the evolution of dynamo geometry and in the maximum dipolar field intensity at the planetary surface.

Figure 16 summarizes the evolution of the dipole moment for planets with long-lived dynamos. For periods $P <$ 1 day and $P > 5 - 7$ days the dipole moment is nearly independent of rotation. Slow rotators have a non-negligible dipole moment which is systematically larger in more massive planets.

It is interesting to compare the predicted values of the maximum dipole moment calculated by ZU13 with the values roughly estimated in previous work (Grießmeier et al. 2005; Khodachenko et al. 2007; López-Morales et al. 2011). For example, Khodachenko et al. (2007) estimate dipole moments for tidally locked planets in the range 0.022-0.15 $\mathcal{M}_\oplus$, ZU13 predict maximum dipole moments almost one order of magnitude larger (0.15-0.60 $\mathcal{M}_\oplus$) with the largest differences at ($M \gtrsim 4M_\oplus$). These differences arise from the fact that none of the scaling laws used by (Khodachenko et al. 2007) depend on the convective power. In our results, the dependency on power explains the differences between massive planets and lighter planets especially at

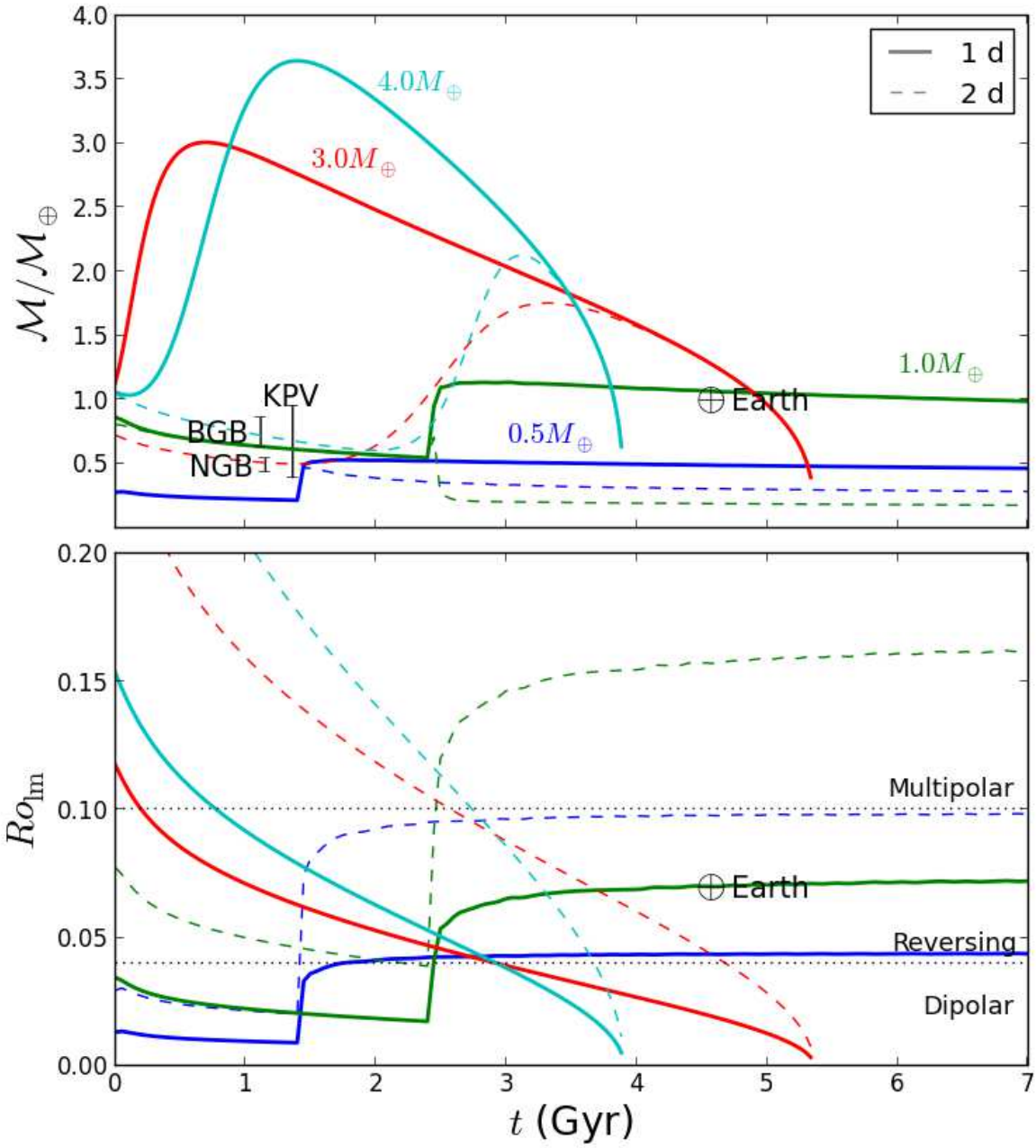

Figure 15. PMF properties predicted using the RTE and equations (93), (94) and (96) for planets masses 0.5-4.0 $M_\oplus$. The local Rossby number (lower panel) and the maximum dipole moment (upper panel). The figure includes the present values of the geodynamo (⊕) and three measurements of paleomagnetic intensities (error bars) at 3.2 and 3.4 Gyr ago (Tarduno et al. 2010). The figure compares the magnetic properties for two periods of rotation, 1 day (solid curves) and 2 days (dashed curves). The effect of a larger period of rotation is more significant at early times in the case of massive planets ($M_p \gtrsim 2\ M_\oplus$) and at late times for lower mass planets. (Figure from ZU13, with permission of the editor)

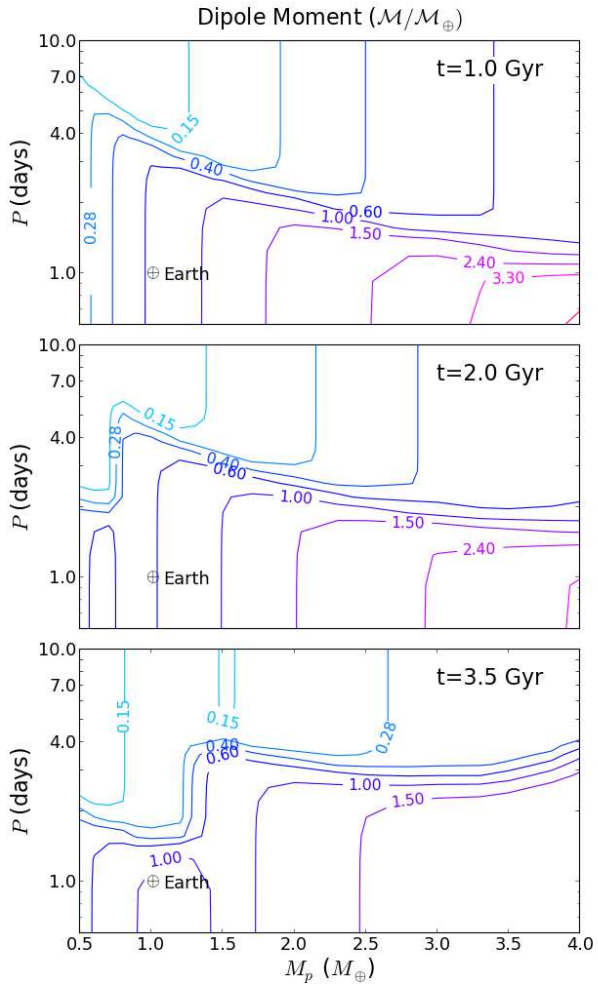

Figure 16. Mass-Period (M-P) diagrams of the dipole moment for long-lived planetary dynamos computed using RTE. Three regimes are identified [ZU12]: rapid rotating planets ($P \sim 1$ day) whose dipole moment are large and almost independent of rotation rate; slowly rotating planets ($1 < P < 5$ days), whose dipole moment are intermediate in value and highly depend of rotation rate; and very slowly rotating planets ($P > 5 - 10$ days) with small but non-negligible rotation-independent dipole moments. At lower masses ($M_p < 2\ M_\oplus$) the shape of the dipole-moment contours is determined by the time of inner-core formation: ~1 Gyr for 0.5 $M_\oplus$, ~2 Gyr for 1.0 $M_\oplus$ and $\gtrsim$ 4.6 Gyr for $M_p \gtrsim 1.5\ M_\oplus$. (Figure from ZU13, with permission of the editor)

early times. On the other hand López-Morales et al. (2011) estimate dipole moments as high as 10-80 $\mathcal{M}_\oplus$ even for tidally locked planets. These values are one to two order of magnitude higher than the most optimistic estimates of ZU13. The main difference with López-Morales et al. (2011) lies in the way that magnetic dipolar moments of tidally locked SEs are estimated in the range 0.1–1.0 $M_\oplus$. The values in López-Morales et al. (2011) are compatible with our results. In their work, they use the same power-based scaling laws that RTE applied, but assume a rather simple interior model and a static thermal model where the convective power is set that maximizes the efficiency with which the convective energy is converted into the PMF.

6.3 Magnetic protection

The PMF properties constrained using RTE and scaling laws are not enough to evaluate the magnetic protection of a potentially habitable planet. It is also necessary to estimate the magnetosphere and stellar properties as a function of time. Combining the PMF properties and the star-planet interaction, ZU13 proposed an upper constraint on magnetic protection. This model can predict certainly which planets may be unprotected, but can not say for sure the level of actual protection.

6.3.1 The HZ and tidally locking limits

Here the properties of the stars are taken from evolutionary models of GKM stars developed by Baraffe et al. (1998), for solar metallicity stars with an age of $t = 3$ Gyr. Since luminosity increases with time in main sequence stars, this assumption guarantee the largest distance of the HZ and hence the lowest effects of the stellar irradiation and wind.

The HZ limits are defined by Kasting et al. (1993) and Selsis et al. (2007). The inner and outer limits, a_{in} and a_{out}, are given in terms of the stellar effective temperature and luminosity by:

$$a_{in} = (a_{in\odot} - \alpha_{in}\Delta T - \beta_{in}\Delta T^2)\sqrt{L/L_\odot} \qquad (98)$$
$$a_{out} = (a_{out\odot} - \alpha_{out}\Delta T - \beta_{out}\Delta T^2)\sqrt{L/L_\odot},$$

where $a_{in\odot}$ and $a_{out\odot}$ are the inner and outer limits of the HZ for the Sun, and $\Delta T = T_\star - T_\odot$, α and β are fitting constants. For "recent Venus" and "early Mars", the values of the parameters are: $a_{in\odot} = 0.72$, $\alpha_{in} = 2.7619\times10^{-5}$, $\beta_{in} = 3.8095 \times 10^{-9}$ and $a_{out\odot} = 1.77$, $\alpha_{out} = 1.3786 \times 10^{-4}$, $\beta_{out} = 1.4286 \times 10^{-9}$ (Selsis et al. 2007).

We know that orbital and rotational properties of close-in planets are affected by gravitational interaction with the star. Tidal torques dampen primordial rotation and axis tilt, driving the planet up to a final resonant equilibrium where the period of rotation P becomes close or even equal to the orbital period. The final resonance is determined by dynamical factors, the most important being the orbital planetary eccentricity (Leconte et al. 2010; Ferraz-Mello et al. 2008; Heller et al. 2011a). In the solar system, Mercury is trapped in a 3:2 resonance. In the case

of GJ 581 d, dynamical models predict a resonant 2:1 equilibrium state (Heller et al. 2011a), for GJ 667 C c the predicted resonance is 1:1 (Cuartas-Restrepo et al. 2016).

The distance a_{tid} at which a planet becomes tidally locked before a given time t can be roughly estimated by (Peale 1977):

$$a_{tid}(t) = 0.5\,AU \left[\frac{(M_\star/M_\odot)^2 P_{prim}}{Q}\right]^{1/6} t^{1/6}. \qquad (99)$$

where the primordial period of rotation P_{prim} should be expressed in hours, t in Gyr and Q is the quality factor. ZU13 assumed a primordial period of rotation $P_{prim} = 17$ hours (Varga et al. 1998; Denis et al. 2011) and $Q \approx 100$ (Henning et al. 2009; Heller et al. 2011a).

6.3.2 Stellar winds

Stellar winds represent the highest risks for an unprotected planet. Its dynamical pressure can sweep the exposed atmosphere, especially at early phase of stellar evolution (Lammer et al. 2003). Additionally, the flux of CR is a risk to life directly exposed (Grießmeier et al. 2005). In order to estimate the level of magnetic protection, ZU13 predict the stellar wind properties for different stellar masses as a function of planetary distance and time.

There are two basic models used to describe the dynamics of the stellar wind: 1) the hydrodynamical model by Parker (1958) that describes the wind as a non-magnetized, isothermal and axially symmetric flux of particles and 2) the magneto-hydrodynamic model developed originally by Weber and Davis (1967) that takes into account the effects of stellar rotation and treats the wind as a magnetized plasma.

Parker's model describes the properties of the stellar winds of stars with periods of rotation of the same order of the Sun, *i.e.* $P \sim 30$ days (Preusse et al. 2005). For rapid rotating stars, as young and active dM stars, the isothermal model underestimates the stellar wind properties almost by a factor of 2 (Preusse et al. 2005). With Parker's model and equations (88)-(92), the systematic errors in the values of the magnetosphere properties will be between 10-40% compared with more detailed models. Magnetopause fields have the largest uncertainties and could be underestimated by ~40%, while standoff distances and polar cap areas will be respectively under and overestimated by just ~10%.

According to Parker's model the stellar wind average velocity v at distance d from the host star is:

$$u^2 - \log u = 4\log\rho + \frac{4}{\rho} - 3, \qquad (100)$$

where $u = v/v_c$ and $\rho = d/d_c$ are the velocity and distance normalized with respect to $v_c = \sqrt{k_B T/m}$ and $d_c = GM_\star m/(4k_B T)$ which corresponds to the local sound velocity and the critical distance where the stellar wind becomes subsonic respectively. T is the temperature of the plasma, which in the isothermal approximation is assumed constant at all distances and equal to the temperature of the stellar corona.

The particles density $n(d)$ is calculated using the equation of continuity:

$$n(d) = \frac{\dot{M}_\star}{4\pi d^2 v(d) m}, \qquad (101)$$

$\dot{M}_\star$ is the rate of stellar mass-loss, which is a free parameter in the model. It is necessary to estimate the evolution of the coronal temperature T and the mass-loss rate $\dot{M}_\star$.

From observational values of the stellar mass-loss (Wood et al. 2002), and models for the evolution of the stellar wind velocity (Newkirk 1980; Grießmeier et al. 2004) developed an expression for the evolution of the long-term averaged density and velocity of the stellar wind for main sequence stars at 1.0 au (see equations 1 and 2 in Grießmeier et al. (2010)). Using these formulae (Grießmeier et al. 2007) devised a way to estimate $T(t)$ and $\dot{M}_\star(t)$ and predict the stellar wind properties as a function of d and t.

For stellar ages $t \lesssim 0.7$ Gyr, equations 1 and 2 in (Grießmeier et al. 2010) are not reliable. These equations are based on the empirical relationship between the X-ray flux and the mass-loss rate $\dot{M}_\star$ (Wood et al. 2002), which has been obtained only for ages $t \gtrsim 0.7$ Gyr. Wood et al. (2005) have shown that an extrapolation to earlier times overestimates the mass-loss by factors of tens. At times $t \lesssim 0.7$ Gyr and over a given magnetic activity threshold the stellar wind of main-sequence stars seems to be inhibited (Wood et al. 2005). The limit at $t \approx 0.7$ Gyr could mark the time where the early stellar wind reaches a maximum. This fact suggests that at early times the effect of the stellar wind on the planetary magnetosphere is much lower than often assumed.

6.3.3 Magnetosphers of SEs

ZU13 have calculated magnetospheric properties of SEs in the mass-range 0.5-6.0 $M_\oplus$ inside the HZ of main sequence G-K-M stars. Their analysis include some well known SEs located inside the HZ: Gl 581 d, GJ 667C c and HD 40307 g. Additionally they include the cases for the Earth and a fictitious Venus as reference.

Planets inside the HZ of late K and dM stars ($M < 0.7 M_{\odot}$) are tidally locked at times $t < 0.7$ Gyr. Planets around G and early K stars ($M \gtrsim 0.7 M_{\odot}$) still have their primordial periods of rotation in the range 1 – 100 days as predicted by models of planetary formation (Miguel and Brunini 2010). Even at early times, tidally locked planets can develop non-negligible magnetospheres with radius up to $R_S > 1.5\ R_p$. For the same planets, Khodachenko et al. (2007) found that magnetospheric radius are below $2\ R_p$, even for tempered conditions, independent of the mass of the planet and age of the system. Conversely, ZU13 predict standoff distances for tidally locked planets in the range of 2-6 R_p depending on planetary mass and stellar age.

Though tidally locked planets seem to have larger magnetospheres than previously expected, they still have large polar caps. As a consequence, even protected atmospheres could have more than 15% of their areas exposed to open field lines where thermal and non-thermal processes remove atmospheric mass. ZU13 predict that these planets would have multipolar PMFs which contribute to an increase of the atmospheric area open to interplanetary space (Siscoe and Crooker 1976). Exposure of magnetized planets to external effects is a function of the standoff distance and polar cap area.

Magnetic protection increases with time as the star evolves and the dynamic pressure of the stellar wind decreases more rapidly than the PMF dipole moment. As a consequence the standoff distance grows in time and the polar cap shrinks. With the reduction in time of the stellar wind pressure the magnetopause field is also reduced, a fact that can also affect the incoming flux of CR at late times.

ZU13 found that planets with $M_p \sim 1.0\, M_{\oplus}$ begin their core nucleation around 2.5 Gyr. The emergence of the inner core enhances and strengthens the PMF. On the other hand, planets with $M_p \sim 1.8\ M_{\oplus}$ and greater still have a completely liquid core and therefore produce a weak PMF.

Unlocked planets are better protected than tidally locked planets. They develop extended magnetospheres $R_S \gtrsim 4.0\ R_p$ and lower polar cap areas $A_{pc} \lesssim 10\%$. In both cases and at early times $t \sim 1.0$ Gyr a smaller planetary mass implies a lower level of magnetic protection. This contradicts the general idea that low-mass planets ($M_p \lesssim 2.0\ M_{\oplus}$) are better suited to develop intense and protective PMFs [GA10, TA11, ZU12]. Magnetic protection as defined by ZU13 depends on the dipole moment instead of surface PMF strength. Since dipole moment scales as $\mathcal{M} \sim B_{dip} R_p^3$, more massive planets will have greater dipole moments, although their dynamos survive for less time.

We can compare the predicted values of the maximum dipole moment calculated by ZU13 with the values estimated in other attempts. For example, Khodachenko et al. (2007) estimate dipole moments for tidally locked planets in the range 0.022-0.15 $\mathcal{M}_{\oplus}$. These values have been systematically used in the literature to study planetary magnetic protection (Lammer et al. 2010). ZU13 predicts maximum dipole moments one order of magnitude greater (0.15-0.60 $\mathcal{M}_{\oplus}$) with the largest differences found for massive planets ($M \gtrsim 4.0\ M_{\oplus}$). These differences arise from the fact that none of the scaling-laws used by (Khodachenko et al. 2007) depend on the convective power. López-Morales et al. (2011) estimate magnetic dipolar moments for tidally locked SEs in the range 0.1-1.0 $\mathcal{M}_{\oplus}$. They use the same power-based scaling laws as ZU13, but assume a simple interior model and a static thermal model where the convective power is set maximize the efficiency with which the convective energy is converted into the PMF.

The evolution of magnetospheres for SEs is presented in figure 17. Although almost all these cases are tidally locked, ZU13 computed the magnetic properties for a primordial period of rotation $P = 1$ day. The case of a fictitious "hydrated" Venus is interesting. The dynamo of Venus probably shut down at $t = 3$ Gyr as a consequence of the drying of the mantle (Christensen et al. 2009). A massive loss of water induced by a runaway greenhouse and insufficient magnetic protection played a central role in the extinction of the early PMF in Venus. The evolution of the PMFs in Gl 581 d, GJ 667C c and HD 40307 g could have a similar fate, even though, their masses are much larger and their atmospheres are bound to the planet by a stronger gravity.

For planet HD 40307 g, ZU13 predicts the shut down of the dynamo at $t_{dyn} \sim 4$ Gyr. So that, currently the planet does not probably have a PMF. However, being around a K star ($M_{\star} \sim 0.7$), the stellar wind and XUV radiation have probably decreased enough to present no real threat to its atmosphere.

Gl 581 d and GJ 667C c are located around dM stars where the stellar wind pressure and XUV radiation are intense enough to erode their atmospheres. ZU13 predicts that Gl 581 d already lost its dynamo and has been exposed for almost 2.5 Gyr to the effects of the stellar wind and CR.

Given the estimated age of the GJ 667C system ($t \approx 2$ Gyr (Anglada-Escudé et al. 2013)), the planet probably still retains its magnetic field. According to ZU13, its magnetosphere properties are close to that of the "hydrated" Venus, at 2 Gyr. The planet is located in the inner part of the HZ, so it is more exposed to XUV radiation. This has

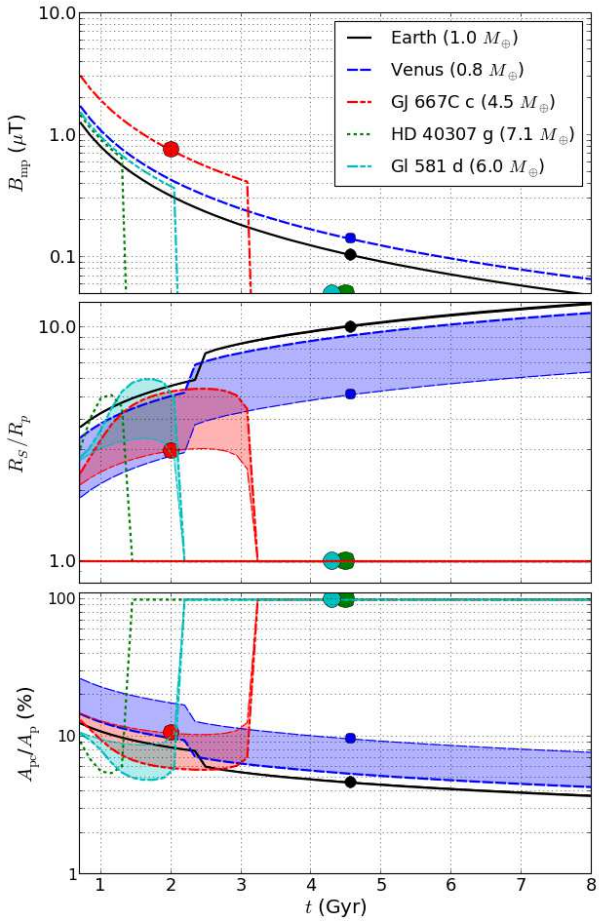

Figure 17. Evolution of magnetospheres. Shaded regions are limited by the properties calculated at a minimum period of rotation of $P \approx 1.0$ day (upper and lower bounds in standoff radius and polar cap area curves respectively) and the maximum period of rotation $P \approx P_o$ corresponding to a perfect match between the rotation and orbital periods (tidal locking). The actual curves should lie inside the shaded regions probably closer to the lower (upper) limits in the case of close-in already tidally locked planets (including Venus). Magnetopause fields do not depend on the rotation period of the planet. (Figure from ZU13, with permission of the editor)

surely led to the loss of its atmosphere, including its water.

6.3.4 Atmospheric mass-loss estimation

There are thermal and non-thermal atmospheric mass loss models that, combined with the evolution model of the magnetosphere, allow us to estimate the rate of loss of atmospheric mass for planets with and without a PMF. It is possible to make estimations based on ZU13 results and atmospheric mass-loss rate computed in previous work (Tian et al. 2008; Tian 2009; Lammer et al. 2012). The model of atmospheric mass loss used by ZU13 is fundamentally the same model of Tian et al. (2008); Tian (2009). It is a hydrodynamic model of the upper layers of the atmosphere (ionosphere/thermosphere), which solves the equations of continuity and momentum, in order to obtain velocities of the particles as well as the densities of the layers. The temperatures are prescribed. It is a model initially developed to analyze the response of heavy molecules such as N_2 and O_2 to XUV radiation and has been validated by comparison with the Earth's ionosphere/thermosphere (Tian 2009). The model has uncertainties mainly because it assumes a CO_2 rate per unit of mass for the SEs as equal as that for the Earth. On the other hand, the model neglects nonthermal escape mechanisms in the atmosphere escape calculations. The SE thermospheres expand up to five planetary radii. This would not be a problem for planets with extensive magnetospheres, but on small planets, especially those tidally locked, the termosphere would be outside the magnetosphere, and the loss by thermal mechanisms would be considerable.

The thermal mass-loss is induced by XUV radiation and have been estimated for Earth-like N_2 rich atmospheres (Watson et al. 1981; Kulikov et al. 2006; Tian et al. 2008) and dry Venus-like CO_2 rich atmospheres (Tian 2009; Lammer et al. 2012). A critical property, essential to evaluate the non-thermal mass-loss is the radius of the exobase R_{exo}, defined as the distance where the mean-free path of the electrically neutral particles could be comparable to the size of the planet. When the exobase size is comparable or larger than the magnetosphere, R_S, then the planet is effectively unmagnetized. In these conditions, the molecules in the exosphere will be picked-up by the stellar wind and lost to the space. On the other hand, if the exobase is well inside the magnetosphere, the molecules escaping by thermal process could stay trapped by the magnetic field forming a plasma-sphere. Planets under this condition will be magnetically protected and the mass-loss rate is much lower.

From the XUV luminosities of main-sequence stars (Garcés et al. 2011), ZU13 estimated the XUV flux at the top of the atmospheres of GL 581 d, GJ 667C c and HD 40307 g during the first Gyr of planetary evolution. The XUV flux is measured in an Earth-like unit, 1 PEV = 0.64 erg cm^{-2} s^{-1} is the XUV *Present Earth Value* (Judge et al. 2003; Guinan et al. 2009).

HD 40307 g receives $F_{XUV} = 10 - 35$ PEV. Gl 581 d was exposed to a flux of $F_{XUV} = 150 - 250$ PEV while GJ 667C c receives $F_{XUV} = 450 - 800$ PEV. Tian (2009) computed the exosphere properties of massive SEs, $M_p \geqslant 6\, M_\oplus$, subjected to different XUV fluxes. ZU13 estimate the exosphere radius and mass-loss rate for these SEs.

The atmospheric mass-loss rate is estimated as $\dot{M} \approx \alpha m n v_{eff}$ (Zendejas et al. 2010), where α is the entrainment efficiency and m, n and v_{eff} are the mass, the density and the effective velocity of the stellar wind at the planet distance (see eq. (87)).

- **HD 40307 g**
  HD 40307 g has a mass $M_p \approx 7\ M_\oplus$. If it possesses a CO_2 rich atmosphere, Tian (2009) predict that the exosphere of the planet and its mass-loss rate was low enough to avoid a significant early erosion of its atmosphere. This is true at least during the first 2 Gyr during which the RTE model predicts the planet was protected by a PMF (see figure 17). After the planetary dynamo has shut down, the atmosphere of HD 40307 g has been exposed to the direct action of the stellar wind. If the star age is 4.5 Gyr (Tuomi et al. 2013), then the atmosphere has been eroding during the last 3-4 Gyrs. Using an entrainment efficiency $\alpha \sim 0.3$, ZU13 calulated that for HD 40307 g has lost less than 1% of its volatile content (Tian 2009) during the unmagnetized phase. Although ZU13 provides an upper limits to magnetic protection and the planet could have a lighter Nitrogen-rich atmosphere which is more susceptible to XUV induced mass-losses (Watson et al. 1981; Kulikov et al. 2006; Tian et al. 2008), this preliminary estimate suggests that HD 40307 g probably still preserves a dense atmosphere able to sustain surface liquid water and hence to be actually habitable.
- **Gl 581 d**
  This SE has a mass $M_p \approx 6\ M_\oplus$. Assuming the estimates from ZU13 for the XUV flux, the exosphere radius predicted by Tian (2009) is $R_{exo} = 1.8 - 2.3\ R_p$ for a time $t \sim 1$ Gyr. The ZU13 model predicts a magnetosphere radius of $R_S > 2.7\ R_p$. It can be concluded that Gl 581 d could have been protected by its PMF during the early phases of planetary evolution and probably it has preserved the volatiles in its atmosphere.
- **GJ 667 C c**
  For GJ 667C c with a mass $M_p \approx 4.5\ M_\oplus$, the minimum exosphere radius predicted at $t \sim 1$ Gyr is $R_{exo} = 3.0 - 4.5\ R_p$ and the standoff distance is $R_S < 3\ R_p$. As the exosphere radius is larger than the standoff distance, and ZU13's model is actually optimistic, probably the planet was unprotected during its first Gyr. For the XUV fluxes estimated at the top of the atmosphere during the first Gyr, the thermal mass-loss rate of Carbon atoms from a CO_2 rich atmosphere will be greater than 2×10^{10} atoms cm^{-2} s^{-1} (Tian 2009). This is the value proposed for a 6 $M_\oplus$ SE, so for the actual mass of the planet the mass-loss rate will be larger. Moreover, if the exosphere were exposed directly to the stellar wind, non-thermal processes can contribute to the mass-loss. At the minimum mass-loss rate, GJ 667C c could have lost more than $\sim 10^{46}$ atoms of Carbon in just $\sim$ 100 Myr and in the first gigayear the amount of carbon thermally lost to space could rise to $\sim 10^{47}$ atoms. The total inventory of CO_2 in the atmosphere, crust and mantle of Venus is $2 - 3 \times 10^{46}$ molecules (Tian 2009), if we scale-up linearly with planetary mass, a 4.5 $M_\oplus$ planet will have a total budget of $\sim 10^{47}$ CO_2 molecules. In summary GJ 667C c could have lost its total inventory of Carbon in the first Gyr. Even assuming that large amounts of CO_2 are still trapped in the mantle and crust of the planet, its atmosphere should be being rapidly eroded by the stellar wind. ZU13 speculate that GJ 667C c is a sort of "Venus-like" planet. Regardless, the fact that the planet is well inside the HZ suggest that it has lost its capacity to support life.

ZU13 used a model of interaction with the stellar wind adapted from previous works (Grießmeier et al. 2004), to compute the properties of the magnetosphere and the level of magnetic protection that SEs could actually have. A non-trivial dependence of the magnetic properties on planetary age, planetary mass and period of rotation has been found in general for SEs inside the HZ. Thermal evolution is responsible for the relationship among all these properties. Contrary to what was found in the works of GA10 and TA11, tidally locked planets could develop relatively intense PMF and extended magnetospheres. However they also have extended polar caps and probably multipolar PMFs where lines open to the space, probably increasing the non-thermal loss of atmosphere.

In the case of SEs Gl 581 d, HD 40307 g and GJ 667C c, assuming a composition and thermal evolution parameters similar to the Earth, ZU13 predicted that dynamos of Gl 581 d and HD 40307 g have been already shut down. A younger GJ 667C c seems to still have an active dynamo. With the available information not much can be said about the magnetic protection of HD 40307 g. ZU13 predicts a large magnetosphere able to protect Gl 581 d against the erosive action of the stellar wind during the first few Gyr of planetary evolution. Further theoretical and observational analyses should be performed to establish the actual magnetic protection of this planet. The ZU13 upper-limit to the standoff-distance and the most optimistic estimate of the exobase radius and mass-loss rate from the atmosphere of

GJ 667C c, suggest that this planet has already lost a large fraction of its atmosphere. All the evidence makes GJ 667C c a sort of "Venus analogue". Despite the fact that it is inside the HZ, the planet is presently uninhabitable.

7 Discussion and perspectives

PMFs are an astrophysical phenomenon widely known in our solar system, PMFs of all planets, and even some of their moons (Bland et al. 2008) have been measured. The measurements has allowed us to infer the possible characteristics of the interior of planets and satellites, possible compositions and structures. The PMF play a fundamental role in the habitability of a planet. In the case of Earth, the PMF protects our atmosphere from the erosive effects of the solar wind and CR. The Earth's PMF is, for obvious reasons, the best studied and the best known. However, the modeling of its properties, its structure and its behavior over time still fails to explain some phenomena such as its non-periodic polarity changes (Valet et al. 2005). An additional problem is the inability to know the value of fundamental rheological parameters, limiting our understanding of the real thermal behavior of the inner layers of a planet, such as viscosity, specific heats or other factors in the EOS. However, taking into account what can be measured from our planet, models of the geodynamo are largely able to adjust to Earth data, despite the lack of information on some of the parameters.

On the other hand, despite having a large amount of data and measurements for the Earth, which allow us to infer the internal structure of the planet, there is still not enough information about the behavior and physicochemical nature of materials such as silicates or iron at very high pressures and temperatures. This is a fundamental problem, especially for planets more massive than Earth, in which the conditions of the interior are much more complex. The characterization of materials at very high pressures and temperatures is one of the main objectives of current research (Jeanloz 2017). The laboratory experiments seek to understand the properties of these materials inside the planets in order to improve theoretical models. These models include quantum behavior of materials, specifically in the case of rocky planets, the experiments seek to analyze whether the rock (SiO_2) behaves like metal under the conditions of the interior of a SE, and if this contributes to the generation and properties of the PMF (Jeanloz 2017).

To scale the behavior of the geodynamo to terrestrial planets with higher masses, as it is the case of the SEs, one must make some suppositions in terms of the possible composition and structure. The models described in this work suppose, in all the cases, that SEs are composed and structured like the Earth, with percentages of iron and silicates equal to the Earth, and arranged in the same way in their interior. This imposes a limitation to the models, since, in principle, they can not tell us anything about the thermal evolution or PMF of SEs with other compositions or different internal structure, such as for planets rich in water or with large atmospheres rich in volatiles such as H or He. It has begun to develop models of the interior of terrestrial planets that include compositions and structures different from those of the Earth. The work of Zuluaga and Bustamante (2018) models the magnetic protection of Proxima b, covering a wide range of possible compositions and masses for the planet using the RTE model. Their results have established a range of masses for Proxima b between 1.3 - 2.3 $M_\oplus$ and a radius between 1.2 - 1.5 $R_\oplus$, in addition to a magnetic dipole moment between 0.11 - 0.74 of the Earth. Their model can be extended to other planets.

In the case of extrasolar planets, the current impossibility of making direct measurements of their PMFs does not allow us to make precise predictions about their structure or about the source of energy that produces the PMF itself. There is still no observational evidence of the presence of atmospheres around terrestrial planets. However, the models of the planetary interior, as well as the models of their possible atmospheres, give us indications of their possible habitability, but again the presence of a protective PMF is required. One possibility of observing the presence of PMFs in extrasolar planets and measuring their intensity comes from radio astronomy. Radio signals produced by electron-cyclotron masers could be measured in the PMFs of extrasolar planets, especially in giants near their stars (Lazio et al. 2018). These electron-cyclotron emissions, which result from the interaction between the magnetosphere and the solar wind, have already been detected for Earth and all the giant planets of the solar system (Lazio et al. 2018). The detection of a PMF would provide information that would expand our knowledge about planetary interiors and their dynamos. The possible observation of magnetic fields should be complemented with the observation in the infrared of the presence of planetary atmospheres and their compositions (Batalha et al. 2018), which will greatly expand the information that could be included in the theoretical models.

Planetary habitability is another of the topics currently open. The modeling of planetary atmospheres and their interaction with their star, in a wide variety of possible worlds, makes this field one of the most prolific in scientific publications of high impact. Currently there is spe-

cial interest in terrestrial planets around red dwarf stars, which would be the most abundant in the galaxy and in the universe. It is widely accepted that the high-energy particles of solar wind and cosmic rays, as well as the XUV radiation, generate a hostile environment around main sequence stars, F-G-K and especially around young red dwarfs (M-dwarfs). There are two harmful effects for life that come from the impact of high-energy particles and XUV radiation:

1. The direct destruction of organic molecules on the surface of the planet, and
2. the erosion of the atmosphere, especially the loss of water from the planet. PMFs prevent both processes.

It is expected to have a large sample of exoplanets with measured PMFs and detected atmospheres with their composition in the coming few decades. This will allow us to consolidate the theoretical models and validate the assumptions or reformulate the proposed theories about the composition, structure and thermal and magnetic evolution of the planets.

Acknowledgment: We thank the reviewers of this manuscript for the valuable insights and comments, all of them have been included in the final version of the text. FACom - SEAP group is supported by Estrategia de Sostenibilidad 2016-2017, Vicerectoría de Investigación - UdeA.

References

Adams, E. R., Seager, S., and Elkins-Tanton, L. 2008, *ApJ* , **673**, 1160–1164.

Amit, H., Leonhardt, R., and Wicht, J. 2010, *Space Sci. Rev.* , **155**, 293–335.

Anglada-Escudé, G., Amado, P. J., Barnes, J., Berdiñas, Z. M., Butler, R. P., Coleman, G. A. L. et al. 2016, *Nature* , **536**, 437–440.

Anglada-Escudé, G., Tuomi, M., Gerlach, E., Barnes, R., Heller, R., Jenkins, J. S. et al. 2013, *A&A* , **556**, A126.

Aubert, J., Labrosse, S., and Poitou, C. 2009, *Geophysical Journal International*, **179**, 1414–1428.

Baraffe, I., Chabrier, G., Allard, F., and Hauschildt, P. H. 1998, *A&A* , **337**, 403–412.

Baraffe, I., Chabrier, G., and Barman, T. 2008, *A&A* , **482**, 315–332.

Barnes, R., Raymond, S. N., Jackson, B., and Greenberg, R. 2008, *Astrobiology*, **8**, 557–568.

Batalha, N. E., Lewis, N. K., Line, M. R., Valenti, J., and Stevenson, K. 2018, *ArXiv preprint arXiv:1803.07983*.

Benneke, B. and Seager, S. 2013, *ApJ* , **778**, 153.

Biggin, A. J., Strik, G. H. M. A., and Langereis, C. G. 2009, *Earth, Planets, and Space*, **61**, 9–22.

Bland, M. T., Showman, A. P., and Tobie, G. 2008, *Icarus*, **198(2)**, 384–399.

Bonfils, X., Delfosse, X., Udry, S., Forveille, T., Mayor, M., Perrier, C. et al. 2011, *ArXiv preprint arXiv:1111.5019*.

Boss, A. P. 2006, *ApJL* , **644**, L79–L82.

Breuer, D., Labrosse, S., and Spohn, T. 2010, *Space Sci. Rev.* , **152**, 449–500.

Busse, F. H. and Simitev, R. D. 2009, *ArXiv e-prints*

Charbonneau, D., Berta, Z. K., Irwin, J., Burke, C. J., Nutzman, P., Buchhave, L. A. et al. 2009, *Nature* , **462**, 891–894.

Chaufray, J. Y., Modolo, R., Leblanc, F., Chanteur, G., Johnson, R. E., and Luhmann, J. G.: 2007, *Journal of Geophysical Research (Planets)*, **112(E11)**, 9009.

Christensen, U., Balogh, A., Breuer, D., and Glaßmeier, K. 2009, *Planetary Magnetism*, Space Sciences Series of ISSI, Springer.

Christensen, U. R. 2010, *Space Sci. Rev.* , **152**, 565–590.

Christensen, U. R.: 2011a, *Physics of the Earth and Planetary Interiors*, **187(3-4)**, 157–169.

Christensen, personal communication, U. R. 2011b, Personal communication

Christensen, U. R. and Aubert, J. 2006, *Geophysical Journal International*, **166**, 97–114.

Christensen, U. R., Aubert, J., and Hulot, G. 2010, *Earth and Planetary Science Letters*, **296(3-4)**, 487–496.

Christensen, U. R., Holzwarth, V., and Reiners, A. 2009, *Nature* , **457**, 167–169.

Correia, A. C. M., Boué, G., and Laskar, J. 2012, *ApJL* , **744**, L23.

Cuartas-Restrepo, P. A., Melita, M., Zuluaga, J. I., Portilla-Revelo, B., Sucerquia, M., and Miloni, O. 2016, *MNRAS* , **463**, 1592–1604.

Denis, C., Rybicki, K. R., Schreider, A. A., Tomecka-Suchoń, S., and Varga, P. 2011, *Astronomische Nachrichten*, **332**, 24–35.

Driscoll, P. and Olson, P. 2009, *Geophysical Journal International*, **178**, 1337–1350.

Driscoll, P. and Olson, P.: 2009, *Earth and Planetary Science Letters*, **282(1-4)**, 24–33.

Driscoll, P. and Olson, P. 2011, *Icarus* , **213**, 12–23.

Dumusque, X., Pepe, F., Lovis, C., Ségransan, D., Sahlmann, J., Benz, W. et al. 2012, *Nature*, **491**, 207–211.

Dziewonski, A. M. and Anderson, D. L. 1981, *Physics of the Earth and Planetary Interiors*, **25**, 297–356.

Elkins-Tanton, L. T. and Seager, S. 2008, *ApJ* , **685**, 1237–1246.

Ferraz-Mello, S., Rodríguez, A., and Hussmann, H. 2008, *Celestial Mechanics and Dynamical Astronomy*, **101**, 171–201.

Foley, B. J., Bercovici, D., and Landuyt, W. 2012, *Earth and Planetary Science Letters*, **331**, 281–290.

Ford, E. B., Seager, S., and Turner, E. L.: 2001, *Nature* , **412**, 885–887.

Fortney, J. J., Glenzer, S. H., Koenig, M., Militzer, B., Saumon, D., and Valencia, D. 2009, *Physics of Plasmas*, **16(4)**, 041003–041003-7.

Fortney, J. J., Marley, M. S., and Barnes, J. W.: 2007, *ApJ* **659**, 1661–1672.

Franck, S., von Bloh, W., Bounama, C., Steffen, M., Schönberner, D., and Schellnhuber, H.-J. 2000, *J. Geophys. Res.* , **105**, 1651–1658.

Gaidos, E., Conrad, C. P., Manga, M., and Hernlund, J. 2010, *ApJ* , **718**, 596–609.

Gaidos, E. 2011, Personal communication.

Garcés, A., Catalán, S., and Ribas, I. 2011, *A&A* , **531**, A7.

Glatzmaier, G. A. and Roberts, P. H. 1995, *Nature* , **377**, 203–209.

Grasset, O., Schneider, J., and Sotin, C. 2009, *ApJ* , **693**, 722–733.

Grießmeier, J.-M., Khodachenko, M., Lammer, H., Grenfell, J. L., Stadelmann, A., and Motschmann, U. 2010, In: A. G. Kosovichev, A. H. Andrei, & J.-P. Roelot (Eds.), *IAU Symposium*, *IAU Symposium*, **264**, 385–394.

Grießmeier, J.-M., Preusse, S., Khodachenko, M., Motschmann, U., Mann, G., and Rucker, H. O. 2007, *Planet. Space Sci.* , **55**, 618–630.

Grießmeier, J.-M., Stadelmann, A., Grenfell, J. L., Lammer, H., and Motschmann, U. 2009, *Icarus* , **199**, 526–535.

Grießmeier, J.-M., Stadelmann, A., Motschmann, U., Belisheva, N. K., Lammer, H., and Biernat, H. K. 2005, *Astrobiology*, **5**, 587–603.

Grießmeier, J.-M., Stadelmann, A., Penz, T., Lammer, H., Selsis, F., Ribas, I. et al. 2004, *A&A* , **425**, 753–762.

Gubbins, D., Alfè, D., Masters, G., Price, G. D., and Gillan, M. 2004, *Geophysical Journal International*, **157**, 1407–1414.

Gubbins, D., Alfè, D., Masters, G., Price, G. D., and Gillan, M. J. 2003, *Geophysical Journal International*, **155**, 609–622.

Guillot, T., Santos, N. C., Pont, F., Iro, N., Melo, C., and Ribas, I. 2006, *A&A* , **453**, L21–L24.

Guinan, E. F., Engle, S. G., and Dewarf, L. E. 2009, In: M. E. van Steenberg, G. Sonneborn, H. W. Moos, & W. P. Blair (Eds.), *American Institute of Physics Conference Series*, *American Institute of Physics Conference Series*, 1135, 244–252.

Haghighipour, N. 2011, *Contemporary Physics*, **52**, 403–438.

Heller, R., Barnes, R., and Leconte, J. 2011a, *Origins of Life and Evolution of the Biosphere*, **41**, 539–543.

Heller, R., Leconte, J., and Barnes, R. 2011b, *A&A* , **528**, A27.

Henning, W. G., O'Connell, R. J., and Sasselov, D. D. 2009, *ApJ* , **707**, 1000–1015.

Herrero-Bervera, E. and Valet, J.-P. 2009, *Earth and Planetary Science Letters*, **287**, 420–433.

Howard, A. W., Marcy, G. W., Johnson, J. A., Fischer, D. A., Wright, J. T., Isaacson, H. et al. 2010, *Science*, **330**, 653–655.

Huang, S.-S. 1960, *PASP* , **72**, 489–493.

Ida, S. and Lin, D. N. C.: 2004, *ApJ* **604**, 388–413.

Jeanloz, R. 2017, *Recreating Planet Cores in the Laboratory*, Technical report, Univ. of California, Berkeley, CA, USA.

Jones, C. 2000, *Philosophical Transactions of the Royal Society of London A: Mathematical, Physical and Engineering Sciences*, **358(1768)**, 873.

Joshi, M. M., Haberle, R. M., and Reynolds, R. T. 1997, *Icarus* , **129**, 450–465.

Judge, P. G., Solomon, S. C., and Ayres, T. R., 2003, *ApJ* , **593**, 534–548.

Kasting, J. 2010, *How to Find a Habitable Planet*, Princeton University Press, USA.

Kasting, J. F., Whitmire, D. P., and Reynolds, R. T. 1993, *Icarus* , **101**, 108–128.

Khodachenko, M. L., Lammer, H., Lichtenegger, H. I. M., Grießmeier, J.-M., Holmström, M., and Ekenbäck, A. 2009, In: K. G. Strassmeier, A. G. Kosovichev, and J. E. Beckman (Eds.), *Cosmic Magnetic Fields: From Planets, to Stars and Galaxies*, *IAU Symposium*, 259, 283–294.

Khodachenko, M. L., Ribas, I., Lammer, H., Grießmeier, J.-M., Leitner, M., Selsis, F. et al. 2007, *Astrobiology*, **7**, 167–184.

Kite, E. S., Gaidos, E., and Manga, M. 2011, *ApJ* , **743**, 41.

Kite, E. S., Manga, M., and Gaidos, E. 2009, *ApJ* , **700**, 1732–1749.

Kopparapu, R. K., Wolf, E. T., Arney, G., Batalha, N. E., Haqq-Misra, J., Grimm, S. L. et al. 2017, *ApJ* , **845**, 5.

Korenaga, J. 2010, *ApJL* , **725**, L43–L46.

Krasnopolsky, V. A. 2015, *Icarus* , **257**, 377–386.

Kulikov, Y. N., Lammer, H., Lichtenegger, H. I. M., Terada, N., Ribas, I., Kolb, C. et al. 2006, *Planet. Space Sci.* , **54**, 1425–1444.

Kutzner, C. and Christensen, U. R.: 2002, *Physics of the Earth and Planetary Interiors* **131**, 29

Labrosse, S. 2003, *Physics of the Earth and Planetary Interiors*, **140**, 127–143.

Labrosse, S.: 2007a, *Encyclopedia of Geomagnetism and Paleomagnetism*, Chapt. Heat flow across the core-mantle boundary, Springer, 127–130,

Labrosse, S. 2007b, *Encyclopedia of Geomagnetism and Paleomagnetism*, Chapt. Energy sources for the geodynamo, Springer, 300–308,

Labrosse, S., Poirier, J.-P., and Le Mouël, J.-L. 2001, *Earth and Planetary Science Letters*, **190**, 111–123.

Lammer, H., Bredehöft, J. H., Coustenis, A., Khodachenko, M. L., Kaltenegger, L., Grasset, O. et al. 2009, *A&A Rev.* , **17**, 181–249.

Lammer, H., Lichtenegger, H. I. M., Khodachenko, M. L., Kulikov, Y. N., and Griessmeier, J. 2012, In: J. P. Beaulieu, S. Dieters, & G. Tinetti (Eds.), *Astronomical Society of the Pacific Conference Series*, 450, 139–146.

Lammer, H., Lichtenegger, H. I. M., Kulikov, Y. N., Grießmeier, J.-M., Terada, N., Erkaev, N. V. et al. 2007, *Astrobiology*, **7**, 185–207.

Lammer, H., Selsis, F., Chassefière, E., Breuer, D., Grießmeier, J.-M., Kulikov, Y. N. et al. 2010, *Astrobiology*, **10**, 45–68.

Lammer, H., Selsis, F., Ribas, I., Guinan, E. F., Bauer, S. J., and Weiss, W. W. 2003, *ApJL* , **598**, L121–L124.

Lazio, J., Hallinan, G., Airapetian, V., Brain, D., Dong, C., Driscoll, P. et al. 2018, *ArXiv preprint arXiv:1803.06487*.

Leconte, J., Chabrier, G., Baraffe, I., and Levrard, B. 2010, *A&A* , **516**, A64.

Léger, A., Rouan, D., Schneider, J., Barge, P., Fridlund, M., Samuel, B. et al. 2009, *A&A* , **506**, 287–302.

Levi, A., Sasselov, D., and Podolak, M. 2014, *ApJ* , **792**, 125.

Lichtenegger, H. I. M., Lammer, H., Grießmeier, J.-M., Kulikov, Y. N., von Paris, P., Hausleitner, W. et al. 2010, *Icarus* , **210**, 1–7.

Lister, J. R. 2003, *Physics of the Earth and Planetary Interiors*, **140**, 145–158.

López-Morales, M., Gómez-Pérez, N., and Ruedas, T. 2011, *Origins of Life and Evolution of the Biosphere*, **41**, 533–537.

Luger, R. and Barnes, R. 2015, *Astrobiology*, **15**, 119–143.

Madhusudhan, N., Lee, K. K. M., and Mousis, O. 2012, *ApJL* , **759**, L40.

Makarov, V. V., Berghea, C., and Efroimsky, M.: 2012, *ArXiv e-prints*.

Makarov, V. V. and Efroimsky, M.: 2012, *ArXiv e-prints*.

Marcus, R. A., Sasselov, D., Stewart, S. T., and Hernquist, L. 2010, *ApJL* , **719**, L45–L49.

Mayor, M. and Udry, S. 2008, *Physica Scripta Volume T*, **130(1)**, 014010+08.

McNeil, D. S. and Nelson, R. P. 2010, *MNRAS* , **401**, 1691–1708.

Mead, G. D. 1964, *J. Geophys. Res.* , **69**, 1181–1195.

Miguel, Y. and Brunini, A. 2010, *MNRAS* , **406**, 1935–1943.

Nettelmann, N., Fortney, J. J., Kramm, U., and Redmer, R. 2011, *ApJ* , **733**, 2.

Newkirk, Jr., G. 1980, In: R. O. Pepin, J. A. Eddy, & R. B. Merrill (Eds.), *The Ancient Sun: Fossil Record in the Earth, Moon and Meteorites*, 293–320.

Nimmo, F. 2009, *Treatise on Geophysics*, Chapt. Enegetics of the Core, Elsevier, 8, 31–68.

Nimmo, F. and Stevenson, D. J. 2000, *J. Geophys. Res.* , **105**, 11969–11980.
Olson, P. 2007, In: T. N. A. of Sciences of the USA (Eds.), *Proceedings of the National Academy of Sciences*, 104, 20159–20166.
Olson, P.: 2007, In: G. Schubert (Ed.), *Treatise on Geophysics: Volume 8, Core dynamics*, Elsevier B.V., 1–30.
Olson, P. and Christensen, U. R. 2006, *Earth and Planetary Science Letters*, **250**, 561–571.
Owen, J. E. and Mohanty, S. 2016, *MNRAS* , **459**, 4088–4108.
Pallé, E., Ford, E. B., Seager, S., Montañés-Rodríguez, P., and Vazquez, M. 2008, *ApJ* , **676**, 1319–1329.
Papuc, A. M. and Davies, G. F. 2008, *Icarus* , **195**, 447–458.
Parker, E. N. 1958, *ApJ* , **128**, 664–685.
Peale, S. J. 1977, In: J. A. Burns (Ed.), *IAU Colloq. 28: Planetary Satellites*, 87–111.
Pozzo, M., Davies, C., Gubbins, D., and Alfè, D. 2012, *Nature* , **485**, 355–358.
Preusse, S., Kopp, A., Büchner, J., and Motschmann, U. 2005, *A&A* , **434**, 1191–1200.
Ranalli, G. 2001, *Journal of Geodynamics*, **32**, 425–444.
Rauer, H., Gebauer, S., Paris, P. V., Cabrera, J., Godolt, M., Grenfell, J. L. et al. 2011, *A&A* , **529**, A8.
Ricard, Y. 2009, *Treatise on Geophysics*, Chapt. Physics of Mantle Convection, Elsevier, Vol. 7.
Rivera, E. J., Lissauer, J. J., Butler, R. P., Marcy, G. W., Vogt, S. S., Fischer, D. A. et al. 2005, *ApJ* , **634**, 625–640.
R.K. Kopparapu, p. c.: 2017, Personal communication.
Roberts, P.: 2009, *Treatise on Geophysics*, Vol. 8, Chapt. Theory of Geodynamo, Elsevier, 67–105.
Roberts, P. H. and Glatzmaier, G. A. 2000, *Reviews of Modern Physics*, **72**, 1081–1123.
Rodríguez, A., Callegari, N., Michtchenko, T. A., and Hussmann, H. 2012, *MNRAS* , **427**, 2239–2250.
Rogers, L. and Seager, S. 2010, In: *American Astronomical Society Meeting Abstracts #215*, *Bulletin of the American Astronomical Society*, 42, 443.
Sasselov, D. D., Valencia, D., and O'Connell, R. J. 2008, *Physica Scripta Volume T*, **130(1)**, 014035.
Scalo, J., Kaltenegger, L., Segura, A. G., Fridlund, M., Ribas, I., Kulikov, Y. N. et al. 2007, *Astrobiology*, **7**, 85–166.
Schubert, G., Cassen, P., and Young, R. E. 1979, *Icarus* , **38**, 192–211.
Schubert, G., Turcotte, D. L., and Olson, P. 2001, *Mantle Convection in the Earth and Planets*, Cambridge University Press, Cambridge, UK.
Seager, S., Kuchner, M., Hier-Majumder, C. A., and Militzer, B. 2007, *ApJ* , **669**, 1279–1297.
Segura, A., Walkowicz, L. M., Meadows, V., Kasting, J., and Hawley, S. 2010, *Astrobiology*, **10**, 751–771.
Selsis, F., Kasting, J. F., Levrard, B., Paillet, J., Ribas, I., and Delfosse, X. 2007, *A&A* , **476**, 1373–1387.
Siscoe, G. and Christopher, L. 1975, *Geophys. Res. Lett.* , **2**, 158–160.
Siscoe, G. and Crooker, N. 1976, *Journal of Geomagnetism and Geoelectricity*, **28**, 1–9.
Siscoe, G. L. and Chen, C.-K. 1975, *J. Geophys. Res.* , **80**, 4675–4680.
Sotin, C., Grasset, O., and Mocquet, A. 2007, *Icarus* , **191**, 337–351.
Sreenivasan, B. and Jones, C. A. 2006, *Geophysical Journal International*, **164**, 467–476.
Stacey, F. D. 1992, *Physics of the Earth.*, Brookfield Press, Kenmore, Brisbane, Australia.
Stadelmann, A., Vogt, J., Glassmeier, K.-H., Kallenrode, M.-B., and Voigt, G.-H. 2010, *Earth, Planets, and Space*, **62**, 333–345.
Stamenković, V., Breuer, D., and Spohn, T. 2011, *Icarus* , **216**, 572–596.
Stevenson, D. J. 1983, *Reports on Progress in Physics* **46**, 555–557, 559–620.
Stevenson, D. J.: 2003, *Earth and Planetary Science Letters* **208(1–2)**, 1–11.
Stevenson, D. J. 2010, *Space Sci. Rev.* , **152**, 651–664.
Tachinami, C., Senshu, H., and Ida, S. 2011, *ApJ* , **726**, 70.
Tarduno, J. A., Cottrell, R. D., Watkeys, M. K., Hofmann, A., Doubrovine, P. V., Mamajek, E. E. et al. 2010, *Science*, **327**, 1238–1240.
Tian, F. 2009, *ApJ* , **703**, 905–909
Tian, F. 2015, *Earth and Planetary Science Letters*, **432**, 126–132.
Tian, F., Kasting, J. F., Liu, H.-L., and Roble, R. G. 2008, *Journal of Geophysical Research (Planets)*, **113(E12)**, 5008.
Tikoo, S. M. and Elkins-Tanton, L. T. 2017, *Philosophical Transactions of the Royal Society of London Series A*, **375**, 20150394.
Tuomi, M., Anglada-Escudé, G., Gerlach, E., Jones, H. R. A., Reiners, A., Rivera, E. J. et al. 2013, *A&A* , **549**, A48.
Valencia, D. 2011, In: A. Sozzetti, M. G. Lattanzi, and A. P. Boss (Eds.), *IAU Symposium*, 276, 181–188.
Valencia, D. and O'Connell, R. J. 2009, *Earth and Planetary Science Letters*, **286**, 492–502.
Valencia, D., O'Connell, R. J., and Sasselov, D. 2006, *Icarus* , **181**, 545–554.
Valencia, D., O'Connell, R. J., and Sasselov, D. D. 2007a, *ApJL* , **670**, L45–L48.
Valencia, D., Sasselov, D. D., and O'Connell, R. J. 2007b, *ApJ* , **665**, 1413–1420.
Valencia, D., Sasselov, D. D., and O'Connell, R. J. 2007c, *ApJ* , **656**, 545–551.
Valet, J.-P., Meynadier, L., and Guyodo, Y. 2005, *Nature*, **435(7043)**, 802–805.
van Hoolts, T. 2009, *Treatise on Geophysics*, Chapt. The Rotation of the Terrestrial Planets, Elsevier, 10, 123–164.
van Thienen, P., Benzerara, K., Breuer, D., Gillmann, C., Labrosse, S., Lognonné, P. et al. 2007, *Space Sci. Rev.* , **129**, 167–203.
Varga, P., Denis, C., and Varga, T. 1998, *Journal of Geodesy*, **25**, 61–84.
Voigt, G. 1995, *Handbook of atmospheric electrodynamics*, Chapt. Magnetospheric Configuration, CRC Press, 2, 333–388.
von Bloh, W., Bounama, C., Cuntz, M., and Franck, S. 2007, *A&A* , **476**, 1365–1371.
Vočadlo, L., Alfè, D., Gillan, M. J., and Price, G. D. 2003, *Physics of the Earth and Planetary Interiors*, **140**, 101–125.
Wagner, F. W., Tosi, N., Sohl, F., Rauer, H., and Spohn, T. 2012, *A&A* , **541**, A103.
Ward, P. and Brownlee, D. 2000, *Rare earth : why complex life is uncommon in the universe*, Copernicus, Springer-Verlag New York.
Watson, A. J., Donahue, T. M., and Walker, J. C. G. 1981, *Icarus* , **48**, 150–166.
Weber, E. J. and Davis, Jr., L. 1967, *ApJ* , **148**, 217–227.
Wood, B. E., Müller, H.-R., Zank, G. P., and Linsky, J. L. 2002, *ApJ* , **574**, 412–425.

Wood, B. E., Müller, H.-R., Zank, G. P., Linsky, J. L., and Redfield, S. 2005, *ApJL* , **628**, L143–L146.
Yamazaki, D. and Karato, S. 2001, *American Mineralogist*, **86**, 385–391.
Zendejas, J., Segura, A., and Raga, A. C. 2010, *Icarus* , **210**, 539–544.
Zeng, L. and Sasselov, D. 2013, *PASP* , **125**, 227.
Zeng, L., Sasselov, D. D., and Jacobsen, S. B. 2016, *ApJ* , **819**, 127.
Zuluaga, J. I. and Bustamante, S. 2018, *Planetary and Space Science*, **152**, 55–67.
Zuluaga, J. I., Bustamante, S., Cuartas, P. A., and Hoyos, J. H. 2013, *ApJ* , **770**, 23.
Zuluaga, J. I. and Cuartas, P. A. 2012, *Icarus* , **217**, 88–102.